MODELING, SENSING AND CONTROL FOR GEOMETRIC ACCURACY IN BAR TURNING

by

ALY M. SHAWKY, B. SC. HONS., M. SC.

A Thesis

Submitted to the School of Graduate Studies

in Partial Fulfillment of the Requirements

for the Degree

Doctor of Philosophy

McMaster University

GEOMETRIC ACCURACY IN BAR TURNING

DOCTORATE OF PHILOSOPHY (1996) **McMaster University**
(Mechanical Engineering) **Hamilton, Ontario**

TITLE:	Modeling, Sensing and Control of Workpiece Geometric Accuracy in Bar Turning.
AUTHOR:	Aly M. Shawky, B. Sc. Hons. (Alexandria University, Egypt) M. Sc. (Alexandria University, Egypt).
SUPERVISOR:	Professor M. A. Elbestawi
NUMBER OF PAGES:	xxii, 201

ABSTRACT

The ability to predict, measure and control the geometric accuracy of the machining process has become of significant importance to industry in its pursuit of successful competition in today's market place. This thesis describes the development and integration of the different subsystems required for the implementation of geometric adaptive control in bar turning. These subsystems include modeling of the machining system, on-line measurement of the workpiece geometry, tool actuation and predictive control design.

A mechanistic dynamic model of the machining system in bar turning is developed. The model accounts for the rather complex geometry of a multi-edged cutting tool and considers the dynamics of both the tool and workpiece. Also, the simulation of machining dynamics is significantly enhanced by incorporating a mechanistic ploughing force model which accounts for process damping. The model enables the simulation of the process for a wide range of cutting conditions and the prediction of cutting forces, workpiece accuracy and machined surface topography. The model predictions are verified using experimental results of turning hardened steel using ceramic inserts.

A novel non-contact sensor is then developed for on-line high speed monitoring of the workpiece diameter while using a cutting fluid. The measurement system employs three ultrasonic transducers and provides an absolute diameter measurement. An algorithm based

on multi-probe measurements is developed to process the radius data and simultaneously compensate for sensor misalignment by tracking the center-line of the workpiece. The system is incorporated into a CNC lathe and provides an accuracy of ±5 μm within a working range of 20 mm. The accuracy and repeatability of the measuring system are tested experimentally under realistic cutting conditions. The applicability of the measurement system to provide complete on-line assessment of workpiece geometry is also demonstrated by evaluating the workpiece geometrical tolerances. The influence of different parameters such as fitting objective functions, size of data sets, and data conditioning on such strategy are investigated.

A model-based predictive controller is designed and implemented to minimize the form error of the workpiece in bar turning. The mechanistic model of the machining system is simplified and reformulated into the state space to permit design and real-time implementation of the control system. The measurement system is set as close as possible to the cutting edge (at a distance of 0.27 mm). An optimal regulator with a Kalman Filter is designed. The on-line measurement of the workpiece diameter is used through the Kalman filter to update the model predictions with unmodeled process disturbances such as tool wear and thermal deflections of the tooling system. The system is implemented on a CNC lathe retrofitted with an Open Architecture Controller. The output of the geometric controller is used to govern the position of the tool tip in real-time by commanding the same servo motor which is driven by the preprogrammed G-code. The control system is tested experimentally under different cutting conditions and is found to provide a significant improvement of more than 90% in workpiece geometric accuracy.

ACKNOWLEDGMENTS

The author would like to express his sincere gratitude and appreciation to his research supervisor, Professor M. A. Elbestawi, for his constructive guidance, continuous encouragement and support throughout the course of this study. Gratitude is also expressed to the members of the supervisory committee: Professors P. Taylor, R. Judd and M. Sklad for their thoughtful suggestions and their willingness to lend their thoughts and insights when they were able to.

I would like to acknowledge the assistance of many other individuals. My great appreciation goes to my wife Sue for her patience and encouragement, without whose support none of this would have been possible. Also, my friends and colleagues at IMMRC labs; I have to express my great appreciation for your friendship, support and team spirit. It is great to always find somebody there, willing and able to help and discuss research issues of mutual interests, as well as anything else. They are a great group to work with.

I also would like to thank the people who provided technical assistance over the course of this research, Joe Verhaeghe, Ron Lodewyks, and David Schick. Your assistance has been invaluable.

Finally, the financial support provided by McMaster University and an Ontario Graduate scholarship is also gratefully acknowledged.

TO THE MEMORY OF MY FATHER

TABLE OF CONTENTS

CHAPTER 3

LIST OF FIGURES

LIST OF TABLES

NOMENCLATURE

A, A_c	System matrices.	AB	Axis of substitute cylinder.
A_c	Chip load.	A_d	Dynamic change in A_s
A_s	Local static contact area.	$a_0 .. a_3$	Regression constants.
B, B_c	Input matrices.	b_o	Constant.
b	Vector representing optimization control variables.		
C	Tool nose arc.	C, C_c	Output matrices.
$C_0 .. C_7$	Regression constants.	C_{tx}, C_{tx}	Tool damping coefficients.
D, D_c	Direct Input matrices.	D	Diameter of piezoelectric element.
d	Depth of cut.	d_a	Actual depth of cut.
d_c	Commanded depth of cut.		
d_d	Nominal depth of cut (output of x-axis servo model).		
d_{min}	Minimum distance from q to AB.	d_m	Master bar diameter.
d_o	Intermediate variable in x-axis servo model.		
doc	Workpiece surface	dr_i	Out of roundness data.
d_{wp}	Workpiece diameter.	E	End cutting edge
$EI(x)$	Workpiece flexural stiffness.	e_i	Measurement error of *ith* sensor.
ϵ_i	Smallest residual.	F	Indicates Cutting Force.
F_L	Longitudinal Cutting Force.	F_N	Normal cutting force.
F_{obj}	Objective function.	F_R	Radial cutting force.

F_T	Tangential cutting force	f	Tool feed, rev/min.
$f(x,t)$	Distributed force as function of time.		
f_c	Cut-off-frequency, Hz.	f_{com}	Commanded tool feed.
f_r	Feed rate [mm/min].	f_{sp}	Proportionality constant.
G, Q	Weighing matrices.	$g's$	Regression constants.
h_a	Actual chip thickness.	h_m	Maximum penetration depth.
h_{nom}	Nominal chip thickness.	h_t	Total penetration depth.
i	Inclination angle.	J	Quadratic cost function.
K_c	Chuck translational stiffness.	K_t	Tail Stock translational stiffness.
K_t	Chuck torsional stiffness.	$k_{f,d}$	Servo dc-gain.
K_{tx},K_{ty}	Tool stiffness.	K	Kalman gain.
$K_{N,T,v}$	Proportionality constants.	L	Feedback gain matrix.
L	Clearance face contact length.	L_p	Distance function (index p, $0<p<\infty$).
l	Workpiece Length.	la	Tool lead angle.
la_e	Effective lead angle.		
l_{cir}	Circumfrencial distance of workpiece surface elapsed per measurement.		
l_c	Chip contact length.	l_o	Distance to point of action of force.
m_{tx},m_{ty}	Tool mass.	$m(x)$	Mass per unit length of workpiece.
$O(t)$	Cutting conditions vector.	O_n	Nominal cutting conditions vector.
$P(t)$	Tool edge profile at time t.		
P_d	Calibrated distance from sensor to datum.		
P_{mi}	Distance measured by the ith sensor.	P_N	Normal ploughing force.
P_T	Tangential ploughing force.	p_x	Vector representation of a point x.

$\mathbf{p}^u_x$	Tangent vector at point x.		
$\mathbf{q}$	Vector representation of a measured point.		
$Q_r(t)$	Generalized modal force.	Q, R	Weighing matrices.
R	Tool nose radius	R_i	ith radius measurement.
R_m	Mean value of radius measurements.	R_{nom}	Nominal radius of the workpiece.
$R_{w,v}$	Covariance matrices.	R_{wp}	Workpiece radius.
r_i	Radius data with low frequency form error.		
r	Tool edge radius.	S	Side cutting edge.
s	Laplace operator.	T	Time of one workpiece revolution.
T_d	Time delay in servo response.	T_m	Time delay in measurement.
T_s	Sampling time interval.	t	Current time instant.
t_c	Equivalent chip thickness.	t_f	Time of flight elapsed.
u	Parametric variable, $u \in [0,1]$.	u,v	Input vectors.
v	Total ploughed volume	v_d	Dynamic ploughed volume
V	Cutting velocity, *m/min*.	v_s	Static ploughed volume.
w_k, v_k	Vectors of noise sequences.	x_a, y_a, z_a	Cartesian coordinates of point A.
x, z	State vectors.		
x,y	Suffices indicating radial and longitudinal directions, respectively.		
$Y_r(x)$	*rth* mode shape.	$Y_{xi}(l)$	*ith* mode shape in radial direction.
y	Output Vector.	ym	Measured output.
y_{tx}, y_{ty}, y_{tz}	Tool displacements.	y_{wx}, y_{wz}	Workpiece displacements.
α_v	Velocity rake angle.	α_n	Normal rake angle.
α_e	Effective rake angle.	Γ	Input matrix of augmented model.

γ	Clearance angle.	Δd	Depth of cut offset.
Δd_c	Commanded depth of cut offset.	δ	Sensor delay in *mm*.
δ	Structural displacement vector.	δV	Change in cutting velocity.
δd	Change in depth of cut.	δf	Change in tool feed.
ϵ	Smallest residual.	$\zeta_{w,x,f,d,}$	Damping ratios.
η	Non-linear transformation matrix.	η	Chip flow angle.
η_x	Workpiece displacement in normal coordinates.		
Θ	Wokpiece torsional vibrations.	θ_i	Inclination angle of the *ith* sensor.
μ	Overlap factor.	μ_p	Proportionality constant.
ξ	Speed of Sound.	Φ	System matrix of augmented model.
$\omega_{w,f,d}$	Natural frequencies [rad/sec].		

CHAPTER 1

INTRODUCTION

Today's innovations in manufacturing technology are driven by demands to maintain a consistent high level of product quality in an unattended manufacturing environment. Consequently, the pursuit of better accuracy, reliability and performance of machined parts is becoming increasingly more important. Dimensional and geometrical accuracies are usually specified in the design stage as tolerances to allow for possible machining errors. Under the requirements of improved accuracy, tighter tolerances and more stringent requirements are being imposed on the machining process. Thus, to be competitive in today's marketplace manufacturers must be able to control the performance of the machining process in order to diminish the effects of machining errors on product quality.

Machining errors are different in nature and can result from several sources. There are three main categories of error sources: a) mechanical hardware deficiencies, such as, backlash, non-straightness of guide ways, ... etc., b) cutting process disturbances, such as, deflections, vibrations, tool wear, ... etc., and c) controller and drive dynamics. The total

machining error is a combination of all errors from the above sources. However, some error sources are of minor importance and can be neglected, and some of them may never be good for automatic compensation.

The turning process is specifically used for machining cylindrical components. This thesis is concerned with the accuracy of the turning process particularly in machining slender shafts. The accuracy of a cylindrical component is defined by its dimensional accuracy, geometrical accuracy and surface finish. Dimensional accuracy refers to the size error of the effective diameter of the machined part from the specified diameter on the part drawing. It determines the clearance or tightness in the assembly of a hole and a shaft. Geometrical tolerances such as roundness, concentricity, straightness and cylindricity become proportionally more critical as tolerances become tighter. Roundness or more specifically out-of-roundness, refers to the deviation of the cross-section of a cylindrical workpiece from a true circle as shown in Fig. 1.1a. Analogously, waviness refers to the deviation of the cylinder generator from a true straight line as shown in Fig. 1.1b. However, more global definitions can be given to the form of a cylindrical workpiece such as cylindricity and runout. Depending on the type of application, these form errors may result in various kinds of problems, such as leakage, stress concentration, noise, vibration and so forth. On the other hand, finish is a microscopic description of the part surface. The machined part usually has many random and high frequency undulations on the surface in addition to waviness and out-of-roundness as shown in Fig. 1.1c. The qualitative interpretation of these small undulations through human sensors (vision and touch) is finish. Its effects on the performance of the product are also of microscopic nature, such as friction, wear, erosion and reflectability.

It can be recognized that the classification of geometrical error components presented above is based on their wavelengths. In another words, referring to the terminology of the type used in Fourier analysis, the distinct components of geometrical error are: a) long-wave component representing overall workpiece dimensions and waviness, b) medium-wave component representing out-of-roundness and lobbing, and c) short-wave component representing surface roughness.

Generally speaking, the accuracy of the machining process is controlled by the relative distance between the cutting tool and the surface to be machined. In conventional Computer Numerically Controlled (CNC) machine tools, feedback control loops are used to precisely position the cutting tool with respect to the workpiece as commanded by preprogrammed (G-Code) values. Figure 1.2 shows a schematic diagram representing the structure of a conventional CNC lathe. The feedback is established through velocity and position measurements taken at the driving units (motors). However, process disturbances such as structural deflections, thermal deformations and tool wear occur at the cutting point. These disturbances cause machining errors and deteriorate the accuracy of the machined surface. Due to the lack of a feedback mechanism from the cutting point, the machine tool controller is unaware of the occurrence of such inaccuracies, and thus, no control action is taken for error compensation.

Based on knowledge of the machined surface deviation from its nominal value, error compensation is possible by making suitable corrections to the tool path. These corrections are typically performed in the direction normal to the machined surface by manipulating the controlled inputs of the process. Error compensation methods are based on modeling the error and then predicting the control actions for compensation. The error models can be

either generated from measured variables or developed mechanistically. There are two methods of error compensation:

a) Pre-calibrated error compensation: This is based on off-line measurement. However, it is applicable to systematic and repeatable errors only. Production time is also wasted in measurement for calibration.

b) Active error compensation: This is based on in-process measurement (i.e. while the workpiece is being machined). Therefore, it emerges as the more promising method for reducing the unpredictable errors. The unpredictable properties of the system can be resolved by devising a model for the control system that is updated according to on-line measurement. This has been termed in the literature as Geometric Adaptive Control (GAC).

The philosophy of GAC is to add a feedback mechanism based on measurement of the machined surface geometry. The GAC system has an inherent time lag due to a delay in the measurement. The schematic diagram shown in Fig. 1.3 presents this concept. The measurement of surface error is taken at point '*b*', while the compensatory control action is taken by the tool at cutting point '*a*'. The difference between points '*a*' and '*b*' represents time lag in the feedback control loop. In order to minimize this time lag, the measurement must be performed on-line, with high speed and as close as possible to the cutting point. Therefore, the sensor must be non-contact and insensitive to temperature fluctuation. Also, its performance must not be influenced by the presence of coolant, chip particles and so forth. Therefore, a certain amount of signal conditioning is always necessary for increasing the reliability and robustness of the whole system.

In terms of hardware, the compensatory control action at the tool tip can be performed either through the machine tool position control system, or by using a completely external

actuating device. While the first approach involves minimal external hardware, it involves changing the pre-programmed G-Code values in real-time which can not be accommodated by conventional machine tool controllers. With the second approach the machine tool controller performs the gross motion of the tool while the fine motion corrections are performed by the external actuating device. While previous researchers were forced to follow the second approach, in the current work the first approach is investigated. This is made possible by implementing the developed GAC system on a CNC turret lathe which is retrofitted with an Open Architecture Controller (OAC).

This thesis describes the development and implementation of a GAC system for workpiece accuracy in bar turning. The system is based on mechanistic modeling of the bar turning process and on-line measurement of the workpiece diameter while using a cutting fluid. The state of the current research in the area is reviewed in Chapter 2; the problems encountered are discussed and the objectives of the current work are listed. The development and verification of a dynamic model of the machining process in bar turning is introduced in Chapter 3. The development of an ultrasonic-based on-line measurement system for monitoring the workpiece diameter in bar turning is presented in Chapter 4. The evaluation of workpiece geometrical tolerances using on-line measurement data is investigated in Chapter 5. In Chapter 6 the integration of the developed model and measurement subsystem into a GAC system is presented. A model-based predictive controller is designed to close the feedback control loop. The chapter also demonstrates the implementation of the GAC system to minimize the form error of the workpiece in bar turning and offers an evaluation of the system performance during real cutting test. Finally, in Chapter 7 the conclusions of the study and recommendations for future research are presented.

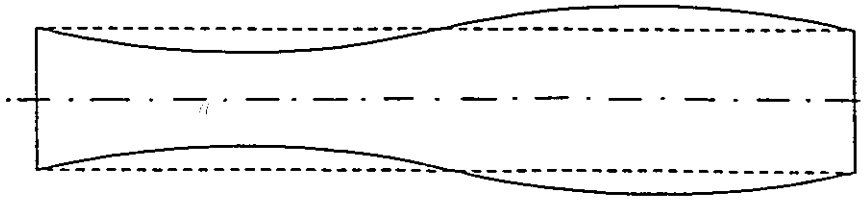

(a)

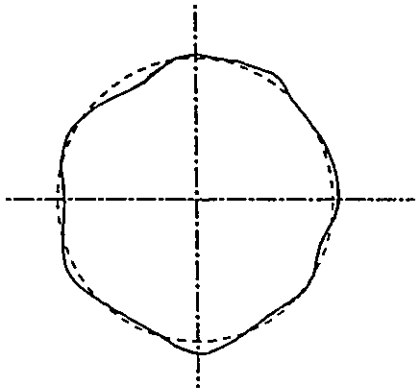

(b)

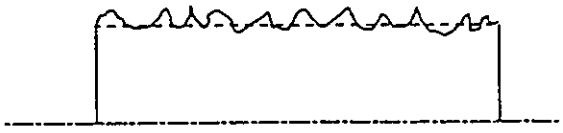

(c)

Fig. 1.1 Classification of Geometrical Errors According to their Wavelengths.
(a) Waviness (long wavelength error).
(b) Out-of-Roundness (medium wavelength).
(c) Surface Roughness (short wavelength).

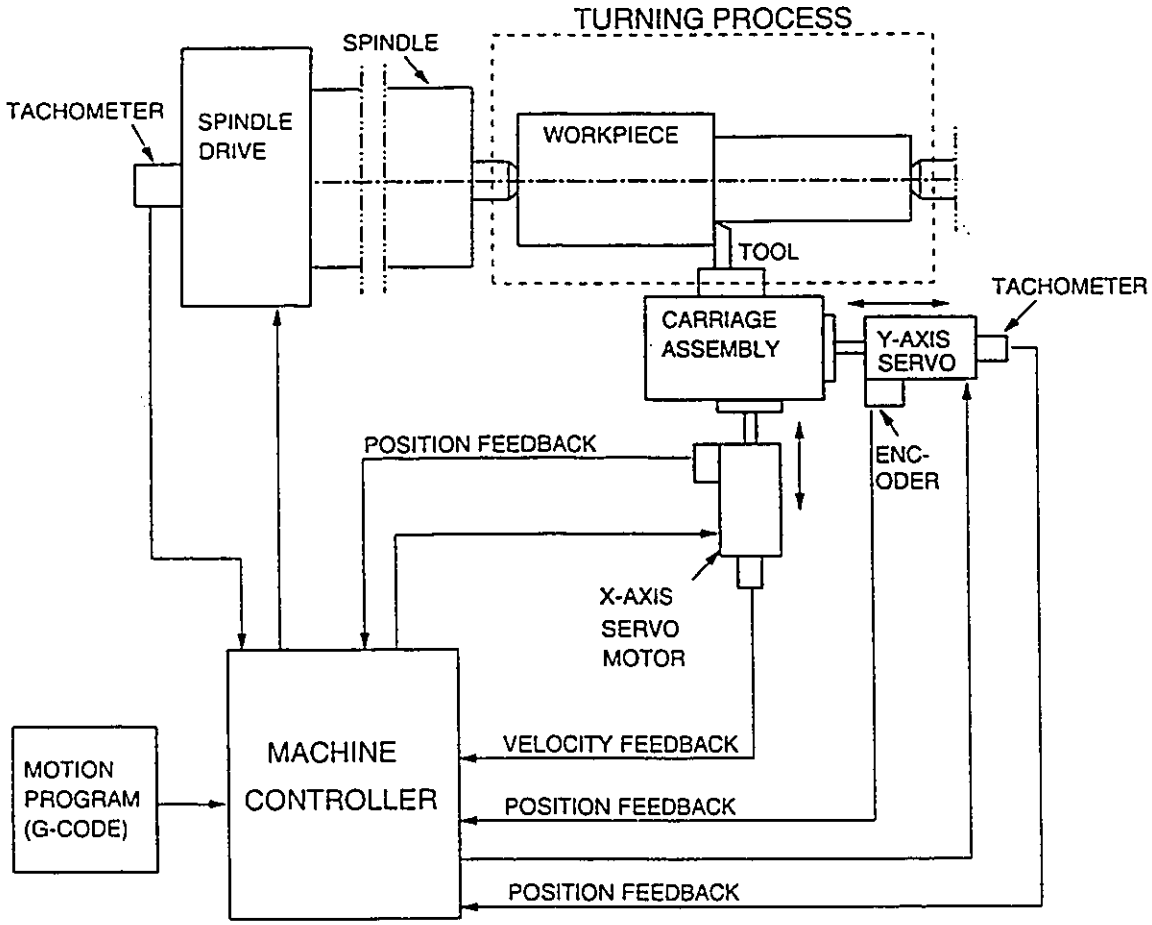

Fig. 1.2 A Schematic Diagram of the Structure of a CNC Lathe.

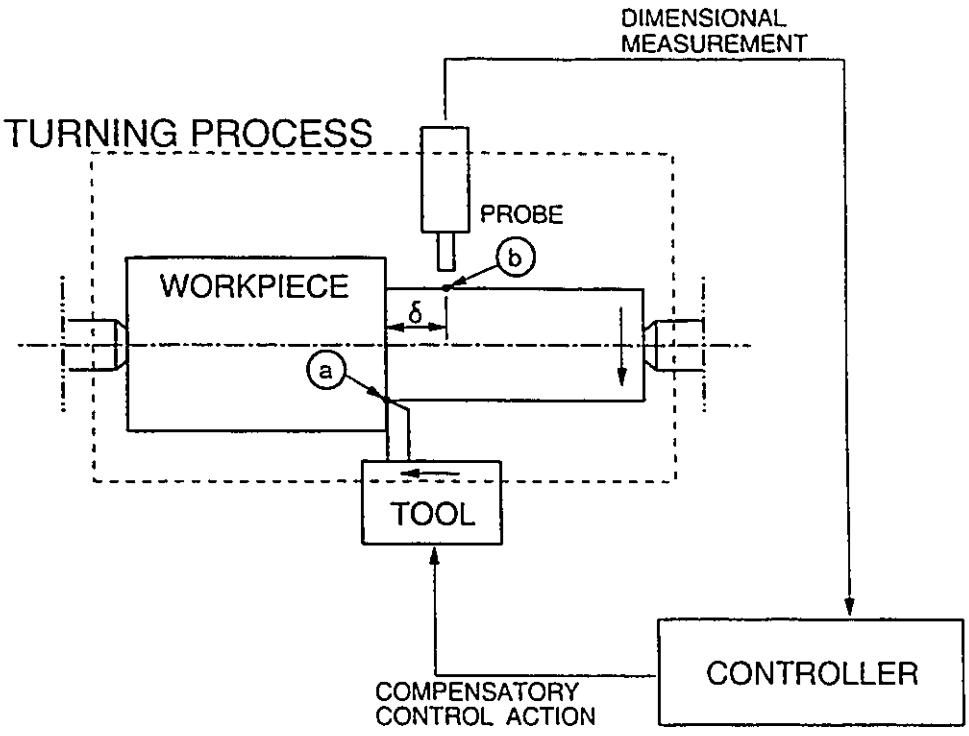

Fig. 1.3 A Schematic Diagram Showing the Concept of a GAC System Applied to Bar Turning.

CHAPTER 2

LITERATURE REVIEW

The literature related to the prediction, on-line measurement, and geometric control of workpiece accuracy in machining is discussed in this chapter. The reviewed literature is somewhat broad in context, but focuses primarily on the three main topics necessary for establishing a GAC system. These topics are: a) modeling of the machining process, b) assessment of workpiece accuracy, and c) geometric control strategies.

2.1 MODELING OF THE MACHINING PROCESS

The performance of the machining process is assessed by dimensional and geometrical accuracy of the part produced in addition to its surface texture. As mentioned in the first chapter, machining errors are due to several sources and result in degrading the quality of the machined part. The prediction of such errors requires the knowledge of some process states such as chip load geometry, cutting forces, and tool/workpiece vibrations. This information can be acquired using a reliable dynamic model of the process. The literature contains much research work on the development of cutting process models for the

prediction of cutting forces. Numerous approaches have been presented and various techniques have been used. In this discussion the topics related to modeling of the machining process are broken down into four areas: cutting mechanics, machining dynamics, ploughing forces and process damping, and recent mechanistic models.

2.1.1 CUTTING MECHANICS

The cutting operation is normally modeled as orthogonal cutting or oblique cutting. The main difference lies in the direction of the tool motion with respect to the cutting edge as shown in Fig. 2.1. In orthogonal cutting, the tool motion is normal to the cutting edge causing the chip to flow right up the tool face normal to the cutting edge. Also, as the width of cut is normally much larger than the undeformed chip thickness, the deformation process is approximated by plane strain conditions (which implies a two dimensional deformation process). Consequently, only two force components act on the tool; F_T acts in the tangential (velocity) direction and F_R acts in the thrust direction. On the other hand, in oblique cutting the cutting edge is not normal to the tool direction of motion and the chip flows at an angle η relative to the cutting edge. Therefore, the deformation process is three dimensional and plane strain conditions cannot be assumed. Also, a third force component F_L acts on the tool in the lateral direction.

The early work by Merchant (1944, 1945a, 1945b) has been a cornerstone for other researchers to follow in the field of modeling the metal cutting process. He analyzed the mechanics of orthogonal cutting and considered the chip as an independent body held in mechanical equilibrium by the action of two equal and opposite forces as shown in Fig. 2.2. Merchant assumed a constant material shear stress equal to that of a perfect plastic material.

He also extended his kinematic model to oblique machining, but he did not account for the effect of strain, strain rate or temperature in the work material properties.

Much research followed and focused more on modeling the complex mechanics of chip formation in oblique cutting. Three different rake angles have been defined for oblique machining: normal rake α_n, velocity rake α_v, and effective rake α_e. The definitions of those angles are given in Appendix A. Some of the models in the literature described the chip formation process in a plane normal to the cutting edge. These models are based on the assumption that the normal rake angle is the most influential rake angle on oblique machining. Such models include those from Merchant (1944, 1945), Rubenstein (1983), Lau and Rubenstein (1983), Armarego (1977), Armarego and Uthaichaya (1977), and Alverio (1984). The other school of thought consists of those researchers who believed that the chip formation in oblique machining can be described in the plane of chip flow, which implies that the effective rake angle is the most relevant rake angle in oblique machining. Research work based on these principles include the models from Shaw, et al. (1952), Luk (1969), Armarego (1970), Usui, et al. (1978a, 1978b), and Nakayama and Arai (1976, 1983).

Several researchers investigated the rake angle that influences the mechanics of deformation in oblique cutting the most. Brown and Armarego (1964) showed experimentally that the tangential cutting force (i.e., the power force) is almost constant as long as the normal rake angle α_n is kept unchanged. Pal and Koenigsberger (1968) also found from their tests that the tangential cutting force is mainly controlled by the normal rake angle, and thus concluded that it is the most significant rake angle in oblique cutting. In addition, the rake angle used by Merchant (1944) in his analysis was the normal rake angle. Therefore, it is reasonable to assume that a model using the normal rake as the most

influential rake angle would be more representative of the oblique cutting process. In the following paragraphs a critical review of those models which describe the oblique cutting process in the normal plane is presented.

Armarego and Uthaichaya (1977) developed a model for oblique cutting based on using a single edged cutting tool. The model does not account for the effect of speed nor rake angle. It also assumes that the feed rate does not affect both the normal shear angle and the apparent coefficient of friction; this has been shown not to be the case (Bisacre and Bisacre, 1948, Chao and Bisacre, 1951, and Chao, etal., 1952).

A general normal plane was defined by Armarego (1977) to allow the modeling of all cutting tools including form tools. This plane is normal to a line adjoining the two extreme points of the engaged cutting edge. Such approach simplifies the multi-edged cutting tool geometry and reduces it to a single edged tool with an equivalent normal shear angle. However, it is not useful for describing the three-dimensional deformation process involved. Also, the inability of the model to account for the variation in the undeformed chip thickness along the cutting edge represents a great limitation to this approach.

Rubenstein (1983) considered a different approach for describing oblique cutting based on a theory he developed with several assumptions. He suggested that the component of the chip velocity in the normal plane is not influenced by the inclination angle i. He then developed relations based on this theory for chip thickness ratio, chip length ratio and normal shear angle in terms of their counterpart in orthogonal cutting. However, he did not attempt to provide a physical explanation either to his theory or to his assumptions. The assumptions were only justified on the basis that the boundary conditions at $i=0°$ and $i=90°$ are satisfied.

Alverio (1984) developed a model for predicting oblique machining forces from the shear angle, apparent friction coefficient and specific cutting energy obtained from orthogonal machining data. The main assumption involved is that the deformation process is independent of the inclination angle when observed in a plane normal to the cutting edge. This assumption limits the validity of the model for only single edged cutting tools (i.e., tools with a single normal plane).

More models were developed for oblique cutting using the Slip-Line Field (Plasticity) Theory. Lin and Oxley (1972) developed a model based on assuming plane strain conditions in the normal plane. Such questionable assumption would have been more reasonable for the chip flow plane. This model was modified by Lin (1978) and Lin, et al. (1982) to eliminate the need for measuring the apparent friction coefficient during machining tests. One of the limitations of this model is that it requires the chip/tool contact length to calculate the shear stress at that interface. The prediction of such contact length has always been a complex problem. Lin, et al. (1982) assumed a simple relationship to hold between the chip contact length and the feed. However, in the early work by Chao and Bisacre (1951), it was shown that the contact length is also a function of cutting velocity and tool geometry. The predictions of the modified model showed more deviations from the experimental values than those from Lin and Oxley's original model. Also, Lee and Shaeffer's (1951) Slip-Line Field solution for orthogonal cutting was generalized by Morcos (1972a, 1972b, 1980) for oblique cutting which he then used in a comparative study with Merchant's model. The results obtained for the normal shear angle deviated considerably from those obtained experimentally and Merchant's model showed better agreement.

A very important factor and a necessary parameter for all oblique cutting models is the chip flow angle η. That is why the chip flow angle has been the subject of many investigations. Based on experimental work, Stabler (1951) proposed a simple relation known by Stabler's Chip Flow Rule. Other models have been proposed by Colwell (1954), Merchant (1944), Shaw, et al. (1952), Russell and Brown (1966), Luk (1969b, 1972), and Usui, et al. (1978a). The most accepted approximation other than Stabler's Rule is Colwell's approximation which is purely heuristic in nature. Also, Usui, et al. (1978a) developed a very complicated model based on a reasonable assumption that the chip flows in a direction that minimizes the total energy used in cutting. The experimental results showed good agreement with theory and revealed that Stabler's Rule is approached as the depth of cut is increased.

2.1.2 MACHINING DYNAMICS

Machining vibrations have always been considered as a serious limiting factor to both product quality and productivity and it becomes hazardous to both the operator and the machine at the onset of chatter (i.e., instability). Vibratory motions of both the tool and workpiece include both transient vibrations induced by shock load and vibrations induced by periodic excitations. In contrast with these forced, damped vibratory motions, chatter is a "self-excited" oscillation. Chatter occurs at certain conditions which excites the system while the energy dissipation (by either the damping of the structure or the friction of the cutting process) is not enough causing the vibratory motion at one of the system's natural frequencies to grow beyond acceptable limits.

Over the years, a large amount of research has been performed in the area of modeling machining dynamics for the goal of analyzing and predicting machine tool chatter. These models are based on combining the effect of tool/workpiece vibrations on varying the instantaneous undeformed chip thickness with dynamic models of the machine tool structure. In the majority of this work transfer function models and the simple case of orthogonal cutting were considered. The block diagram shown in Fig. 2.3 shows the transfer functions upon which early models of the machining dynamic systems were based. This model is due to Merritt (1965); it consists of a cutting process, a flexible machine tool, and a feedback loop. The cutting process generates a cutting force which acts on the machine tool structure and causes it to deflect. This deflection results in a change of the tool position and the cutting conditions and thus a change in the force. Also, the additional feedback loop accounts for the regenerative effect defined by Hahn (1953).

Doi and Kato (1956), and Smith and Tobias (1961) observed the existence of a phase difference between the position of a harmonically oscillating cutting tool and the magnitude of the resulting oscillating cutting forces. More studies were carried out to explain the mechanism responsible for the phase shift between forces and displacements of the tool (Field and Merchant, 1949, Kegg, 1965, and Cook, 1966). Hanna and Tobias (1969) studied the non-linear behavior in the structural dynamic response and its dependence on the exciting force amplitude. They introduced non-linearities into the stiffness and cutting force functions. Tlusty and Ismail (1981) introduced the basic non-linearity in machining chatter and revealed its effect on the predicted stability boundary. They used in their simulation an average value of the undeformed chip thickness rather than an instantaneous value. More investigations by Tobias and Fishwick (1958) and Albrecht (1965) revealed the effect of the

tangential vibration derivative on the cutting speed. Tlusty and Polacek (1963) proposed the regeneration and the mode coupling as the principal chatter mechanisms and applied their theory to study the stability of a multi-degree of freedom machining system.

Other researchers in the field of modeling machining dynamics concentrated on the development of a standardized model structure based on experimentally determining a set of Dynamic Cutting Force Coefficients (DCFCs). For example, significant contributions in this area are due to Nigm, et al. (1972), Peters, et al. (1972), Tlusty (1978), and Tlusty and Heczko (1980). The main drawback of this approach lies in the large number of cutting experiments required to determine the DCFC components for different workpiece materials and cutting conditions.

Further research was directed towards the development of more quantitative analysis techniques and methods for the prediction of stability limits against chatter. Several methods were developed to predict the critical width of cut. Some methods are graphical such as those developed by Gurney and Tobias (1962), and Merrit (1965), while other methods are analytical such as those developed by Andrew (1964) and Tlusty (1965). Also, Nigm (1981) developed a rather strong analysis method that could be implemented either graphically or analytically and accounted for the full range of regeneration. Lemon and Ackerman (1965), applied the developed theory experimentally to actual machine tools. Tlusty (1978) summarized the work in the area of cutting process dynamics and machine tool chatter and tied many of these results together.

Other work related to the application of the developed chatter prediction theory focused on identification of the actual machine tool's dynamic response using well-established methods employed in structural dynamics. Tobias (1965) and Koenigsberger,

and Tlusty (1971) used sinusoidal forced vibration tests using special electromagnetic exciters. Sadek and Knight (1975) demonstrated the influence of different factors on these tests, such as weight and support of the workpiece, position of the exciting force, etc. Kim, et al. (1984) performed tests using an electromagnetic exciter to generate a random input force, and then applied an Auto Regressive Moving Average (ARMA) modeling technique to the measurements. Brown (1976) demonstrated the simplicity and the validity of impact tests. Taylor (1977) assessed the advantages and disadvantages of various identification techniques. Note that all of the above mentioned techniques can only be applied when the machine tool is inactive. Other researchers such as Kwiatkowski and Al-Samarai (1968) and Moriwaki and Iwata (1976) argued that there is a difference between modal parameters identified during cutting and those from conventional frequency response tests. However, it is not clear how these researchers addressed the intrinsic coupling between the machine tool structure and the cutting process during cutting. Recent work by Minis, et al. (1990) showed that the difference between the modal parameters measured during interrupted cutting and those extracted using impact tests lies only in the damping factor which increases during cutting by 20 to 40 percent.

2.1.3 PLOUGHING FORCES AND PROCESS DAMPING

The significance of the ploughing force has been recognized by many researchers since the early work of Albrecht (1960). These forces arise from the rubbing of the cutting edge against the workpiece and the chip. The complex nature of the interference at the clearance face has promoted most researchers to determine its parameters experimentally. The most illusive of these parameters has been the damping generated, which is termed

process damping. The amount of damping (positive or negative) arising in the chip formation process at the various cutting conditions was formulated by Das and Tobias (1967) using the Dynamic Cutting Force Coefficient (DCFC). Methods used for measurement of DCFC's were reported for example by Tlusty et al. (1976). Tlusty also presented clear evidence of the strong effect of tool wear on the measured DCFC's.

The most common method used for calculating the rubbing forces from dynamometer measurements consists of extrapolating the thrust and cutting forces to zero feed. This value is said to be the rubbing or parasitic component since it does not contribute to chip flow. This method assumes that ploughing forces are independent of feed; this had been proven by Spanns (1967a, 1967b, 1970) not to be the case. Another method was developed by Spanns for calculating the ploughing forces for oblique machining from measured forces, chip thickness and chip flow angle. The main limitation of this method is that it is only applicable to free-end cuts (i.e., single edge cutting).

More recent research work brought more insight into the ploughing action. Merwin and Johnson (1963) recognized ploughing as a loading and unloading cycling process. They also showed that, although the majority of the ploughed material is elastically deformed, plastic flow always takes place at the vicinity of contact surface. This deformation creates contact pressures normal and tangent to the tool surfaces and causes non-uniform distribution of the stress field under the tool. Recently, Wu (1988) based his ploughing model on Shaw and DeSalvo's (1970) assumption that a ploughing force (in equilibrium with the stress field) is proportional to the total volume of the work material displaced by the tool. This same concept was further pursued by Wu (1989) to obtain an enhanced model for the limit of stability in continuous cutting. Wu's model dealt with an orthogonal cutting system with a

single degree of freedom assuming a sinusoidal tool trajectory. Wu also introduced in his model the specific ploughing force as the proportionality constant between the normal ploughing force and the extruded material volume. Elbestawi, et al. (1991) used Wu's model to enhance the prediction of cutting dynamics in milling and extended the theory for worn tools. Both, their computer simulations and experimental results agreed on demonstrating the effect of the ploughing action on process dynamics as a source of process damping.

2.1.4 RECENT MECHANISTIC MODELS

The majority of the models discussed so far requires the knowledge of "difficult-to-obtain-parameters" such as chip/rake face friction angle and contact length, as well as material shear strength and strain hardening coefficient at very large strain rates and high temperatures. Also, most of these models do not account for one or more of the following factors:

- effect of feed on both normal shear angle and apparent coefficient of friction,
- effect of speed , rake angle and or approach angle,
- effect of feed on the clearance face contact and hence on ploughing forces, and
- effect of the complex geometry of a multi-edged cutting tool on varying both undeformed chip thickness and normal rake angle along the tool edge profile.

In addition, the methods used in modeling machining dynamics such as transfer function modeling and the DCFC approach require a large number of experiments to be performed for each workpiece and machining system structure. Recently, a number of researchers have pursued the development of the so called mechanistic machining models. The transfer functions used in the block diagram of early developed models (refer to Fig. 2.3)

have been replaced in the mechanistic modeling approach by the complex geometrical relations and mechanics of material relations as shown in Fig. 2.4 (Endres, 1990). The mechanistic machining models have the "difficult-to-obtain-parameters" replaced with semi-empirical (and variable) specific material cutting resistance. This greatly reduces the experimental amount of work required for model calibration over a wide range of process inputs (such as, cutting conditions, tool geometry, and tool/workpiece material combination). Moreover, such models are inherently developed as computer simulations and can easily accommodate the more complex geometry involved in oblique multi-edged tool dynamics.

All of the work published in the area of mechanistic modeling of machining systems has been contributed by research done at University of Illinois, Urbana-Champaign. Different static and dynamic mechanistic models were developed for end milling (by DeVor, et al., 1980, and Babin, et al., 1985, and Sutherland, 1988a), face milling (by Fu, et al., 1984a and 1984b, and Subramani, et al., 1987a), cylinder boring (by Zhang and Kapoor, 1985, and Subramani, et al., 1987b), and turning (by Kuhl, 1987, Gustafson, 1990, and Endres, et al., 1990). For the turning process, two out of the three models developed are static while the third is dynamic. These three models are discussed in the following paragraphs.

Kuhl (1987) developed a static mechanistic model for turning based on viewing the three dimensional oblique cutting process in terms of an equivalent two dimensional cutting force system in the normal plane. The milling relationships for Sabberwal's power and friction forces (1960) have been used in this normal plane strategy. Kuhl also used the approach suggested by Subramani, et al. (1987b) in calculating the effective lead angle, which indicates that the pressure distributed around the tool nose radius is actually proportional to the chip thickness. In fact, the effective lead angle was first suggested by Fu,

et al. (1984a) and Zhang and Kapoor (1985) as a compensation for the effect of the tool nose radius and a uniform pressure distribution was assumed. Sutherland, et al. (1988b) modified the friction force calculation to be related directly to the projected chip area instead of being proportional to the normal force. Modeling the friction force in this manner reduces the error in the friction force prediction, because it no longer includes noise transmitted from the normal force prediction. Gustafson (1990) further developed a static model for both sharp and worn tools. He modified Kuhl's modeling strategy by both introducing the unweighed effective rake angle parameter and simplifying the chip flow angle calculation using Stabler's Rule. Compared to Kuhl's model, Gustafson's predictions of the cutting forces for sharp tools showed better accuracy. However, the longitudinal force was consistently over-predicted at higher depths of cut and under-predicted at lower depths. On the other hand, the radial force errors changed inconsistently. These errors are attributed to a combination of prediction errors of both specific cutting friction K_N and effective lead angle la_e.

Endres, et al. (1990) developed a dynamic model for the cutting forces by extending Kuhl's static model to account for the effect of tool and workpiece dynamics on changing the cutting conditions and tool geometry continuously during the cut. They based the effective lead angle model on a uniformly distributed friction force. The approach used to determine the chip load is similar to Kuhl's in dividing the chip area into elements which are presumed for a specific tool edge profile. The chip load is evaluated using elemental area integrals with integration limits which are functions of the cutting geometry. The solution to these integrals as well as the integration limits used are complicated and quite lengthy. This model was used in the prediction of cutting forces. The tail-stock was modeled as a rigid support ignoring its flexibility which resulted in over estimation of the steady state force levels.

Also, intermittent cutting results showed over prediction of the force overshoots indicating lack of process damping in the model. This implies the need to include the tool/workpiece interference mechanism which takes place at the flank face of the tool.

2.2 ASSESSMENT OF WORKPIECE ACCURACY

Due to quality control requirements, workpiece accuracy is assessed by comparing dimensional measurements to design specifications. Design specifications are usually represented by both dimensional and geometrical tolerances. In bar turning applications diameters are often measured in workshop conditions. Measurements are performed both as post-process inspection and while the workpiece is still on the machine. Measurement is generally costly and in some cases the costs of part inspection by conventional methods equal or exceed machining costs. According to Novak (1981), "quality costs" are usually estimated to be at least 10-15 percent of the product cost; 60-70 percent of which depend on the control of the machining process accuracy. The trend is to bring quality control close to the machining process by means of on-line dimensional sensing. The full (or partial) replacement of off-line measurement and statistical quality control with complete on-line part inspection would greatly reduce "quality costs" and improve process control. The ultimate goal is the ability to measure and compensate on-line for part errors (either every pass or in real time) using GAC without a need for post process inspection afterwards. A prerequisite for the realization of this GAC strategy is a dimensional on-line measurement system. Such system is required to permit the measurement of workpiece critical dimensions and the evaluation of its dimensional and geometrical tolerances while cutting. The material

discussed in this section is divided into two subsections: a) Machining errors and on-line measurement, and b) coordinate and computational metrology.

2.2.1 MACHINING ERRORS AND ON-LINE MEASUREMENT

The roundness and straightness errors in the production of cylindrical features depend on the compliance of the head stock, the tail-stock, the carriage and the workpiece. In the case of turning, the variation in workpiece stiffness due to the chucking jaw arrangement can cause roundness errors depending on the chucking force and chucking length (Bajpai, 1972, Rahman and Ito, 1979). This variation in stiffness has directional orientation which depends on the position of the jaw with respect to the radial component of the cutting force. Also, the variation in stiffness along the workpiece length (i.e., longitudinal axis) can cause straightness and cylindricity errors. Therefore, in cylindrical parts, form errors are present in both longitudinal and radial (lobbing) directions.

In a survey by Wilson (1992) it was shown that for most manufacturing processes, the dominant lobbing is of low order (two to seven) and the lobe amplitude reduces dramatically with the number of undulations per revolution. Lobbing with two and three lobes is commonly seen due to spindle runout and chucking forces, respectively (Rahman and Ito, 1979). Longitudinal form errors are also of relatively low order and depend greatly on the length-to-diameter ratio of the workpiece. They can be classified as barrel, hourglass, banana, undulated, and bell mouth, as shown in Fig. 2.5 (Wilson 1992). In case of turning, thermal expansion of the tool generates a bell-mouth shape (e.g., Asao, et al., 1992), while structural deflection of the workpiece generates a form error depending on the method of fixation; for example, a centered workpiece is normally expected to generate a barrel shape.

The roundness and straightness errors can also be characterized by examining certain parameters such as the radial cutting forces, the depth of cut, the cutting tool approach angle, and the overhang length of the part. The radial cutting force has a significant effect on the geometrical errors of turned workpieces; higher radial cutting forces result in larger geometrical errors. In general, both straightness and roundness errors increase as the distance measured from the chuck along the workpiece length is increased.

Surface and form errors of a machined part can be classified by spectral analysis into three main components: a) surface roughness (high-frequency component); b) waviness (medium-frequency component); and c) form error (low-frequency component). Surface and form errors developed in turning have detailed relationships to process parameters, and thus, their amplitudes could be predicted by mechanistic models.

In another classification the errors encountered in any machining process can be divided into two main classes. The first includes machine tool errors such as misalignment of guide-ways and spindle runout. These errors are determined from machine tool metrology. The second class includes errors inherent in the cutting process such as thermal expansions, vibrations and structural deflections. These errors can be referred to as "process errors" and they are usually determined off-line by workpiece metrology.

In-process metrology involves the measurement of workpiece geometry and machine tool errors, both superimposed on each other. This superposition of errors does not represent a problem for the "direct measurement" of workpiece diameter. However, it is not always easy to perform direct diameter measurement, and generally large scale equipment are required for direct measurement; see for example Novak (1981), Badiv, et al. (1980), and Bath and Sharp (1972). On the other hand using "indirect measurement" by evaluating the

diameter of the workpiece from the "radius change" proved to be simpler in construction and more feasible; see for example Haibao, et al. (1990), Shiraishi and Sato (1990), Kohno, et al. (1989), Kim, et al. (1987), Shiraishi (1979), and Shiraishi and Uehara (1979). However, the major drawback of the radius method is that the measurement depends on the basic accuracy of the machine tool. In addition, any deflections of the workpiece are misinterpreted as radius changes. In order to compensate for these effects, Shiraishi (1984) designed a system based on actuating the sensor itself using several stepping motors to continuously track the workpiece axis. However, such approach seems impractical due to its complexity and high cost. In another domain, it was shown by Kakino and Kitazawa (1978), and Whitehouse (1976), that the radius method can be improved by using a multi-probe technique (three point method) to separate workpiece surface profile from significant machine tool errors. This method is based on modeling the cylindrical form using Fourier series and orthogonal polynomials expansion with respect to a datum line determined by the method of least squares. Therefore, it is based on a relative evaluation scheme and hence, it is applicable to the evaluation of form tolerances but is not valid for absolute size measurement.

Moreover, the literature shows that practically machine tool errors and process errors range on the average between 0.1-3.0 μm and 10-70 μm (e.g., Moriwaki, et al., 1990), respectively. Thus, there is at least an order of magnitude difference between both classes, and separating both errors from in-process measurements would be of more interest to machine tool metrology.

On-line dimensional sensing requires non-contact measuring methods with high speed and robustness. In the literature, several types of instruments have been developed

for on-line measurements, the most promising of which are those based on both pneumatic and optical sensors. Pneumatic sensors (e.g., Tillen, 1964, Bath and Sharp, 1972) provide a relatively simple measurement at lower cost. Their primary advantage lies in the continuous flow of air through the gauge head which can be arranged to blow away cutting fluid and chips. However, the measurement range of pneumatic sensors is typically small. It is usually limited by the nonlinear behavior expressed by the back pressure over wider ranges of the measured air gap. Also, pneumatic sensors seem to have very high dimensional sensitivity, which together with their limited range make them more suitable for non-contact surface roughness measurement. On the other hand, optical sensors exhibit better performance, compared to other methods, with regard to both resolution and measuring range. A number of optical sensors were developed based on different optical techniques including light projection, light-spot detection and light sectioning. (A comprehensive survey of these methods can be found in Shiraishi, 1989.) However, the majority of these developments were successful only in laboratory setups and under dry cutting conditions. In fact, no work in the literature have been exclusively directed to solve the problem in the "wet" cutting environment (i.e., while using a cutting fluid). Shiraishi (1984) developed an optical sensor which he combined with an air blast system to blow away chips and cutting fluid. This system was used on a medium bench type lathe. The air blast system worked well for dry cutting, and seemed sufficient for eliminating sharp disturbances during wet cutting as well. However, it was concluded that the accuracy of the measurement is deteriorated during wet cutting due to the scatter of the light through the oil film on the machined surface.

The use of a reliable on-line measurement of the machined diameter can be extended to evaluate the form tolerances of the workpiece. For achieving this goal, it is important to realize the analogy between on-line measurement on a machine tool and off-line measurement on a Coordinate Measuring Machine (CMM). The data provided by on-line measurement is inherently discrete and can be viewed in the three dimensional (3D) space as the Cartesian coordinates of those points sampled on the machined surface of the workpiece. In this sense, the analogy depicted above is emphasized; both are Coordinate Measuring Systems (CMSs) to which "coordinate metrology" applies. Usually in the case of on-line measurement, the density of the sampled points can be greatly increased at no extra cost, unlike the situation with CMMs. Note that despite the fact that the accuracy provided by a CMM is superior to that of a machine tool-based-measuring system, the latter can still provide great improvement for on-line process control applications. It also permits the inspection of 100% of the parts produced at no extra cycle time. However, the evaluation of dimensional and geometrical tolerances based on coordinate metrology involves different sources of errors which have to be addressed. These issues are discussed in the following section.

2.2.2 COORDINATE AND COMPUTATIONAL METROLOGY

The term "Computational Metrology" refers to the study of the effects of data analysis computations on the performance of measurement systems (Hopp, 1993). It is well understood that the accuracy of any measuring system depends on the hardware, consisting of both the machine and the probe. However, in coordinate metrology, the data analysis strategy represents another major source of error. The coordinate data has to be analyzed by

algorithms to create a geometric model, usually called the "substitute geometry", which represents the perfect geometric form (line, plane, circle, cylinder, sphere, ... etc.) that best fits the set of points measured on the part surface. The fitting process is usually viewed as an optimization problem to find the parameters of substitute geometry that optimize a particular fitting objective for a given set of points. Different form tolerances are evaluated using different substitute geometries. The form tolerances are compared with the design specification for process control. Despite, the obvious benefits of using data analysis software, computations to convert raw data to final results (called "data reduction") can be a major source of error in measurement systems. The alert issued by Walker (1988) on using CMMs to inspect mechanical parts drew both industrial and academic attention to what has been called a crisis of CMMs. There were "methods divergence" problems in using CMMs to check the dimensional correctness of parts: different measurement techniques, using the same data analysis algorithms, resulted in different measurement results; different data analysis algorithms calculated different measurement results using the same technique. In the case of CMMs methods divergence due to software problems led to relative errors of up to 50% in accepting bad parts or rejecting good parts. Feng and Hopp (1991) attributed this situation to several factors occurring at the same time: conflicting interpretation of the ANSI Y14.5 National Standard on Dimensioning and Tolerancing (1982) by part designers and part inspectors; lack of standard measurement practice; and performance problem of CMM software, due to flaws embedded in the post-inspection data analysis algorithms.

Hopp identified three aspects of computational metrology that are particular to CMSs: the objective of the computation i.e. (fitting objectives), how these functions are carried out in software, and how software performance can be tested. Hocken, et al. (1993) presented

a comprehensive review covering the different sources of errors in measuring systems and data analysis, and discussed the form and magnitude of the normally encountered machine and part errors and emphasized the fact that measurement data contain systematic and pseudo-random errors that ultimately must affect the sampling strategy (i.e., number and distribution of points) in addition to the algorithm used to process the data. It was concluded that current inspection techniques, used daily in manufacturing, drastically under-sample geometric features in the presence of unknown part form and measuring machine errors.

Several possible sampling strategies have been addressed in the literature. These include uniform sampling, random sampling and stratified sampling. Uniform sampling has proven to be the most practical for most users Hocken, et al. (1993). Also, Odayappan (1992) showed using computer simulations that random and stratified sampling have a high degree of uncertainty and often failed to detect the correct form error. Odayappan's study resulted in recommendations regarding the acceptable sampling densities for circles in the presence of form error for different algorithms, however, no explanation was given for the randomness of the recommended figures. Computer simulations carried out by Babu, et al. (1993) for cylindrical workpieces using the least squares algorithm showed that the number of sampled points should be maximized in order to achieve stable results.

The choice of the fitting objective is a major factor in determining the fitting software performance. Part tolerances are generally interpreted in terms of "extremal fits". That is the fitting objective is to find the geometry that fits the extremes of the data: the largest inscribed, smallest circumscribed, or minimum separation geometry. On the other hand, measurement practice most commonly involves averaging fits, typically least-squares. The most frequently used fitting algorithms are based on the L_p-norm: (Gonin and Money, 1989)

$$L_p = \left[\frac{1}{N} \sum_{i=1}^{N} | \epsilon_i |^p \right]^{\frac{1}{p}} \quad (2.1)$$

where $0<p<\infty$, N is the total number of data points, and ϵ_i is the smallest residual (i.e., distance between the i^{th} data point and the considered feature). The best fit feature is the feature that minimizes the L_p-norm. When $p=1$, the fitting problem is least-sum-of-distances fitting, a generalization of finding the median of a data set. When $p=2$, it is total least squares fitting (called orthogonal distance regression). The limit of L_p as p goes to infinity is the largest magnitude residual, so that the L_p-norm problem is minimizing the maximum magnitude residual (i.e., finding the minimum zone fit).

Generally, the bias and sensitivity errors of the fit will vary with p. This relationship is shown in Fig. 2.6. Hopp (1993) showed that least square fitting commonly used in metrology is biased with respect to the extremal fit objectives suggested by tolerancing theory; on the other hand, extremal fits will propagate more of the point measurement error than least square fitting. The precise shape of the curves depends on the distribution of the residuals, the geometry of the particular fitting problem, the configuration of measured points, and the measurement uncertainty of the points.

It can be concluded from the above discussion that it is still very difficult to develop general guidelines for sample set sufficiency and appropriate data reduction. In fact, it is common knowledge in practice that information on how a part was manufactured will help an experienced inspector to do a better job. Despite the inconsistency of this fact with the process independence principle in tolerancing, it is customary that process knowledge be used based on spectral analysis in order to determine sampling sufficiency and data reduction adequacy. Knowledge of the process and its error dynamics can be provided by reliable

mechanistic process models or in the form of extended empirical data-rich environments based on non-contact sensing.

2.3 GEOMETRIC CONTROL STRATEGIES

The current state of the art for GAC systems is based on in-process measurement, on-line error modeling and real-time control. The application of GAC to manufacturing systems was first suggested by Peklenik (1970). Also, Jona (1971) presented a visualization of a GAC system applied to the finish turning process. The time lag inherent in a GAC system due to measurement delay was discussed by those early researchers. An essential characteristic of a GAC system is thus its predictive ability to ensure the generation of control commands in advance. This allows the system to overcome the problems associated with the response time of the controller and providing the proper relative position, of the tool and workpiece, at the moment actual metal removal takes place. Although, much research work has been directed towards the development of on-line dimensional measurement systems (as mentioned in the previous section), fewer publications have been dedicated to the development, implementation, and the machine tool controls involved in GAC systems.

Watanabe and Iwai (1983) developed a GAC system for milling based on indirect measurement of workpiece dimensional errors using strain gauges attached to the tool holder. The dimensional and waviness errors of the finished surface are corrected by controlling the tool path and changing the feed rate, respectively. Another end milling application was developed by Albrecht and McCabe, et al. (1985) using the light sectioning method to

monitor the edge of the machined surface and correct the tool path accordingly. More GAC systems were developed based on the Forecasting Compensatory Control (FCC) technique. FCC was proposed by Rao and Wu (1982). It was further expanded by Kim, et al. (1986), and used in developing a GAC system for cylindrical chuck grinding. Several GAC systems based on FCC were developed later for milling applications (e.g., Parl et al., 1988) and boring applications (e.g., Kim, et al., 1987). FCC is based on stochastic time series Auto-Regressive (AR) modeling of the workpiece form error. The AR-model parameters are updated using on-line measurement of machining errors which allows compensation for not only deterministic errors but also correlated stochastic errors. Nevertheless, the parameters of those time series models can hardly be related to the physical parameters of the process. Wu and Ni (1989) recognized the effects of cutting process and structural dynamics on the compensation accuracy of FCC and suggested using an additional feedback loop in the conventional FCC system. This feedback loop is based on force measurements and accounts for the input/output relationships of the process ignored by FCC. The results of their simulations using the modified control scheme showed an improvement of 34%.

For turning applications, not much work has been published on developing "real-time" GAC systems. The work by Wu and Haboush, et al. (1986) addressed the problem during batch production where the compensatory control action is taken between parts based on process intermittent gauging of the machined surface. Shiraishi (1984) developed a GAC system based on continuous monitoring of the workpiece diameter using an optical measurement system. A unity gain feedback GAC was used to control the radial position of the tool using the drive circuit of the NC unit. This made it customary to stop the machine for a short time (about 2 s) to compensate the error in an off-line fashion. In a theoretical

study by Lin (1985) the performance of GAC in plunge turning using both Self Tunning Control (STC) and FCC was compared. It was argued that FCC is less effective than STC in fully tracking the specified output and in stabilizing the system.

2.4 SUMMARY

This chapter presented a review of previous developments in the different areas related to modeling, on-line sensing and GAC in machining with particular emphasis on turning applications. The discussion furnished a general background and provided an insight into the current state of the art for this field of research. It also offered a critical assessment of the different theoretical and experimental approaches followed and their outcomes. Based on this critical review, it can be concluded that there are a number of problems that have not been fully resolved yet, and therefore, require more research work. These problems can be summarized as follows:

a) ***Problems in machining system modeling:*** A thorough understanding of the machining process has been elusive for the inconsistencies of experimental findings caused by different process inputs. Traditional models are deficient in handling complex tool geometry, wide ranges of cutting conditions and versatility of tool/workpiece material combinations. In these aspects, and with particular emphasis on the more popular oblique cutting situation using a multi-edged cutting tool, recent mechanistic modeling has shown to be more capable and promising. However, there is a lack of mechanistic models that describe the dynamics of the machining system

including the tool flank face interference and its influence as a source of process damping on the machined surface errors.

b) ***Problems in on-line measurement:*** The robustness of on-line sensing against the severe environment of metal cutting is a major concern. The introduction of this technology to the industrial production floor for either the implementation of GAC or just product inspection has been hampered by the uncertainty of its performance under normal cutting conditions (with the presence of smoke, chips and cutting fluid). In addition to robustness there are other challenging concerns that have to be addressed as well, such as, compactness, accessability and closeness to the cutting point. Although a number of optical sensors were developed for on-line measurement of workpiece diameter in turning applications, they have only been successful in the laboratory for dry cutting conditions. The fact is that the majority of metal cutting in North America is performed while using a cutting fluid. Therefore, it is believed that solving the on-line sensing problem in the wet cutting environment is the key to unlocking the passage towards the industrial floor and allowing the industry to benefit from such technology.

c) ***Problems in control strategies:*** The predictive ability of the control strategy is necessary to account for the measurement delay inherent in the GAC system. However, in order to set up an effective control system valid for a decent range of cutting conditions, it is important as well to realize the input/output relationships of the machining process and how does each of the different error components relate to the controlled inputs of the process. Such relationships can be derived by mechanistic modeling of the process. The process models can then provide the basis

to predict and control the accuracy of the machined surface. In the absence of appropriate models for machining processes, most of the control strategies of GAC developed are inadequate in assuring neither the stability of the GAC system nor the convergence of the parameter estimator. A more systematic approach for the design of the geometric controller is thus still needed.

d) ***Problems in conventional CNC machine tool controllers:*** In order to perform the real-time compensatory control action as commanded by the GAC controller, the position of the tool is changed in real-time (i.e., while cutting). The current conventional CNC machine tool controllers are neither flexible nor open enough to permit altering the position command in real-time. Position commands are normally preprogrammed in G-code and are interpreted by the machine controller to drive the servo motor of the respective axis accordingly. This problem forced previous researchers to employ external actuating devices instead of using the machine tool servo system, which added more cost and impracticality to the implementation of the GAC system.

2.5 RESEARCH OBJECTIVES

The main purpose of this work is to improve the accuracy of the turning process in order to meet tighter tolerances without slowing down productivity. This requires reliable tools for predicting, measuring and compensating machining errors. The development of such tools and their integration to implement a GAC system represent the goals of this research. The research objectives can thus be summarized as follows:

a) Develop a mechanistic model which describes the machining system dynamics in turning for the general oblique longitudinal cutting case, while including the effect of ploughing forces. The model should allow the prediction of cutting forces, tool/workpiece structural dynamics, and ultimately the machined surface topography with all structural error dynamics superimposed.

b) Develop an accurate, reliable and compact on-line measurement system for the workpiece diameter to operate during cutting while using a cutting fluid. The system should have the capability of performing adequately and close enough to the cutting point. Sensor immunity against the severe environment of the production floor can be provided by using a suitable filtering method and/or fusion of other sensory data.

c) Design a suitable systematic control strategy which ensures the performance of the GAC system under a wide range of cutting conditions. The control strategy should provide regulation against both deterministic and stochastic disturbances. This can be made possible by employing the developed mechanistic process model and using the provided on-line measurement data in a feedback control loop. The controller should provide predictive control actions and compensate machining errors by regulating the position of the tool tip. Also, the control actions should account for servo dynamics and the other input/output relationships of the machining system model.

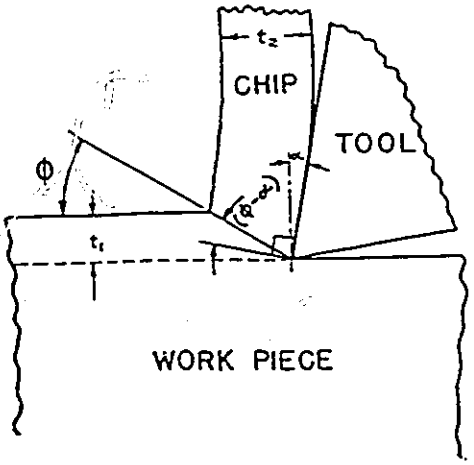

(a)

t_1 Undeformed Chip Thickness.
t_2 Deformed Chip Thickness.
ϕ Shear Angle.
α Rake Angle.

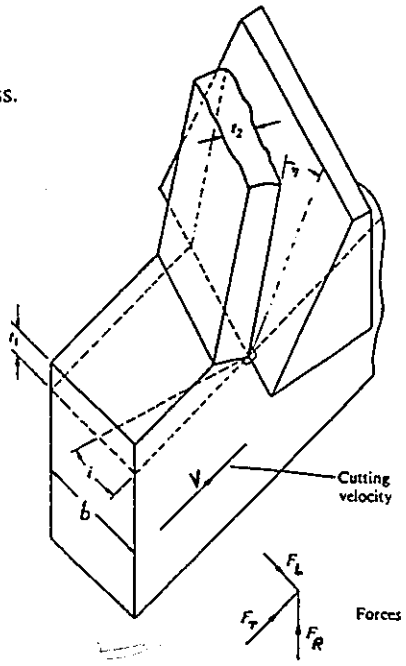

(b)

Fig. 2.1 Models of the cutting process.
a) Orthogonal Cutting.
b) Oblique Cutting.

t_1 Undeformed Chip Thickness.
t_2 Deformed Chip Thickness.
ϕ Shear Angle.
α Rake Angle.

F Rake Face Friction Force
N Rake Face Normal Force
τ Friction Angle
F_N Shear plane Normal Force
F_S Shear plane Shear Force

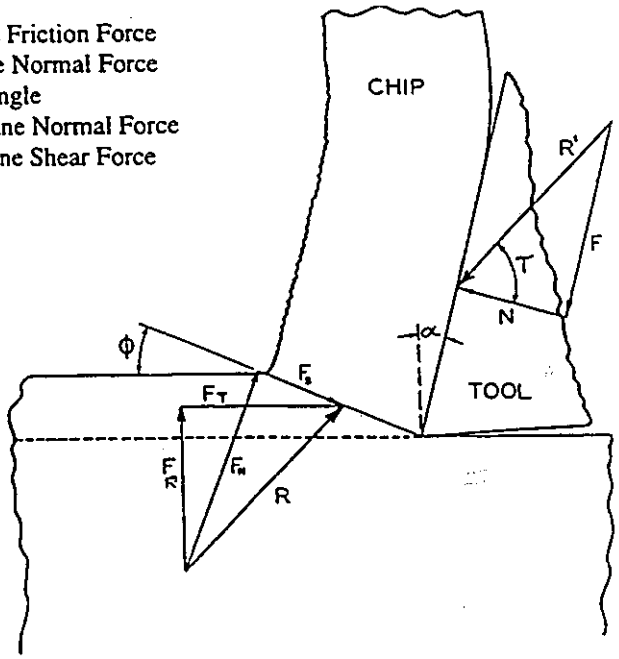

Fig. 2.2 Force System Acting in Case of Orthogonal Cutting, showing Chip in Equilibrium Under Action of Equal and Opposite Resultant Force R and R'. (Merchant, 1944)

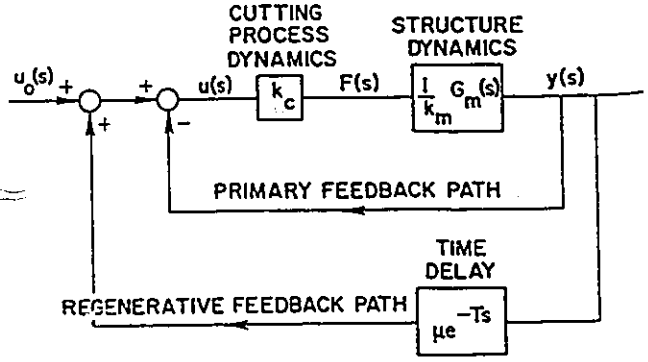

Fig. 2.3 Transfer Function Model Block Diagram. (Merritt, 1965)

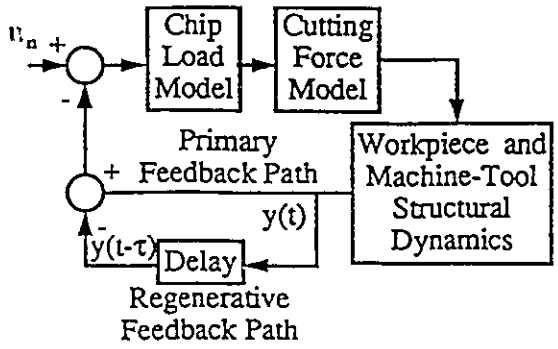

Fig. 2.4 Mechanistic Model Block Diagram. (Endres, et al., 1990)

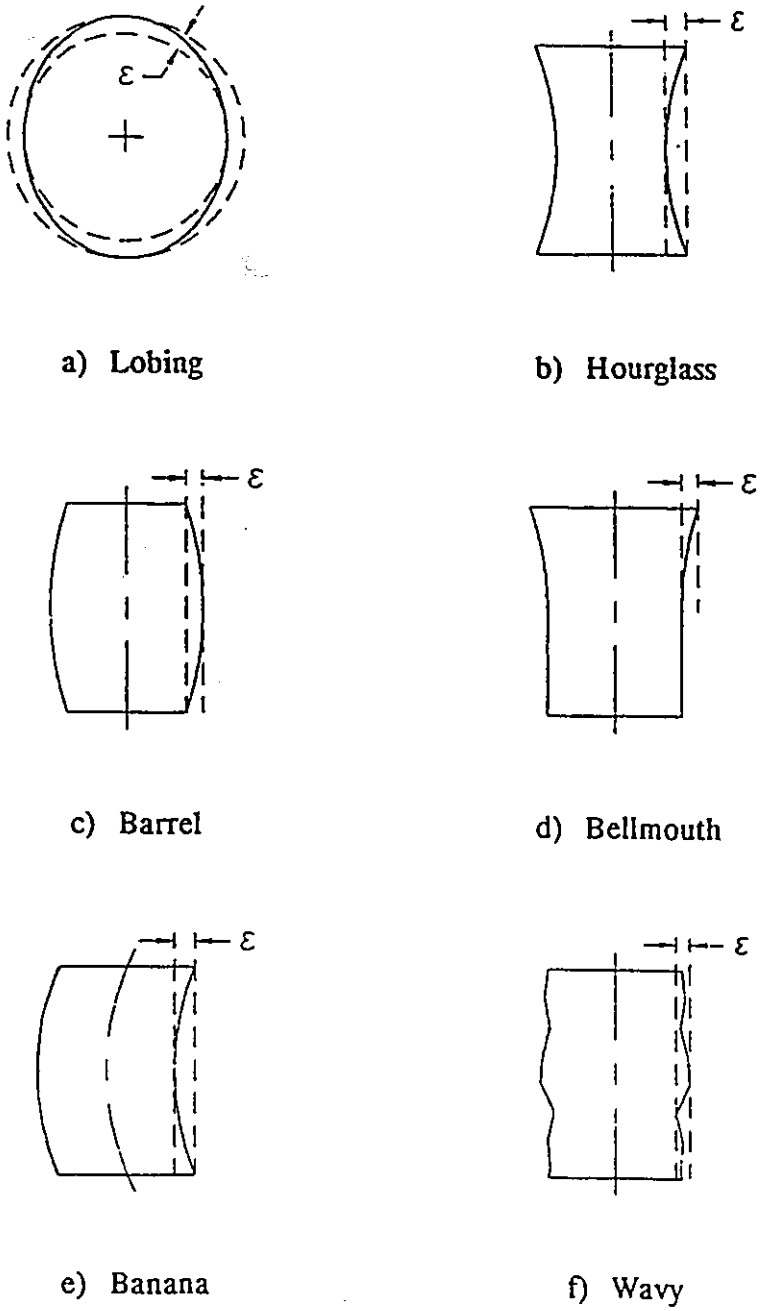

Fig. 2.5 Possible Form Errors For Cylindrical Features. (Wilson, 1992)

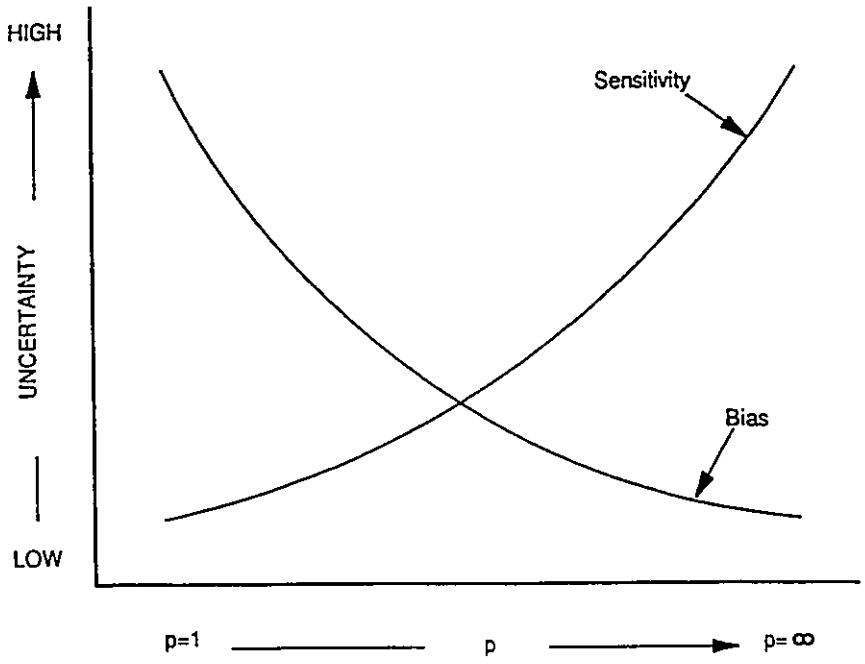

Fig. 2.6 L_p-Norm Uncertainties. (Hopp, 1993)

CHAPTER 3

MACHINING SYSTEM MODEL DEVELOPMENT

This chapter presents the development and verification of an enhanced dynamic process model of the machining process (Shawky and Elbestawi, 1996a). The model is based on the mechanistic model structure developed by Endres, et al. (1990). This model structure is represented by the block diagram shown in Fig. 3.1. The different modules of the model which are modified and newly developed (in the current work) are indicated on the figure by the dotted and hatched blocks, respectively. The simulation of machining dynamics is significantly enhanced by incorporating a mechanistic ploughing force model which permits the prediction of cutting process damping. Also, the structural dynamic models of both the tool and the workpiece are modified by using more realistic boundary conditions based on experimental measurements.

The chapter proceeds with a description of the chip load geometry and proposes a simple method for calculating the chip load area. The chip load area is used in determining the cutting forces. Next, the geometry of the tool-workpiece interface along the clearance face is considered. A new mechanistic approach is introduced for modeling the effect of

ploughing forces on process damping during longitudinal bar turning. The approach is based on the decomposition of ploughing forces into static and dynamic components. The chapter then discusses the modeling of tool/workpiece structural dynamics. This is followed by a description of the surface generation model. The machining system model developed is used in computer simulations to predict cutting forces, surface roughness and workpiece form error. The chapter concludes by experimental verification of the model predictions.

3.1 CHIP LOAD AND CUTTING FORCES

The tool edge profile *P(t)* can be represented in a plane as shown in Fig. 3.2 by two lines joined by a circular arc. Such geometric elements are the side cutting edge *S(t)*, end cutting edge *E(t)*, and tool nose arc *C(t)*. Figure 3.3 shows the chip load $A_c(t)$ as the area contained between the three profiles '*doc*', *P(t)*, and *P(t-T)*, where, '*doc*' represents the original work surface to be machined, *P(t)* represents the tool edge profile at time *t*, *T* is the time for one workpiece revolution, and thus *P(t-T)* represents the tool edge profile of the previous revolution. A data structure is designed to handle the tool edge profile *P(t)* based on its geometrical elements. Using analytical geometry these elements can be defined in the *xy*-plane by the following slopes and *y*-axis intercepts, (refer to Fig. 3.4)

$$\begin{aligned} slope_S &= \tan(\pi/2 - la) \\ slope_E &= \tan(\pi - ea) \\ intercept_S(t) &= y_{LIM1(t)} - x_{LIM1(t)} * slope_S \\ intercept_E(t) &= y_{LIM2(t)} + x_{LIM2(t)} * \tan(ea) \end{aligned} \qquad (3.1)$$

where, *la* and *ea* are the lead and end angles of the cutting edge, respectively. *LIM1(t)* and *LIM2(t)* are the points where the side and end cutting edges join the nose portion of the tool

edge profile, respectively, and their coordinates are given by,

$$\begin{aligned} x_{LIM1}(t) &= x_o(t) + (R * \cos(la)) \\ y_{LIM1}(t) &= y_o(t) - (R * \sin(la)) \\ x_{LIM2}(t) &= x_o(t) - (R * \sin(ea)) \\ y_{LIM2}(t) &= y_o(t) - (R * \cos(ea)) \end{aligned} \tag{3.2}$$

where, x_o and y_o are the coordinates of the nose arc center, while R is the nose radius.

It is essential to determine the time varying chip load configuration according to the instantaneous and previous values of the time changing cutting conditions and tool geometry. Endres, et al. (1990) used an integration method based on incorporating integration limits which are functions of the cutting geometry. In the current work a simpler approach is proposed based on utilizing the two basic area shapes shown in Fig. 3.5.

Due to the nature of the tool edge profile geometry and the vibrations which may be encountered during a cut, the chip load configuration may vary. The geometric profiles which compose the chip load intersect together at some points (for example, like those marked with squares in Fig. 3.3). By solving the analytical equations of these profiles their mutual intersection points can be located. These intersections are used to define the chip load configuration. In this analysis the tool edge profiles of the current and the two previous workpiece revolutions are considered in order to account for large vibrations. The flow chart shown in Fig. 3.6 presents the search sequence used in determining the correct intersection between the tool edge profiles. The knowledge of the intersection point coordinates completes the description of the chip load geometry. The chip load $A_c(t)$ is evaluated in a closed form by addition and subtraction of areas based on the two basic shapes given in Fig. 3.5. The first is the area under a line '*ab*' and the second is the area under a circular arc '*oab*'; they are referred to by the functions *ATRP(line)* and *AUC(arc)*, respectively.

Accordingly, the chip load $A_c(t)$ is calculated from,

$$A_c(t) = A(q_1, q_2) \qquad for, \quad q_1 = t \ \wedge \ q_2 = T \tag{3.3}$$

where,

$$\begin{aligned} A(q_1,q_2) = & ATRP(E(q_1-q_2)) + AUC(C(q_1-q_2)) + ATRP(S(q_1-q_2)) + \\ & ATRP(doc) - ATRP(E(q_1)) - AUC(C(q_1)) - AUC(S(q_1)) \end{aligned} \tag{3.4}$$

and in the case of large vibrations (i.e., when a valid intersection is encountered between $P(t)$ and $P(t-2T)$),

$$A_c(t) = A(q_1 = t, q_2 = 2T) - A(q_1 = t-T, q_2 = T) \tag{3.5}$$

Both functions $ATRP(\ )$ and $AUC(\ )$ are forced to return "*null*" if the area calculated has a negative sign (i.e., the area element calculated does not exist) which allows the use of the general solution given by Eqs. (3.3-3.5) for different chip load geometry configurations. This also accounts for the basic non-linearity in the cutting force system (when "air cutting" occurs) as indicated by Tlusty and Ismail (1981).

The mechanistic structure of the cutting force model is based on proportionality to the chip load. Tangential and normal cutting forces $F_T(t)$ and $F_N(t)$ are determined using the proportionality constants $K_T(t)$ and $K_N(t)$, respectively. The normal component is further resolved using the unweighed effective lead angle la_e into the longitudinal and radial force components $F_L(t)$ and $F_R(t)$, respectively, as shown in Fig. 3.7. The force equations are given by,

$$\begin{aligned} F_T(t) &= K_T(t) * A_c(t) \\ F_N(t) &= K_N(t) * A_c(t) \\ F_L(t) &= F_N(t) \cos(la_e) \\ F_R(t) &= F_N(t) \sin(la_e) \end{aligned} \tag{3.6}$$

K_T and K_N are empirical in nature and are known to be dependent on the tool geometry, cutting resistance and tool-workpiece material combination. They also account for random excitation due to material hardness inhomogeneity (Zhang and Kapoor, 1991a). The random excitation is introduced by a normally distributed, zero mean, percent of $\bar{K}_T$ and $\bar{K}_N$, variable called δ_{norm}, thus

$$\begin{aligned} K_T(t) &= (1 + \delta_{norm})\,\bar{K}_T(t) \\ K_F(t) &= (1 + \delta_{norm})\,\bar{K}_N(t) \end{aligned} \tag{3.7}$$

The values of $\bar{K}_T$ and $\bar{K}_N$ are functions of both the equivalent chip thickness t_c and cutting speed V as will be explained later in this chapter. The equations used to determine the equivalent chip thickness and effective lead angle are given in Appendix B.

3.2 THE PLOUGHING FORCES

The ploughing forces are generated due to the indentation of the tool into the workpiece material at the clearance face. These forces act on the clearance face of the tool in two main directions as shown in Fig. 3.7. P_N acts in the direction of F_N due to the elasto-plastic deformation and P_T acts in the direction of F_T due to friction. Wu (1988) gave the equations for the ploughing forces as,

$$\begin{aligned} P_N &= f_{sp} * v \\ P_T &= \mu_p * P_N \end{aligned} \tag{3.8}$$

where, v is the total volume of the ploughed material, f_{sp} and μ_p are proportionality constants.

3.2.1 DECOMPOSITION OF THE PLOUGHING FORCES

During stable cutting the ploughed volume v_s is static and influences the cutting forces by increasing its mean value. When vibrations are encountered, a dynamic ploughing force component is generated proportional to a change v_d in the indented volume. Thus, both the total volume v and the corresponding ploughing forces can be decomposed into static and dynamic components.

3.2.1.1 Static Ploughed Volume: It has been long understood since the early work of Albrecht (1960) that the small radius of the tool edge causes part of the workpiece material to be extruded beneath the tool in a loading and unloading cycle (Merwin and Johnson, 1963) giving rise to a maximum penetration depth h_m as shown in Fig. 3.8. Also, it is known that the ploughing forces depend on the feed; as the feed is increased the area of contact of the clearance face rises and this influence becomes more significant at larger values of the ratio of feed f to depth of cut d (Zorev, 1966). To model this effect mechanistically consider the plunge cut configuration shown in Fig. 3.9 (and assume first that the tool edge is infinitely sharp). The tool feed motion and the workpiece surface motion are discretized at points 'T_1', 'T_2', ...etc. and points 'W_1', 'W_2' ... etc., respectively. At a starting point in time the tool edge (at point 'T_1') will coincide with point 'W_1' on the workpiece surface. The machined surface has a speed V (*m/min*), and 'W_1' will travel to 'W_2' while 'T_1' will translate to 'T_2' with the tool feed rate f_r (*mm/min*). This results in penetration of the tool into the newly machined surface at 'W_2'. Such penetration may also take place at regions 'W_2', 'W_3', ...etc. depending on the clearance angle, wear land, the ratio of the feed rate to the cutting speed and the diameter of

the workpiece. Notice that in the case of radial tool feed, the rotary motion of the workpiece causes the machined surface points to retract away from the tool flank non-linearly (as they leave the cutting point 'T_1').

Thus the tool indentation is a summation of two effects that happen simultaneously; the sliding-extrusion effect due to the radius r of the tool edge and the effect of tool feed f in increasing the clearance face contact. This results in a total indentation depth h_t that varies along the flank length as shown in Fig. 3.10 governed by the equation,

$$h_{t_i} = \frac{f_r}{1000\,V} * y_i - R_{wp}(1 - \cos\theta_i) + h_{e_i} - y_i \tan\gamma$$

where,

$$\theta_i = \sin^{-1}\frac{y_i}{R_{wp}}$$

$$h_{e_i} = (r - h_m) - \sqrt{r^2 - (r\sin\beta - y_i)^2} \qquad \forall\ y_i < r\sin\beta \tag{3.9}$$

$$h_{e_i} = h_m \qquad \forall\ y_i \geq r\sin\beta$$

$$\beta = \cos^{-1}\left(1 - \frac{h_m}{r}\right)$$

R_{wp} is the workpiece radius, γ is the clearance angle and y is the spatial independent variable. The second term in Eq. (3.9) represents the retraction effect due to workpiece curvature in the case of radial feed. This term, however, tends to be zero for practical values of R_{wp}. In the case of longitudinal feed, if the lead angle is zero, the workpiece radius (of curvature) is effectively infinite. Also, if the lead angle is not zero, then the workpiece radius is somewhere between R_{wp} and infinity. Thus, the retraction term is considered insignificant and can be safely neglected. The static contact area A_s is determined by integrating over the clearance face contact length L ($\forall$*positive* h_t),

$$A_s = \int_L h_{t_i} / \cos\phi_i \; dL$$

where,

$$\phi_i = \beta - 2 * \sin^{-1}\left(\frac{\sqrt{y_i^2 + h_{e_i}^2}}{2r}\right) \qquad \forall \quad L \le r\beta$$

$$\phi_i = \gamma \qquad \forall \quad L > r\beta \tag{3.10}$$

ϕ_i is the local rotation angle from y domain to L domain. The static indentation volume v_s is then determined by integrating the local contact area A_s along the chip contact length l_c of the tool edge profile,

$$v_s = \int_{l_c} A_{s_i} \cdot \frac{t_i}{t_c} \; dl_c \tag{3.11}$$

where, the variation of the pressure distribution along the cutting edge profile is represented by a weighing factor taken as the ratio of the local chip thickness t_i to the equivalent chip thickness t_c.

3.2.1.2 Dynamic Ploughed Volume: The penetration of the tool presented above is due to static effects only. However, when machining vibrations are encountered, undulations are generated on the machined surface leading to more interaction between the tool clearance face and the wavy surface. This interaction is of a dynamic nature and causes a change v_d in the static volume v_s. The corresponding dynamic change in the area of contact A_d (as indicated in Fig. 3.11) is determined by the dynamic depth of penetration h_d which is solely due to surface undulations. The surface undulations are determined from the workpiece/tool vibrations encountered during the current and the two previous revolutions of the workpiece.

Note that if the frequency of surface undulations is high enough, discontinuities in the tool penetration might be encountered.

In an orthogonal cutting process, the surface undulations and the dynamic area of contact on the clearance face are strictly due to the system vibrations in the feed direction. But in the case of a multi-edged cutting tool the surface undulations are due to an interaction of both longitudinal and radial vibrations and it will depend greatly on the effective lead angle. For example, in a longitudinal bar turning situation, with an ideal single edge tool and zero lead angle, radial vibrations have no effect on surface undulations. If the lead angle is increased the ploughing action due to these vibrations will increase. In the current work, local resultant vibration values 'vib_h' are determined at several discrete points along the cutting edge profile by the projection of both radial and longitudinal vibrations (vib_R and vib_L, respectively) on the direction normal to the local lead angle 'la_i',

$$vib_{h_i} = vib_R \sin la_i + vib_L \cos la_i \qquad (3.12)$$

Consequently, the dynamic ploughed volume v_d is determined by the integration of local dynamic contact areas A_d along the chip contact length l_c (similar to Eq. 3.11 used for v_s).

3.2.2 CALIBRATING THE PLOUGHING MODEL

The separation of ploughing forces from dynamometer force measurements has always been an obstacle in studying the ploughing mechanism. The dynamometer force measurements inherently include the effect of the static ploughing component v_s. This indicates that the cutting force calibration system of K_T and K_N already accounts for this effect and thus the determination of v_s is not essential. Moreover, the decomposition of the

total volume presented above reduces the amount of error (due to the estimation of h_m) in determining the dynamic ploughing volume v_d. Eqs. (3.8) are used to determine the dynamic ploughing forces by substituting v_d for v. However, in order to calibrate this model, information on the resistance of the workpiece material to tool indentation is required. Such information is present in the measured data of the normal force.

As opposed to forces on the rake face, forces on the clearance face do not take part in the chip formation process and represent a parasitic load on the cutting tool. It has been concluded by Zorev (1966) that the nature of the forces acting on the rake and flank surfaces is different so the majority of the cutting parameters influence these forces in a different manner and to different degrees. Thus, the value of the ratio of these forces may vary over a wide range. When machining soft materials with a large depth of cut and with a tool having small wear on the clearance face, the forces on the clearance face are negligibly small by comparison with the forces on the rake face. On the other hand, when machining hard materials at small depths of cut with a tool having a large amount of clearance contact, the forces on the clearance face may exceed the forces on the rake face. The latter case for example describes quite well the cutting conditions of the hard turning process. In other words, under controlled cutting conditions the information content about work material indentation in the dynamometer measured forces (and specially in the normal cutting component) will exceed that due to chip removal. Accordingly, dynamometer force measurements for hard turning using ceramic inserts with zero clearance angle were used to investigate the correlation between the measured cutting forces and the static ploughing volume v_s. The friction conditions on the clearance face are assumed to be coulombic. Hence, it has a constant friction coefficient which depends on the softer material (i.e.,

workpiece material) and a value of *0.4* was estimated (Bailey, 1975). The tool edge radius was measured using a tool makers microscope, and was found to be *0.02 mm*. There is no straightforward means of measuring the maximum depth of penetration h_m, (and there is also little information available in the literature), thus an approximate value of *0.006 mm* was chosen as suggested by Thomsen et al. (1962).

As expected, the normal force F_N showed a relatively high correlation with v_s in comparison with the tangential force F_T. A multi-linear regression analysis was conducted to determine a proportionality constant K_v that would relate F_N to v_s. The analysis resulted in a model for K_v with *88.6%* R^2 of the form,

$$\ln K_v = a_0 + a_1 \ln t_c + a_2 V + a_3 \ln V \qquad \textbf{(3.13)}$$

It is concluded that the static ploughing effect has a principal contribution to the normal force component F_N for the ranges of cutting conditions used, and that K_v as determined by Eq. (3.13) is a good approximation of f_{sp} which can be used to determine the dynamic ploughing force using Eq. (3.8). The dependence of f_{sp} on the amount of thermal energy generated at the shear zone (Wu, 1988) is modeled here by the velocity terms in Eq. (3.13).

3.3 THE STRUCTURAL DYNAMICS

The structural dynamics represent the relationship between the cutting force and the response of the structure. In this analysis, the dynamics of both the tool and workpiece are considered, while the remainder of the machine tool structure is assumed rigid. This assumption is reasonable for the machining of a slender workpiece. In such case, the

flexibility of the machine tool structure is negligible as compared to that of the cutting process components. The tool and workpiece were modeled as continuous beams and there equations of motion were derived for the appropriate boundary conditions. The forced response is solved using the principle of mode superposition based on the orthogonality of the eigen functions. The global coordinates were chosen in the three axes of the cutting force system.

3.3.1 EXPERIMENTAL SETUP

The machine tool used in this study is a STANDARD MODERN NC17 lathe with a sixty inch bed and a *10 hp* AC induction spindle motor. The lathe is retrofitted with servo motors on its two axes, that are controlled by a FANUC 3TC digital controller. The lathe is equipped with a tool-post force dynamometer that uses three triaxial piezoelectric load cells to measure the three main cutting forces. A slender shaft workpiece made of case hardened steel *AISI 1552* of *60 Rc* hardness (refer to Fig. 3.12) is used in the experimental work.

3.3.2 WORKPIECE DYNAMICS

The workpiece is modeled as a continuous beam with three different sets of boundary conditions that correspond to three different clamping setups. In case '*a*' the workpiece has one end supported by the chuck and the other end free. While, in case '*b*' the workpiece has one end supported by the chuck and the other end supported by the tail stock. In case '*c*' the workpiece is supported between two centers. Endres, et al. (1990) considered the chuck to be an infinitely stiff clamp. A more realistic representation is used in the current work which

was suggested by Lu and Klamecki (1988) for an onset of chatter detection model (for cases '*a*' and '*b*'). The chuck is modeled by a rotational spring attached to a simple support hinge as shown in Fig. 3.13a. The rotational stiffness K_t depends on the clamping torque of the chuck and the jaws flexibility, and is found to greatly affect both the eigen values and the eigen functions of the system. The tail stock is modeled by a translational spring of stiffness K_l as shown in Fig. 3.13b. In the third case, the center on the spindle side is modeled by a translational spring K_c as shown in Fig. 3.13c. For the torsional vibrations, the workpiece is modeled as a clamped-free cantilever, as shown in Fig. 3.13d.

3.3.2.1 Lateral Vibrations of the Workpiece: The workpiece has flexural vibrations in both the radial and tangential directions. The equation of motion of flexural vibrations in each direction is in the general form,

$$-\frac{\partial^2}{\partial x^2}\left(EI(x) . \frac{\partial^2 y(x,t)}{\partial x^2} \right) + f(x,t) = m(x)\frac{\partial^2 y(x,t)}{\partial t^2} \qquad \textbf{(3.14)}$$

where, $EI(x)$ flexural stiffness of the workpiece, $f(x,t)$ distributed force as a function of time, and $m(x)$ mass per unit length. To solve the eigen value problem, the free vibration characterized by $f(x,t)=0$, is considered, in which case the solution of Eq. (3.14) becomes separable in space and time. Letting,

$$y(x,t) = Y(x) . F(t) \qquad \textbf{(3.15)}$$

and assuming that both the material properties and the cross sectional geometry of the workpiece are constant with position x, the eigen value problem reduces to

$$\frac{d^4 Y(x)}{dx^4} - \beta^4 . Y(x) = 0 \qquad \textbf{(3.16)}$$

where,

$$\beta^4 = \frac{\omega^2 m}{EI} \tag{3.17}$$

which has the general solution of the form, (Meirovitch, 1986)

$$Y(x) = C_1 Sin\beta x + C_2 \cos\beta x + C_3 \sinh\beta x + C_4 \cosh\beta x \tag{3.18}$$

By applying the appropriate boundary conditions, the eigen values and the eigen functions can be determined. The boundary conditions at the chuck end are:

$$Y(x)|_{x=0} = 0, \quad EI\frac{d^2Y(x)}{dx^2}|_{x=0} = K_t\frac{dY(x)}{dx}|_{x=0}, \tag{3.19}$$

for cases '*a*' and '*b*', and

$$EI\frac{d^3Y(x)}{dx^3}|_{x=0} = -K_c . Y(x)|_{x=0}, \quad EI\frac{d^2Y(x)}{dx^2}|_{x=0} = 0, \tag{3.20}$$

for case 'c'. The boundary conditions at the other end are:

$$EI\frac{d^3Y(x)}{dx^3}|_{x=l} = 0, \quad EI\frac{d^2Y(x)}{dx^2}|_{x=l} = 0, \tag{3.21}$$

for a free end (case '*a*') where, l is the length of the workpiece, and

$$EI\frac{d^3Y(x)}{dx^3}|_{x=l} = K_t . Y(x)|_{x=l}, \quad EI\frac{d^2Y(x)}{dx^2}|_{x=l} = 0, \tag{3.22}$$

for a tail stock supported end (cases '*b*' and '*c*').

Applying the appropriate boundary conditions yields the characteristic determinant,

$$\begin{pmatrix} 0 & 1 & 0 & 1 \\ -\sin\beta l & -\cos\beta l & \sinh\beta l & \cosh\beta l \\ -\cos\beta l & \sin\beta l & \cosh\beta l & \sinh\beta l \\ -K_t & EI\beta & -K_t & EI\beta \end{pmatrix} * \begin{pmatrix} C_1 \\ C_2 \\ C_3 \\ C_4 \end{pmatrix} \tag{3.23}$$

for case '*a*',

$$\begin{pmatrix} 0 & 1 & 0 & 1 \\ -\sin\beta l & -\cos\beta l & \sinh\beta l & \cosh\beta l \\ \sin\beta l + \dfrac{EI\beta^3}{K_t}\cos\beta l & \cos\beta l - \dfrac{EI\beta^3}{K_t}\sin\beta l & \sinh\beta l - \dfrac{EI\beta_3}{K_t}\cosh\beta l & \cosh\beta l - \dfrac{EI\beta_3}{K_t}\sinh\beta l \\ -K_t & -EI\beta & K_t & EI\beta \end{pmatrix} * \begin{pmatrix} C_1 \\ C_2 \\ C_3 \\ C_4 \end{pmatrix} \tag{3.24}$$

for case '*b*', and

$$\begin{pmatrix} -EI\beta^3\cos\beta l - K_t\sin\beta l & EI\beta^3\sin\beta l - K_t\cos\beta l & EI\beta^3\cosh\beta l - K_t\sinh\beta l & EI\beta^3\sinh\beta l - K_t\cosh\beta l \\ -EI\beta^3 & K_c & EI\beta^3 & K_c \\ \sin\beta l & \cos\beta l & -\sinh\beta l & -\cosh\beta l \\ 0 & 1 & 0 & 1 \end{pmatrix} * \begin{pmatrix} C_1 \\ C_2 \\ C_3 \\ C_4 \end{pmatrix} \tag{3.25}$$

for case '*c*'. Solving for the eigen values $\beta_r l$ we can get the characteristic frequencies ω_r from,

$$\omega_r = (\beta_r l)^2 \cdot \sqrt{\frac{EI}{m l^4}} \tag{3.26}$$

then substituting back in Eq. (3.18) we get the set of eigen functions:

$$Y_r(x) = C_1 * \left[\sin\beta_r x + A_1 \sin\beta_r x + \left(\frac{\sinh\beta_r l . A_1 - \sin\beta_r l}{\cos\beta_r l - \cosh\beta_r l} \right) . \cosh\beta_r x - \left(\frac{\sinh\beta_r l . A_1 - \sin\beta_r l}{\cos\beta_r l - \cosh\beta_r l} \right) . \cos\beta_r x \right]$$

where,

$$A_1 = \frac{\left(2\frac{EI\beta_r}{K_t} . \sin\beta_r l + (\cos\beta_r l - \cosh\beta_r l) \right)}{\left(2\frac{EI\beta_r}{K_t} . \sinh\beta_r l - (\cos\beta_r l - \cosh\beta_r l) \right)}$$

(3.27)

$$Y_r(x) = C_1 * \left[\sin\beta_r x + A_1 \sinh\beta_r x + \left(\frac{A_1\sinh\beta_r l - \sin\beta_r l}{\cos\beta_r l - \cosh\beta_r l} \right) . \cosh\beta_r x - \left(\frac{A_1\sinh\beta_r l - \sin\beta_r l}{\cos\beta_r l - \cosh\beta_r l} \right) . \cos\beta_r x \right]$$

where,

$$A_1 = -\frac{\left[\left(\sin\beta l + \frac{EI\beta^3}{K_l}\cos\beta l \right) - \frac{\sin\beta l . \left(\cosh\beta l - \frac{EI\beta^3}{K_l}\sinh\beta l - \cos\beta l + \frac{EI\beta^3}{K_l}\sin\beta l \right)}{\cos\beta l - \cosh\beta l} \right]}{\left[\left(\sinh\beta l - \frac{EI\beta^3}{K_l}\cosh\beta l \right) + \frac{\sinh\beta l . \left(\cosh\beta l - \frac{EI\beta^3}{K_l}\sinh\beta l - \cos\beta l + \frac{EI\beta^3}{K_l}\sin\beta l \right)}{\cos\beta l - \cosh\beta l} \right]}$$

(3.28)

and,

$$Y_r(x) = C_1 * \left[\sin\beta_r x + EI\beta_r^3 A_1 . (\cos\beta_r x + \cosh\beta_r x) + (1 - 2K_c A_1) . \sinh\beta_r x \right]$$

where,

$$A_1 = \left(\frac{\sinh\beta_r l - \sin\beta_r l}{\sinh\beta_r l . (\cos\beta_r l - \cosh\beta_r l) + 2K_c \sinh\beta_r l} \right)$$

(3.29)

for cases 'a', '*b*' and '*c*', respectively, while the constant C_1 is determined by mass normalization of the eigen functions; i.e., to satisfy the relation,

$$\int_0^L m(x)\ Y_r(x)\ Y_s(x)\ dx = \delta_{rs} \qquad r, s = 1,2,\ldots \qquad \textbf{(3.30)}$$

where δ_{rs} is the Kronecker delta function.

Since the eigen functions are orthogonal, the displacement of the workpiece as a function of position x can be obtained by superposition of the normalized eigen functions, thus,

$$y(x,t) = \sum_{r=1}^{\infty} Y_r(x)\, \eta_r(t) \qquad (3.31)$$

where $\eta_r(t)$ is the generalized modal displacement which is governed by the second order differential equation,

$$\ddot{\eta}_r(t) + 2\zeta\omega_r\dot{\eta}_r(t) + \omega_r^2\eta_r(t) = Q_r(t) \qquad r=1,2,... \qquad (3.32)$$

(which resemble the equation of motion of a damped single-degree-of-freedom system subjected to external excitation) where $Q_r(t)$ is the *rth* generalized modal force which is obtained from,

$$Q_r(t) = \int_0^l f(x,t)\, Y_r(x)\, dx \qquad r=1,2,... \qquad (3.33)$$

This reduces to

$$Q_r(t) = F(t)\, .\, Y_r(x^*) \qquad (3.34)$$

in the case of a concentrated single load, where x^* is the point of action of the force $F(t)$.

3.3.2.2 Torsional Vibrations of the Workpiece: Similarly the torsional vibrations of the workpiece (θ) are modeled by the following equation of motion,

$$\frac{\partial^2 \theta(x,t)}{\partial x^2} = \frac{1}{b^2} \cdot \frac{\partial^2 \theta(x,t)}{\partial t^2} \qquad (3.35)$$

$$where, \quad b = \sqrt{\frac{G}{\rho}}$$

where, G and ρ are the modulus of rigidity and the material density, respectively. By the separation of variables, Eq. (3.35) reduces to

$$\frac{d^2 \theta(x)}{dx^2} + \frac{\omega^2 \theta(x)}{b^2} = 0 \qquad (3.36)$$

which has a general solution of the form, (Meirovitch, 1986)

$$\theta_r(x) = C_1 * \left(\cos \frac{\omega_r x}{b} + \sin \frac{\omega_r x}{b} \right) \qquad (3.37)$$

The workpiece is assumed completely fixed (i.e., clamped) in the chuck while free at the other end as shown in Fig. 3.13d. Thus applying the geometric boundary conditions:

$$\theta(x)|_{x=0} = 0, \qquad \frac{d\theta}{dx}|_{x=l} = 0 \qquad (3.38)$$

we get the characteristic equation,

$$\cos \frac{\omega l}{b} = 0 \qquad (3.39)$$

which solves for the characteristic frequencies,

$$\omega_r = \frac{r\pi b}{2l} \qquad r = 1,3,5,\ldots \qquad (3.41)$$

and the eigen functions are found to be

$$\theta_r(x) = \sin\frac{r\pi x}{2l} \qquad (3.41)$$

The forced response of the torsional vibrations is determined analogously to that of the lateral vibrations derived above using the principle of modes superposition.

3.3.2.3 Identification of the Boundary Conditions: The identification of the boundary conditions involved measurements of the static stiffness of the joints (i.e., chuck and tail-stock). The dynamometer was used to measure a static applied force while a dial gauge was employed to measure the corresponding deflection. The results obtained demonstrated that the stiffness of the joints (and hence the eigen values of the structure) are influenced by the following factors:

a) the clamping torque of the chuck,

b) the axial load applied by the tail-stock,

c) the sequence of clamping the workpiece,

d) the portion of the workpiece length held by the chuck jaws,

e) whether the workpiece had a shoulder bearing against the chuck jaws or not.

Thus, for consistent experimental conditions, the chuck was tightened with *160 N.m* and the tail stock was clamped to apply an axial load of approximately *100 N*. Finally, an HP-modal analyzer (model *3566A*) was used to analyze hammer impact test data and the predicted natural frequencies were verified. The rotational and translational stiffnesses were identified as *26500 N.s.rad*$^{-1}$ and *9.5 MN/m*, respectively, and the natural frequency of the first mode for both the free-end and the centered workpieces were *167 Hz* and *738 Hz*, respectively.

3.3.3 TOOL DYNAMICS

Initially the tool holder was modeled as a clamped continuous cantilever beam (following Endres, et al., 1990). However, for a *25x25 mm*^{2} cross-section of a typical tool holder, with *40 mm* overhang the natural frequencies obtained were too high. Experimental modal analysis techniques were used to identify the structural dynamic characteristics of the tool. Interestingly the results revealed that the tool-post dynamics are dominant. The three transfer functions of the tool post measured in the three global axes (tangential, longitudinal, and radial) are shown in Fig. 3.14. Two coupled modes can be recognized in each of the transfer functions. Therefore, a lumped mass model of the form,

$$\begin{bmatrix} m_1 & 0 \\ 0 & m_2 \end{bmatrix} \begin{bmatrix} \ddot{x}_1 \\ \ddot{x}_2 \end{bmatrix} + \begin{bmatrix} c_1 & -c_2 \\ -c_1 & c_1 + c_2 \end{bmatrix} \begin{bmatrix} \dot{x}_1 \\ \dot{x}_2 \end{bmatrix} + \begin{bmatrix} k_1 & -k_1 \\ -k_1 & k_1 + k_2 \end{bmatrix} \begin{bmatrix} x_1 \\ x_2 \end{bmatrix} = \begin{bmatrix} F \\ 0 \end{bmatrix} \qquad (3.42)$$

is used to represent the tool dynamics in each axis, and F represents the cutting force component in that axis. The dynamic characteristic parameter identified for each axis are listed in Table 3.1.

Table 3.1 Characteristic Parameters of the Tool Structural Dynamic Model

Direction	m = **Mass** [Kg]	c = **Damping** [N.s.m^{-1}]	k = **Stiffness** [MN.m^{-1}]	**Frequency** [Hz]
Radial	4.74 1.45	1425 578	33.0 14.5	420 504
Longitudinal	3.45 1.68	1040 595	26.9 16.8	444 504
Tangential	2.48 3.1	620 940	18.3 28.5	432 484

3.3.4 STRUCTURAL DISPLACEMENT FEEDBACK

The integrated displacements $\delta(t)$ of workpiece/tool dynamics are used to feedback the instantaneous change in the nominal cutting conditions vector O_n. The updated cutting conditions vector $O(t)$ is given by, (Endres, et al., 1990)

$$O(t) = O_n - \eta \cdot \delta(t) \tag{3.43}$$

where η is a *6x10* non-linear transformation matrix. In the current work, due to the reduction of the model order for the tooling system structural dynamics, all the tool angle-related terms in vectors O_n and $O(t)$ (namely, lead, end and back rake angles) are eliminated and by effect the size of the transformation matrix is reduced to *3x8*. Hence, Eq. (3.43) is given by,

$$\begin{aligned}
\delta d &= -y_{tz} \cdot \tan\left[\frac{1}{2}\sin^{-1}\left(\frac{y_{tz}}{R_{wp}}\right)\right] \\
&\quad -y_{wz} \cdot \tan\left[\frac{1}{2}\sin^{-1}\left(\frac{y_{wz}}{R_{wp}}\right)\right] + y_{tx} - y_{wx}, \\
\delta f &= -\dot{y}_{ty}, \\
\delta V &= \dot{y}_{tz} - \dot{y}_{wz} + \dot{\Theta} \cdot R_{wp}
\end{aligned} \tag{3.44}$$

3.4 MACHINED SURFACE GENERATION

The function of the surface generation model is to keep trace of the tool motion along the cut during the simulation and use it to construct the machined surface. In this model the three elements '*S*', '*C*' and '*E*' of the tool edge profile are considered. The workpiece is assumed stationary, while the tool has two motions. One type of motion is vibratory due to

system dynamics while the other is the spiral trajectory of the tool which represents both the workpiece rotation and the longitudinal tool feed. The tool motion is traced by pursuing the variation in the coordinates of the tool edge profile *P(t)*. These coordinates are provided during the simulation by the chip load geometry model and are updated every time step. The construction of the surface is performed at each time step of the simulation in the two dimensional xy-plane of the tool edge profile *P(t)* as follows: (refer to Fig. 3.15)

a) Determine the elements (*S*,*C*,*E*) which contribute to the surface generation at the current time step. This is based on a knowledge of the "start point" and "end point" of the tool edge profile portion which is engaged with the work material.

b) Interpolate *8* intermediate points between the "start" and "end" points along the portion of the tool edge profile engaged with the work material. The interpolation is done at equal intervals along the x-axis while the y-coordinates represent the surface errors.

The two above steps are repeated for *n* number of times during the simulation, where *n* is the number of time steps per one workpiece revolution. This constructs the part of the surface machined in one workpiece revolution and adds the third dimension along the cutting speed direction. Reiterating the above procedure for subsequent workpiece revolutions results in the generation of the whole machined surface.

It should be noted that the methodology explained above allows the generation of the machined surface topography in 3D without holding the feed, depth of cut or the nose radius below any limiting values. The simulated surface topographies provide a qualitative visualization of the mechanism of surface irregularity generation during machining. They also offer a means to directly and quantitatively evaluate the quality of the machined surface.

Roughness indices such as *Ra* and Peak-to-Valley can be determined by assessment of the y-coordinates of the surface along one of the generators of the cylindrical surface for a small cut-off length. Similarly, if the whole machined length is considered, this analysis can result in the longitudinal form error along the workpiece. Also, measurements on single cross-sections of the workpiece (i.e., in the direction of the cutting velocity) can provide the out-of-roundness.

3.5 MODEL VERIFICATION

3.5.1 STATIC LEVELS OF THE CUTTING FORCES

Experimental cutting force data for turning hard steel using ceramic inserts from Mohamed (1994) were used to calibrate the models of $\overline{K_T}$ and $\overline{K_N}$. An extensive multi-linear regression analysis was carried out and resulted in models of the form,

$$\begin{aligned} \ln \bar{K}_T(t) &= C_0 + C_1 \ln t_c(t) + C_2 V(t) + C_3 \ln V(t) \\ \ln \bar{K}_N(t) &= C_4 + C_5 \ln t_c(t) + C_6 V(t) + C_7 \ln V(t) \end{aligned} \qquad (3.45)$$

with correlation coefficients (R^2) of *92.7%* and *89.2%*, respectively. The factorial design matrix used for model conditioning is given in Table 3.2. The R^2 values achieved indicate good association of the model with variations of the data around its mean values. This is attributed to the predictor variables chosen as well as the accuracy of their prediction. The dependence of material cutting resistance on feed and chip load geometry is represented by the equivalent chip thickness t_c; a decrease in the effective chip thickness results in an increase of the material cutting resistance. Moreover, the velocity term represents the softening effect of the work material at higher cutting speeds due to increase in temperature.

The natural logarithmic transformation is used in Eq. 3.45 to eliminate curvature detected in the data.

Table 3.2 Factorial Design Matrix for Model Conditioning.

CUTTING CONDITIONS			
VARIABLE	**LOW LEVEL**	**HIGH LEVEL**	**UNITS**
Speed	90	495	m/min
Feed	0.025	0.15	mm/rev
Depth of Cut	0.1	1.5	mm
Side Rake	0	1.6	deg

The use of weighed versus unweighed effective lead angle in the decomposition of the normal cutting force was also investigated. The weighed effective lead angle la_e showed better correlation with the measured forces. This resulted in model parameters of higher *t-values*, thus, indicating better statistical significance of the model within the *95%* confidence interval. However, further analysis of the residuals indicated larger variance. Therefore, the unweighed effective lead angle was ultimately used.

The cutting conditions and the tool geometries used in the model verification experiments are listed in Table 3.3a and 3.3b. Figure 3.16 shows a comparison of the cutting force results: a) predicted by the model, b) measured, and c) predicted using an empirical model for hard turning by Mohamed, (1994). The results indicate the ability of the model to closely follow the measured forces for different cutting conditions and demonstrate clearly the advantage of employing a mechanistic model over an empirical one in predicting the cutting forces over wide ranges of cutting conditions.

Table 3.3a Force Model Verification Tests.

TEST	*f* mm/rev	*d* mm	*V* m/min	TOOL	TEST	*f* mm/rev	*d* mm	*V* m/min	TOOL
1	0.150	1.5	122	1	30	0.075	0.5	90	1
2	0.125	1.5	122	1	31	0.050	0.5	90	1
3	0.100	1.5	122	1	32	0.025	0.5	90	1
4	0.075	1.5	122	1	33	0.150	0.3	90	1
5	0.150	1.0	122	1	34	0.125	0.3	90	1
6	0.125	1.0	122	1	35	0.100	0.3	90	1
7	0.100	1.0	122	1	36	0.025	0.3	90	1
8	0.075	1.0	122	1	37	0.050	0.2	90	1
9	0.050	0.5	122	1	38	0.025	0.2	90	1
10	0.150	0.5	122	1	39	0.075	0.1	90	1
11	0.125	0.5	122	1	40	0.050	0.1	90	1
12	0.100	0.5	122	1	41	0.100	0.3	90	1
13	0.075	0.5	122	1	42	0.050	0.3	457	1
14	0.050	0.5	122	1	43	0.100	0.2	444	2
15	0.025	0.5	122	1	44	0.050	0.2	455	1
16	0.150	0.3	122	1	45	0.150	1.0	488	1
17	0.100	0.3	122	1	46	0.150	0.5	495	1
18	0.075	0.3	122	1	47	0.050	0.2	90	1
19	0.050	0.3	122	1	48	0.050	0.3	122	1
20	0.025	0.3	122	1	49	0.075	0.5	203	1
21	0.125	0.2	122	1	50	0.075	0.5	261	4
22	0.075	0.2	122	1	51	0.075	0.3	270	1
23	0.050	0.2	122	1	52	0.075	1.0	272	1
24	0.025	0.2	122	1	53	0.075	0.5	273	1
25	0.075	0.1	122	1	54	0.050	0.5	120	3
26	0.050	0.1	122	1	55	0.075	0.5	120	3
27	0.150	0.5	90	1	56	0.075	0.2	120	3
28	0.125	0.5	90	1	57	0.075	0.2	120	5
29	0.100	0.5	90	1					

Table 3.3b Tool Geometries Used in Model Verification Cutting Tests.

TOOL GEOMETRY (Clearance Angle = 0 and Back Rake Angle= -6 deg.)			
TOOL	**LEAD ANGLE [deg]**	**SIDE RAKE [deg]**	**NOSE RADIUS [mm]**
1	0	0	1.2
2	30	1.6	1.2
3	30	1.6	1.6
4	0	1.6	2.4
5	30	1.6	3.2

3.5.2 DYNAMICS OF THE CUTTING SYSTEM

In this section the capabilities of the model in predicting the dynamic response of the machining system are determined. The model predictions of the machined surface errors are investigated and the increase in process damping as a result of including the ploughing force model is demonstrated. The computer simulations were performed on a SUN SPARC station *4/330*. A Hommel Tester *T6D* surface measuring machine was used for surface roughness measurements.

3.5.2.1 Steady State Cutting Forces: The cutting forces vary across the workpiece length due to the varying stiffness and this variation depends on the boundary conditions of the system. This is evident in the cutting force data presented in Fig. 3.17. At the start of the cut (tail-stock end) the force decreases to a minimum then starts increasing again till it reaches almost a flat maximum at the chuck end. The forces predicted by the model, shown in the same figure, follow rather closely the measured values. A slight consistent under-prediction is noticed at the tail-stock end in all three force components. This can be caused by the increase of the workpiece diameter in that vicinity as shown in Fig. 3.12. Such effect leads to an in increase in the stiffness of the shaft which is not included in the model.

3.5.2.2 Process Damping: To demonstrate the effect of the ploughing mechanism on process damping, simulation runs with and without ploughing were performed. Fig. 3.18 presents the lateral tool vibrations induced due to a *3* percent sudden increase in the depth of cut. From the logarithmic decrement of the dynamic responses shown it can be deduced that the damping coefficient has increased approximately from $\zeta=0.04$ (the structural damping) to $\zeta=0.12$ due to cutting process damping.

Figure 3.19 presents the result of two simulation runs with and without ploughing showing the effect on the stability limit of the process. The feed and speed used were *0.05 mm/rev* and *122 m/min*, respectively. Without ploughing the dynamic system chattered at a depth of cut of *2 mm* as shown in Fig. 3.19a. When the ploughing model was incorporated both simulation and experimental results agreed and no chatter was detected as shown in Fig. 3.19b indicating that the model with damping is closer to correct than without damping.

3.5.2.3 Surface Roughness: The surface topographies resulting from simulation runs provide a data base to assess surface roughness indices and form error. For each cut *1000* longitudinal profiles across the workpiece were generated from simulation runs, and an average *Ra* was calculated and its standard deviation was determined. A cut-off-length of *0.36 mm* was used. Simulated machined surface topographies are presented in Fig. 3.20a, b and c for different feeds; *0.05*, *0.075* and *0.1 mm/rev*, respectively. The depth of cut, cutting velocity and tool nose radius were *0.5 mm*, *120 m/min*, and *1.6 mm*, respectively.

Experimental surface roughness results for hard turning by Elwardani, et al., (1992) were used for comparison with model predictions. Figure 3.21a presents a comparison between measured and predicted *Ra* values for *R=1.2 mm*. Each of the measured values is an average of the measurements of three different surface profiles. Both, the measurements and the simulations took place at approximately *20 mm* away from the chuck. The results show that both experimental and predicted variations of *Ra* values for different feeds are in agreement and both show a minimum at an optimal feed of *0.05 mm/rev*. However, the 6σ error bars (shown on the same figure) reveal a rather consistent under-prediction specially at smaller feeds. This is attributed to a slight underestimation of the variation in the hardness measurements of the work material. The results given in Fig. 3.21b, present two different

simulations; the first (marked with '*o*') represents normal cutting (including random excitation due to material inhomogeneity), while the second represents cutting without random excitation (i.e., deterministic portion). The dashed line represents *Ra* values calculated based on the geometry using the formula given by Boothroyd, (1975)

$$R_a = \frac{0.0321 * f^2}{R} * 10^3 \quad [\mu m] \tag{3.46}$$

where, f and R are in *mm/rev* and *mm*, respectively. Interestingly enough, the model predictions depart away from the results obtained using the latter formula as the feed is decreased. The difference between *Ra* values with and without random excitation gives the random portion of surface roughness. The random portion of *Ra* is noticed to be much larger at small feeds and it decreases as feed increases. This explains the large standard deviation at small feeds that can be recognized in Fig. 3.21a, and confirms that the strength of random excitation increases as feed decreases. Although good *Ra* predictions can be made at large feeds using Eq. (3.46), the results would be rather questionable for small feeds due to the large additional irregularities introduced by the random excitation mechanism. The results by Zhang and Kapoor (1991b) for low carbon steel indicated that the random *Ra* portion can reach twice or three times as high as the deterministic *Ra*. Here, Fig. 3.21b indicates that for hard turning the latter multiplier can reach a value of *10* for relatively small feeds.

To determine the influence of process damping on the machined surface, the same cutting conditions of Fig. 3.21a were used with and without the ploughing model for different cutting locations along the workpiece length. The results indicated a decrease in *Ra* values due to process damping. This decrease is shown in Fig. 3.21c for three different locations (*50 mm*, *100 mm*, and *160 mm* from the chuck) as a percentage of the *Ra*

determined without ploughing. It can be noticed that the effect of process damping on decreasing the *Ra* values is more emphasized at locations where the dynamic system is more flexible and when smaller feeds are used, reaching a maximum of approximately *50* percent close to the middle of the workpiece. It should be noted that the results considered here are for stable cuts and thus the excitation encountered is mainly due to the material inhomogeneity mechanism. The noticed reduction in the influence of process damping on *Ra* with increasing the feed is thus due to the corresponding decrease in the strength of the random excitation mechanism. Process damping is rather governed by the machined surface undulations. At larger excitations, these undulations exhibit larger amplitudes and hence process damping is more intensified. In Fig. 3.21c the influence of process damping on the machined surface during large vibrations due to chatter. Fig. 3.22a and 3.22b show the surface topographies corresponding to the simulation results in Fig. 3.19a and 3.19b, respectively. The effect of process damping on the process stability limit is interpreted here as a significant difference in the appearance of the machined surface and its *Ra* values due to chatter marks.

3.5.2.4 Form Error: To determine the surface form error on the machined work length of 160 mm, several surface profiles were measured with a reading taken every *0.2 mm* giving a total of *200* points per profile. Eleven profiles were used to obtain the average surface profile. Figure 3.23 presents a comparison of the average surface profile predicted by the model with the measured one for a straight cut of *d=0.5 mm*, *f=0.05 mm/rev*, *V=122 m/min* and *R=1.6 mm*. The form error on the workpiece radius is found to be within *35 μm*. Both measured and predicted surface profiles agree with a maximum deviation of *≈5 μm* at

the tail-stock end. This maximum deviation is located at the ends of the workpiece where its cross-section changes. Such change is not accounted for in the model.

From the dynamics point of view, the form error is seen as a low frequency type error and it is a superposition of both tool and workpiece deflections. The tool contribution to the form error throughout the cut is only static while the workpiece contribution is both static and dynamic. It is that variation in the workpiece stiffness which causes the curved surface profile. Thus, a key issue in eliminating the form error would be defining the flexibility of the workpiece across the cut and compensating for it. It should be noted at this point that there are other factors such as tool wear and thermal deformations that contribute to the form errors of the workpiece. In this experiment the effect of tool wear is naturally negligible while the tool thermal condition was stabilized as much as possible by performing several cuts with the same tool without allowing it enough time to cool down. Therefore, the form error due to thermal expansion of the tool is minimized in this case. However, in the case of dry cutting a workpiece of a relatively small length-to-diameter ratio, a model of the tool thermal expansion would be essential to achieve accurate prediction of the machined surface form error.

3.6 SUMMARY

A significant enhancement to the prediction of process dynamics in turning was developed. The interference at the clearance face was modeled mechanistically for a multi-edged cutting tool. The cutting process damping is predicted by tracking the dynamic ploughed volume of the work material. Machined surface undulations are determined based

on integrated tool/workpiece vibrations in both radial and longitudinal directions. The ploughing model was calibrated based on static ploughed volume calculations and normal cutting force measurements. Experimental identification of the system dynamic characteristics brought more insight into the influence of workpiece clamping and led to more realistic boundary conditions, as well as a reduced order model of the tool.

The model was tested through computer simulation of longitudinal turning of slender hardened steel shafts. By comparison to experimental evidence, the theoretical predictions showed good agreement with the test results for a wide range of cutting conditions. The results indicate clearly the effects of including the interference model on machining dynamics and the improvements in predicting the machined surface errors and process stability. The *Ra* values demonstrated that including ploughing forces for cutting process damping is not only important for stability prediction but also necessary for surface roughness prediction specially in low feed finishing pass scenarios. It is shown that the magnitude of process damping is governed by the nature of surface undulations and thus it varies with the level of excitation and the dynamic response of the structure. Also, the study shows that in hard turning the ratio of deterministic *Ra* to random *Ra* can reach *1:10* for relatively small feeds. This indicates the vital importance of random excitation due to material inhomogeneity. Additional research will be required to verify the calibration of the ploughing model for applications with larger depths of cut.

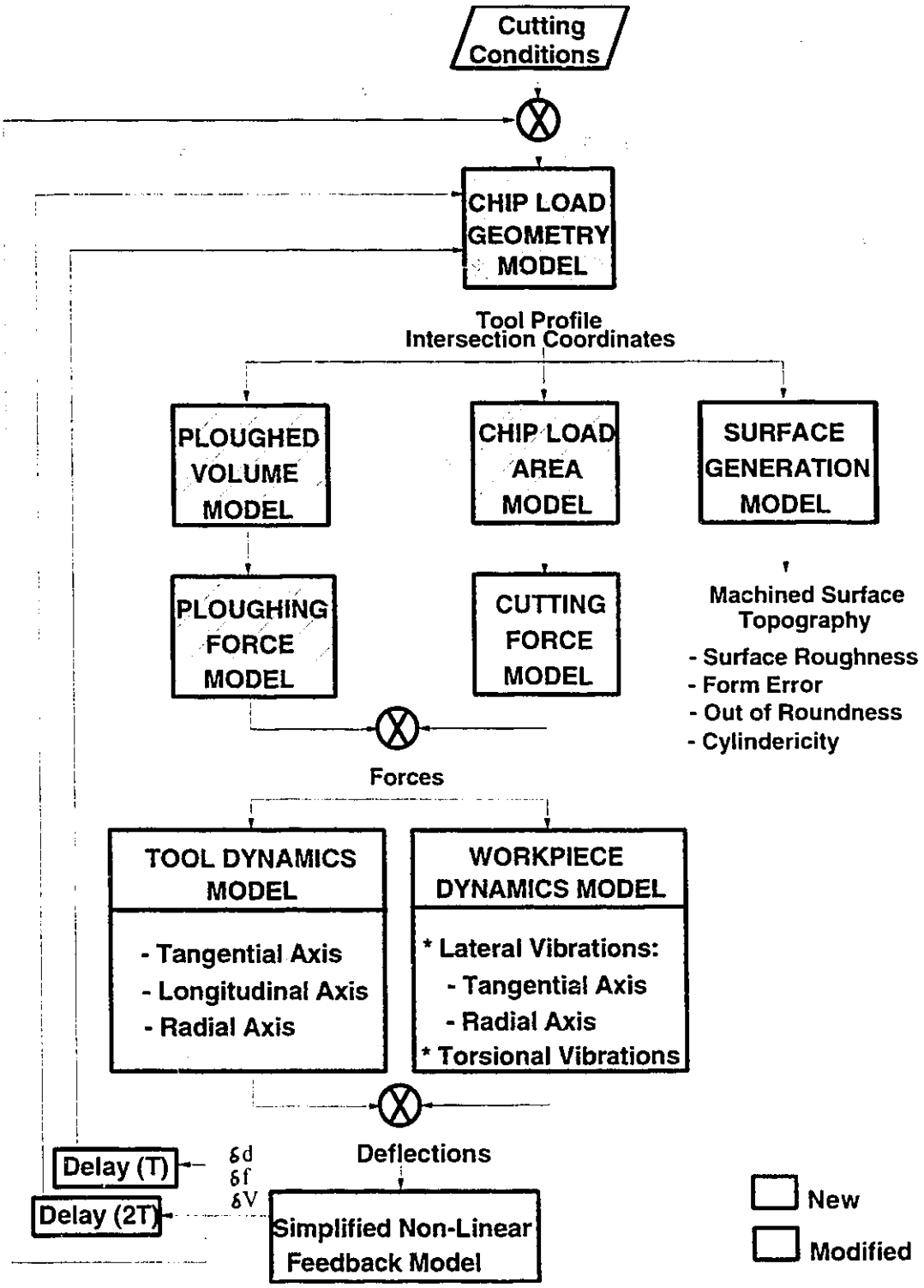

Fig. 3.1 A Block Diagram of the Machining System Enhanced Dynamic Model Structure.

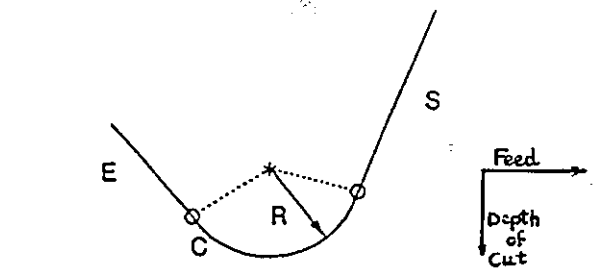

E End Cutting Edge
C Nose Radius
S Side Cutting Edge

Fig. 3.2 Tool Edge Profile P.

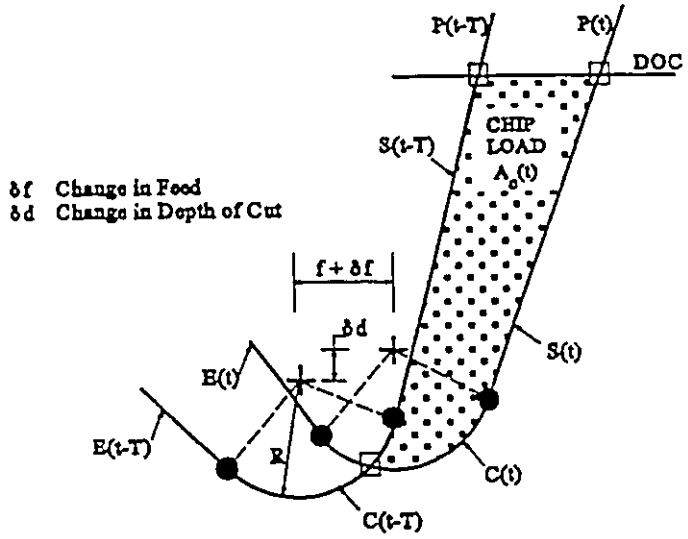

Fig. 3.3 Chip Load Geometry.

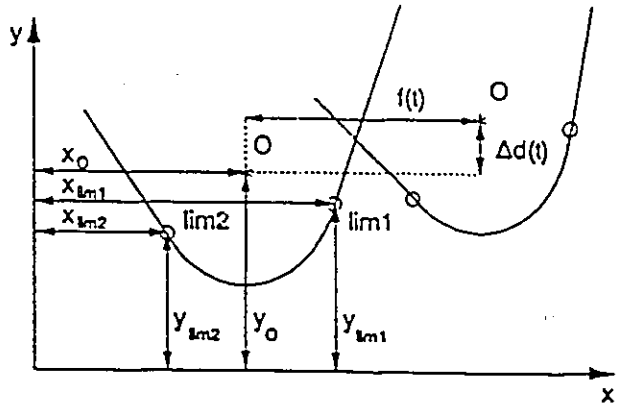

Fig. 3.4 Coordinates of Tool Edge Profiles in the xy-plane.

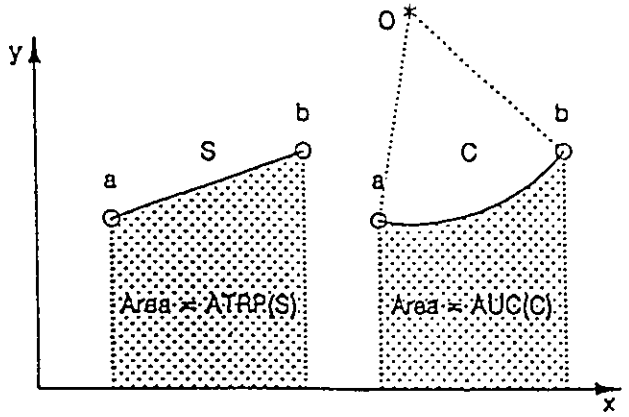

Fig. 3.5 The Two Standard Area Shapes Used in Calculating the Chip Load Area.

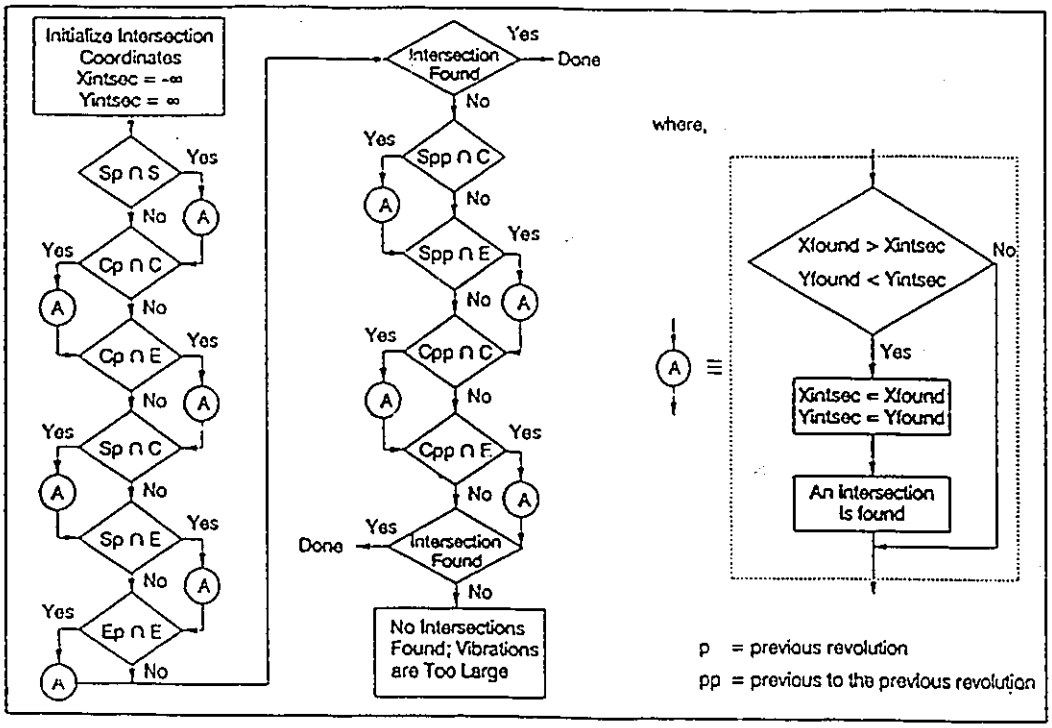

Fig. 3.6 Intersection Search Flow Chart.

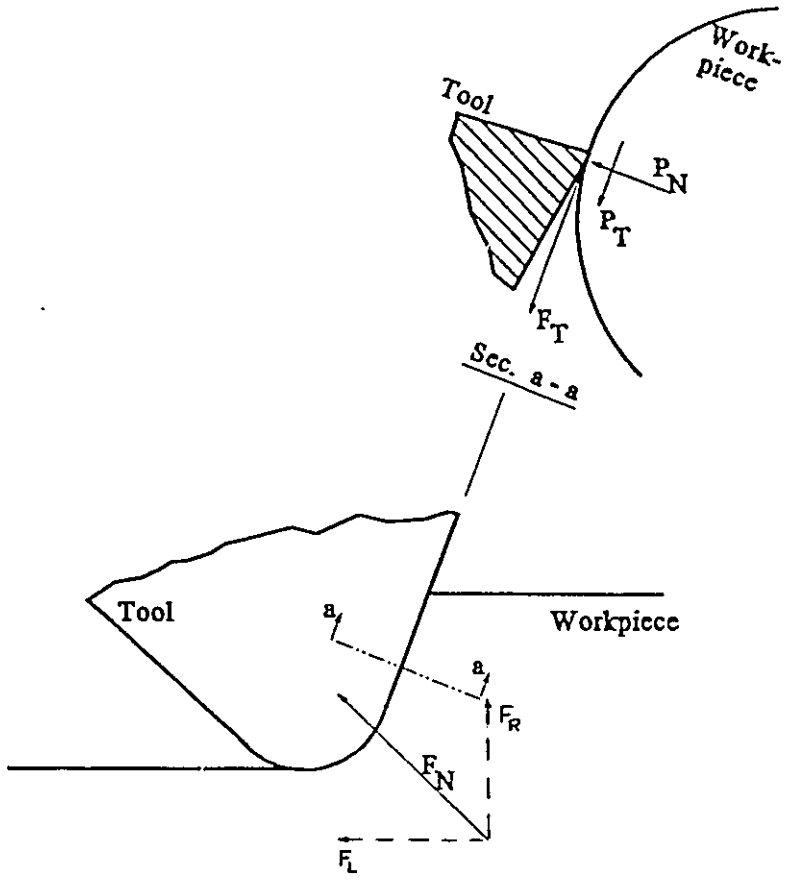

Fig. 3.7 Cutting and Clearance Face Forces.

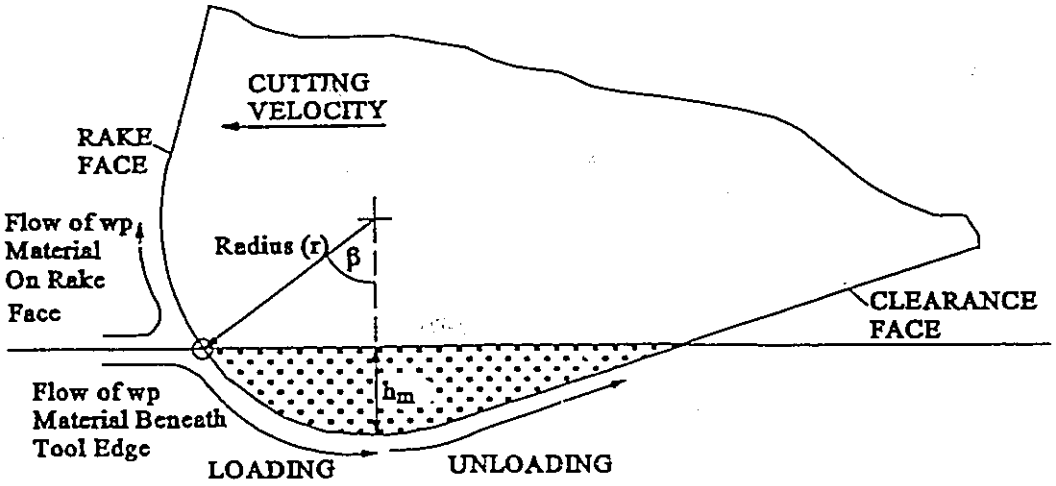

Fig. 3.8 Volumes Extruded Under a Sliding Indentor with a Small Edge Radius *r*.

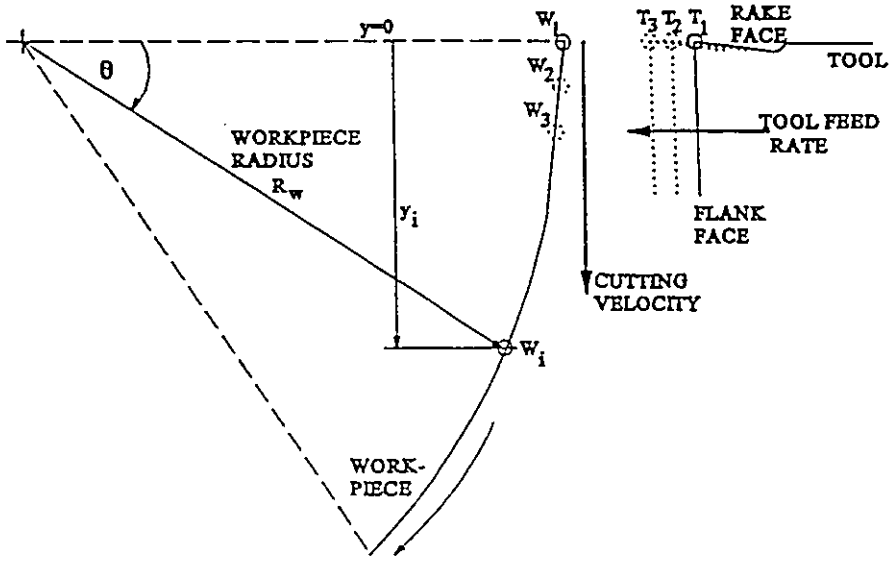

Fig. 3.9 Schematic Diagram Showing the Effect of Tool Feed on Increasing Contact on Clearance Face.

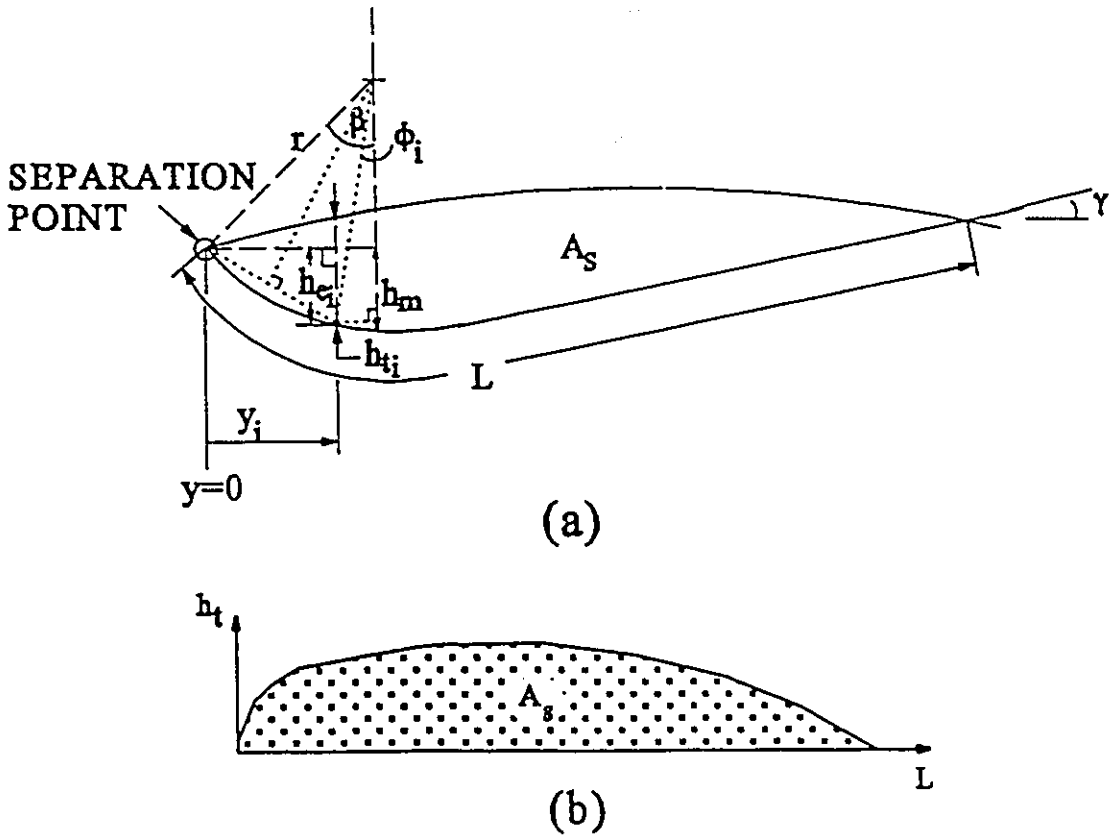

Fig. 3.10 Static Area of Contact A_s.
(a) Clearance Face Contact Geometry.
(b) Total Depth of Penetration h_t.

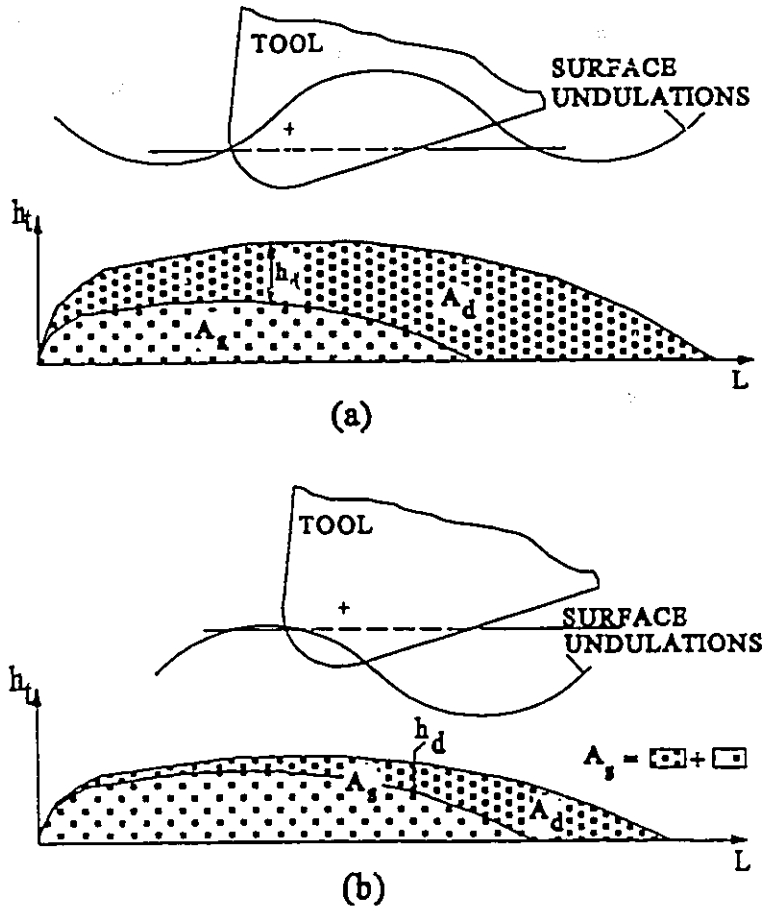

Fig. 3.11 The Dynamic Ploughed Area A_d.
(a) Positive Change.
(b) Negative Change.

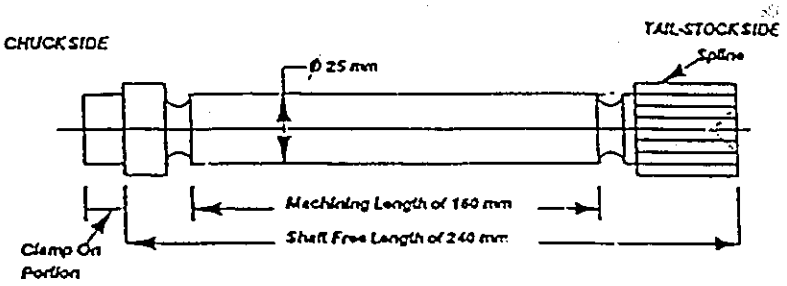

Fig. 3.12 Hardened Steel Workpiece.

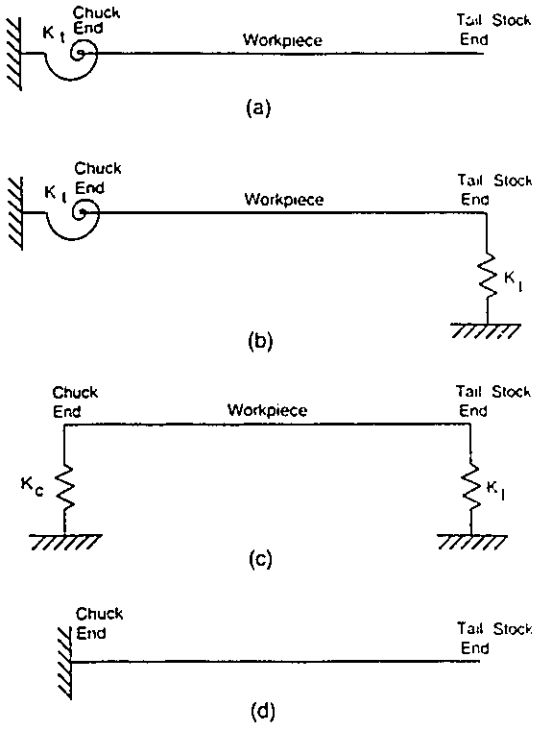

Fig. 3.13 Workpiece Dynamic Models.
(a) Lateral Vibrations of a Free End Workpiece.
(b) Lateral Vibrations of a Centered/Clamped Workpiece.
(c) Lateral Vibrations of Two Ends-Centered Workpiece.
(d) Torsional Vibrations.

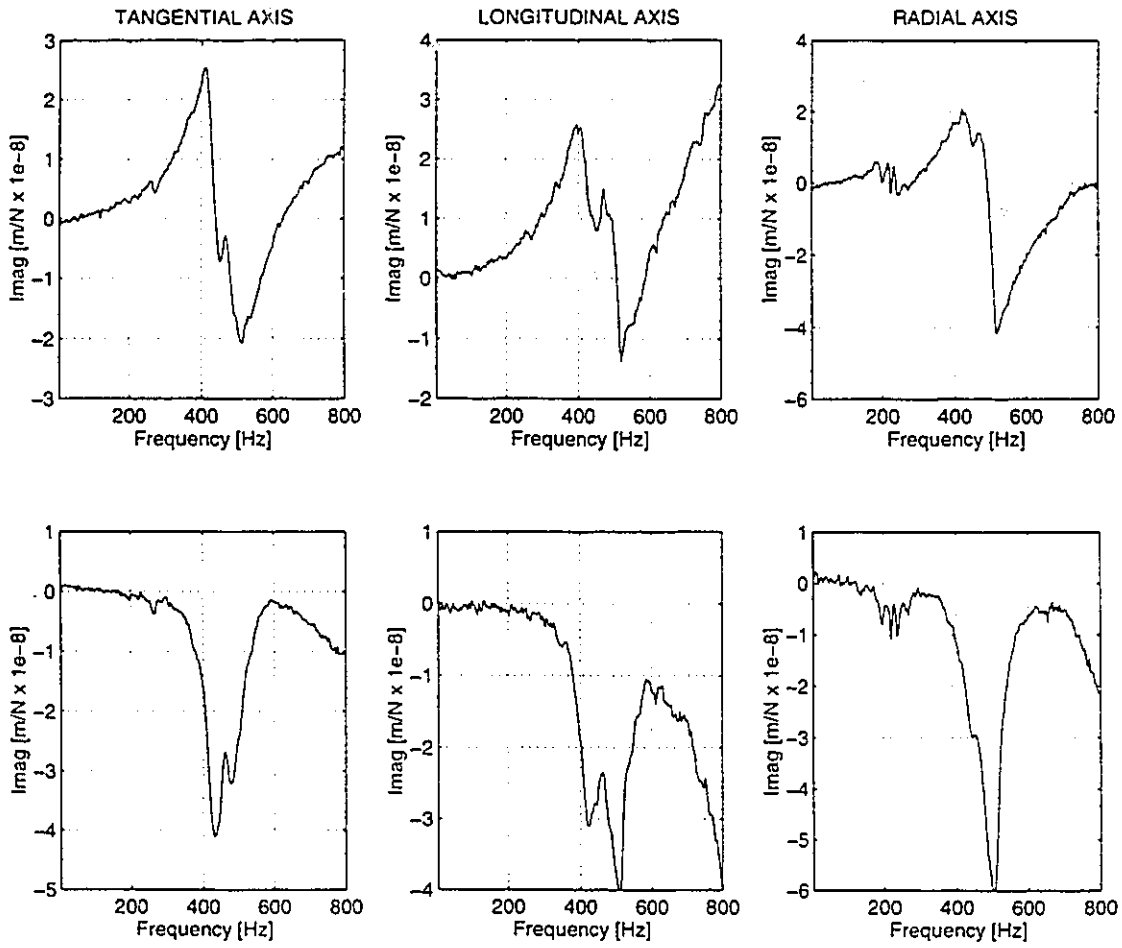

Fig. 3.14 The Structural Transfer Functions of the Tool as Measured in the Tangential, Longitudinal and Radial axes.

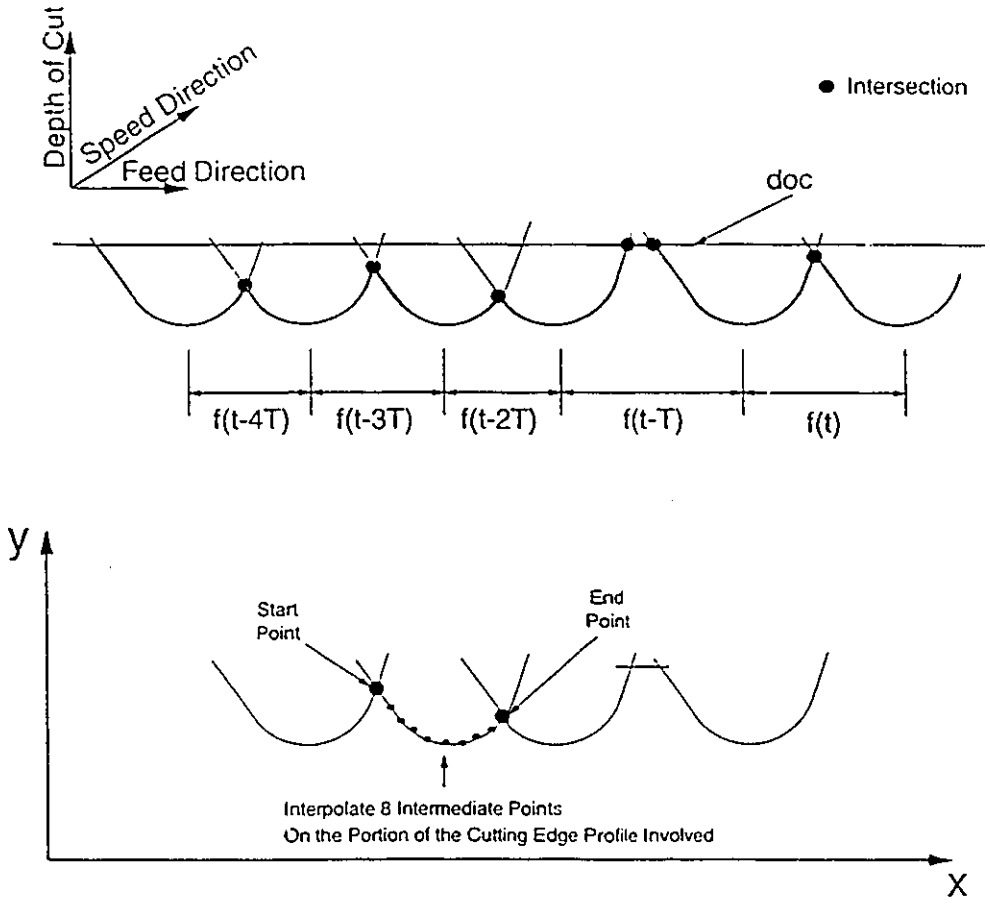

Fig. 3.15 Generation of the Machined Surface.

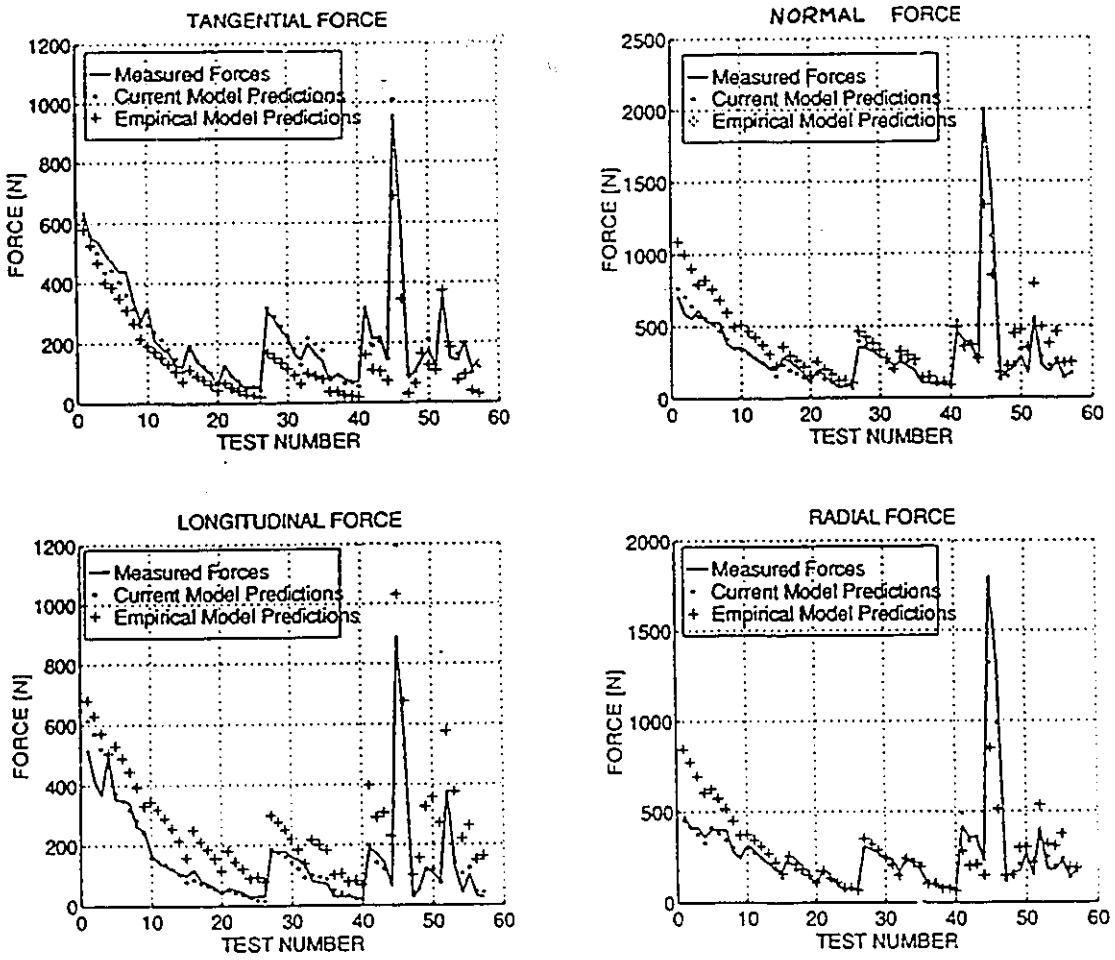

Fig. 3.16 Comparison of the Measured and Predicted Cutting Forces for the Rigid System.

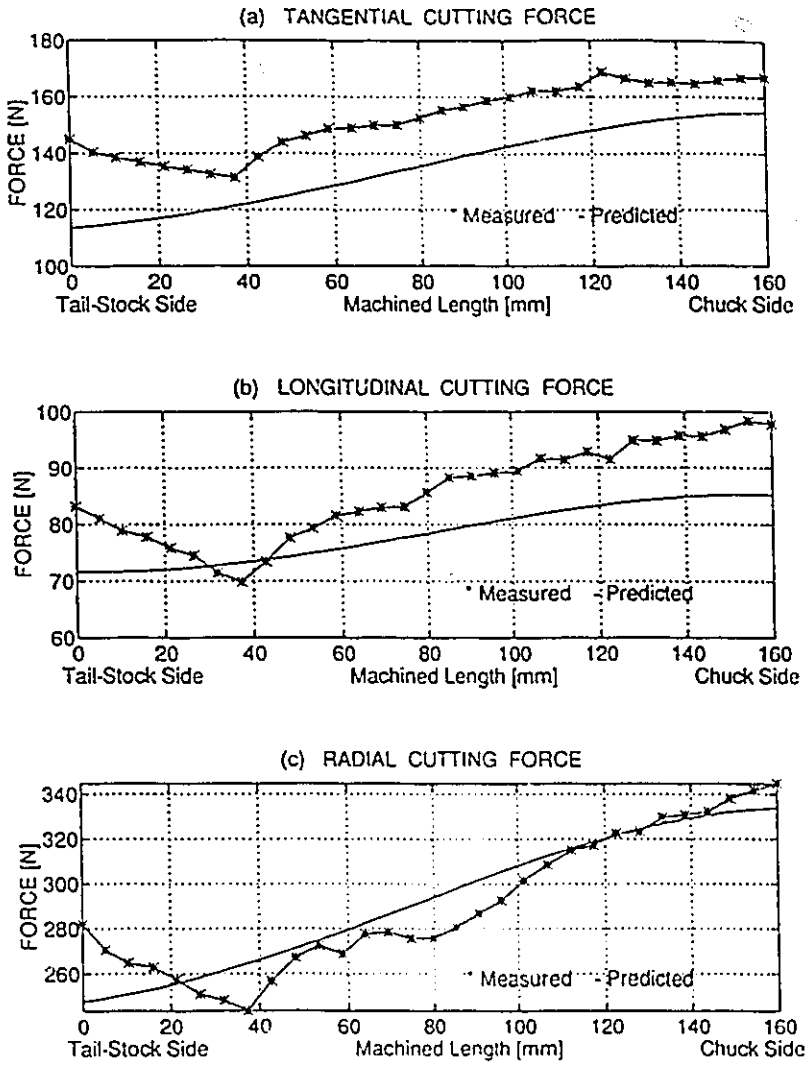

Fig. 3.17 Comparison of Predicted and Measured Cutting Forces along the Workpiece Length. (d=0.25 mm, f=0.0762 mm/rev, V=122 m/min, R=5 mm.)

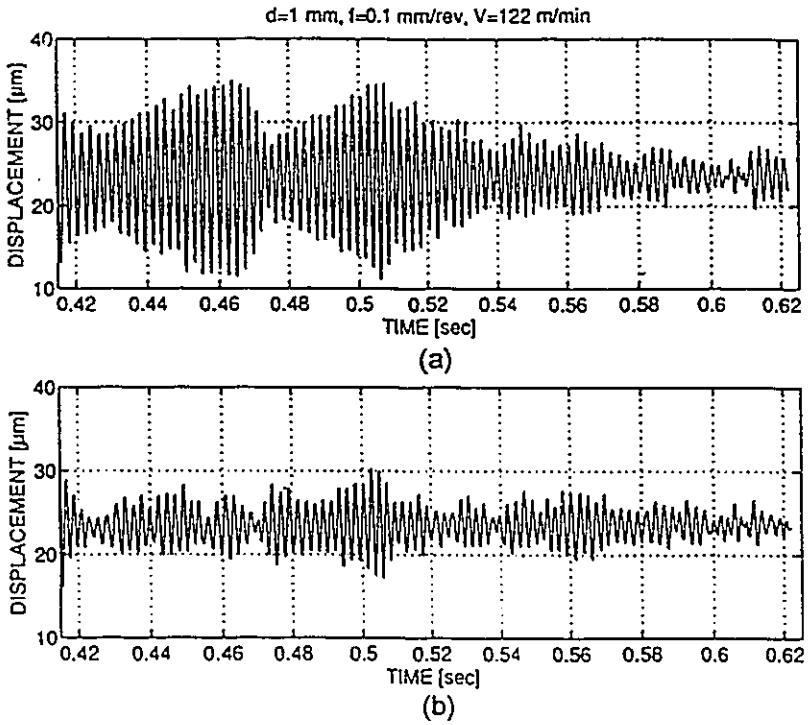

Fig. 3.18 Lateral Tool Vibrations due to a 3% Sudden Increase in the Depth of Cut.
(a) Without Ploughing.
(b) With Ploughing.

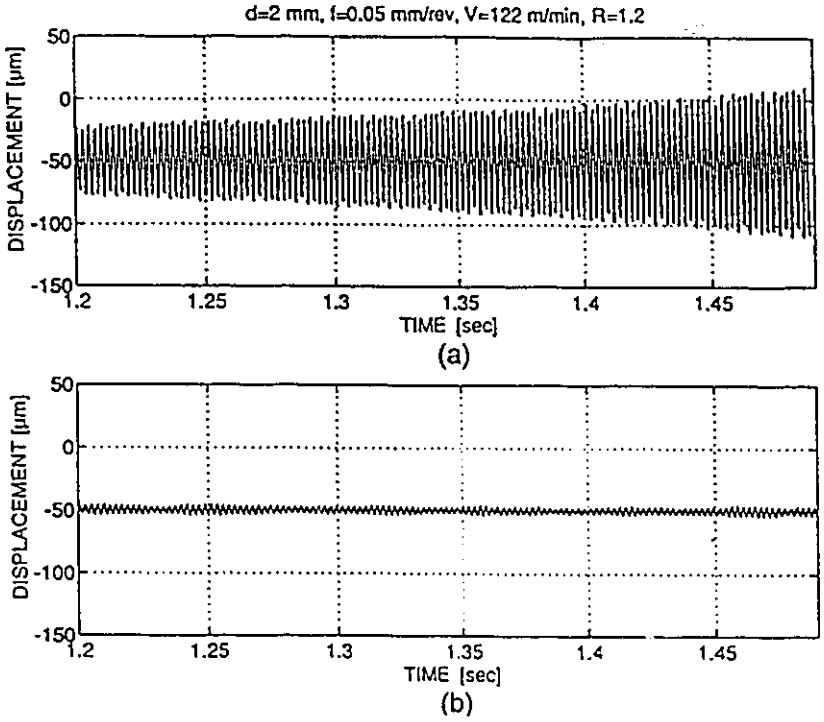

Fig. 3.19 Effect of Process Damping on the Stability Limit and Vibrations due to Chatter.
(a) Without Ploughing.
(b) With Ploughing.

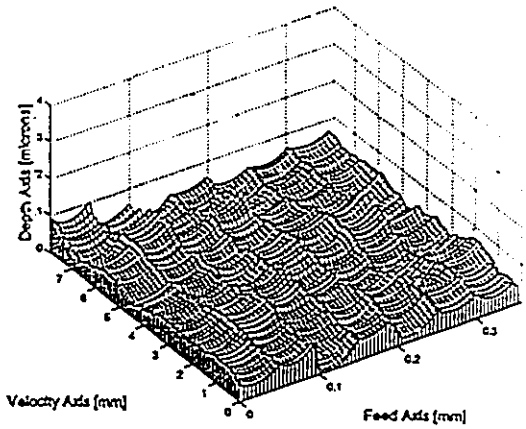

(a) f=0.05 mm/rev, d=0.5 mm, V=120 m/min, R=1.6 mm

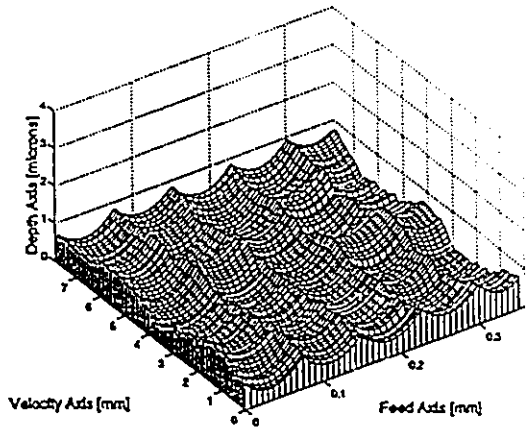

(b) f=0.075 mm/rev, d=0.5 mm, V=120 m/min, R=1.6 mm

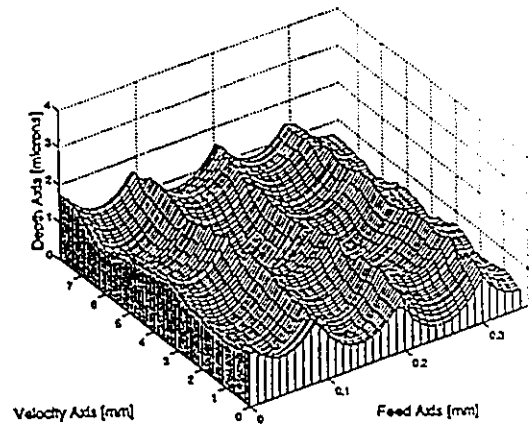

(c) f=0.1 mm/rev, d=0.5 mm, V=120 m/min, R=1.6 mm

Fig. 3.20 Predicted Surface Topographies for different tool feeds.

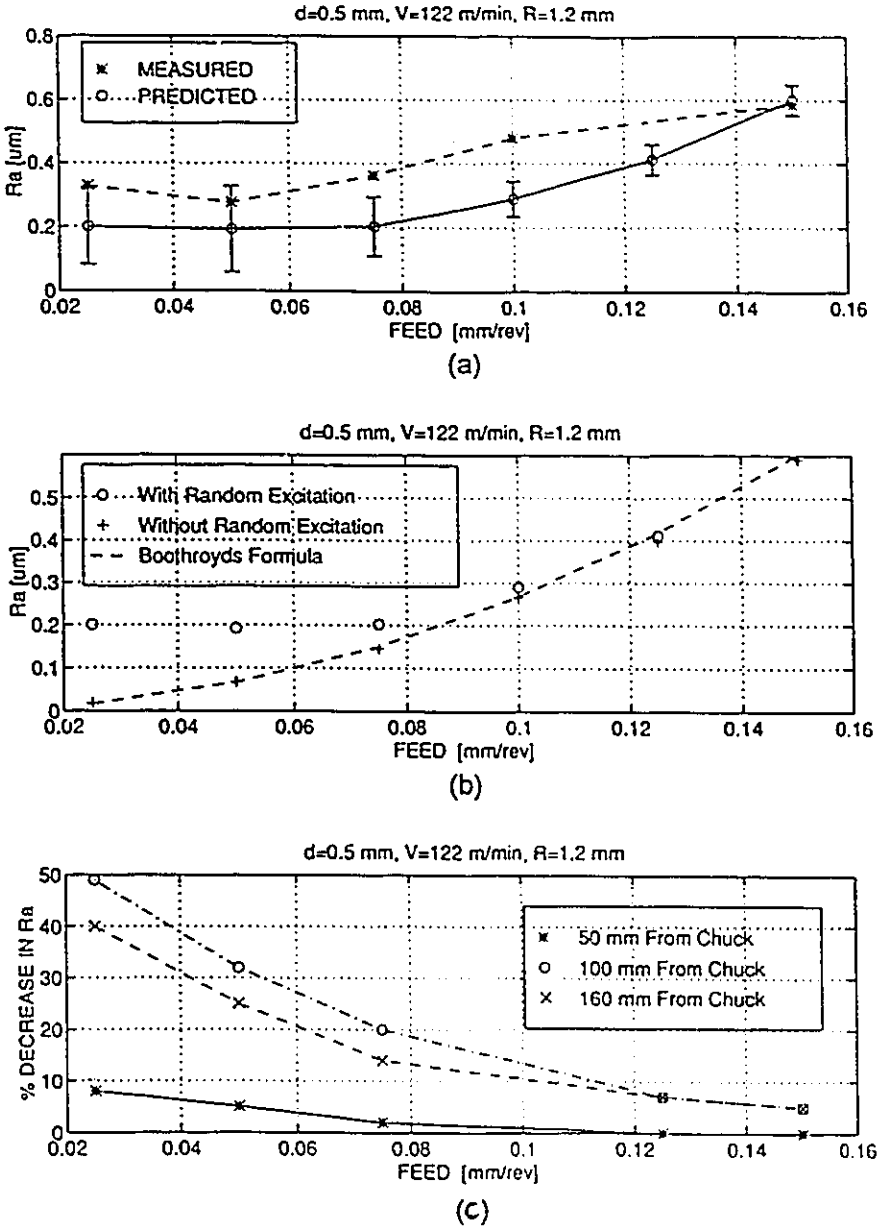

Fig. 3.21 Surface Roughness Results.

(a) Comparison of Predicted and Measured Ra for Different Feed Rates.

(b) Effect of Random Excitation due to Material Inhomogeneity on Ra Predictions.

(c) Percentage Decrease in Ra due to Process Damping.

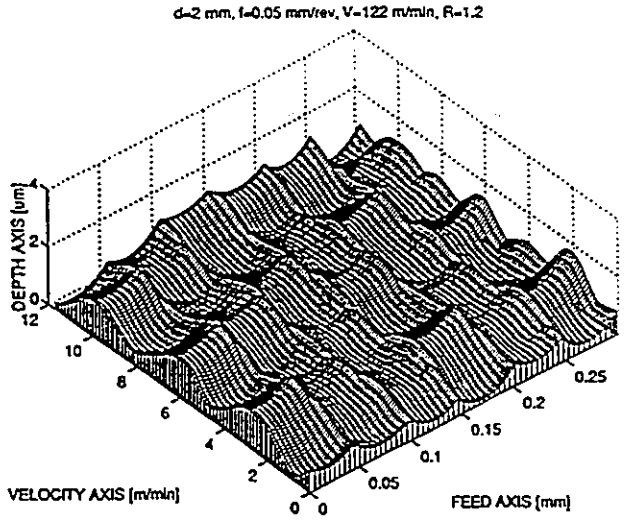

(a)

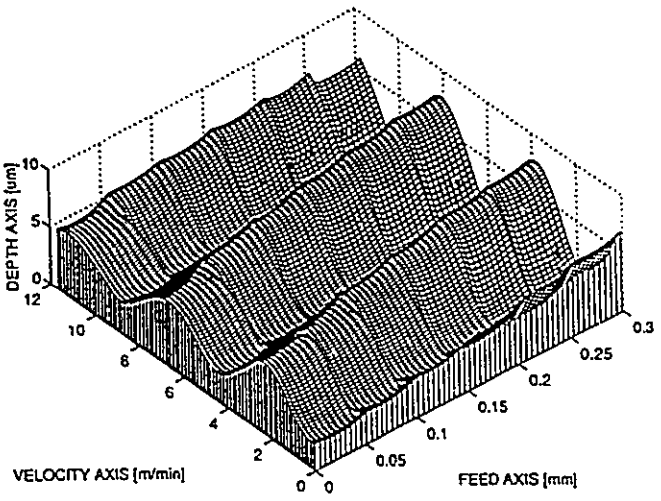

(b)

Fig. 3.22 The Effect of Process Damping on Machined Surface Topography.
(a) With Ploughing.
(b) Without Ploughing.

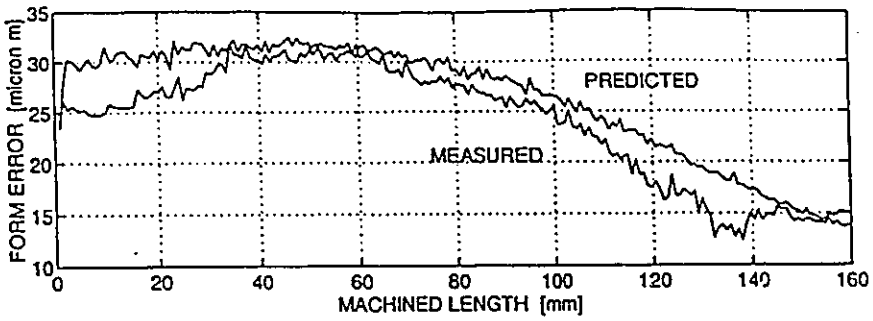

Fig. 3.23 A comparison of the Predicted and Measured Form Error Profiles.

CHAPTER 4

MEASUREMENT SYSTEM DEVELOPMENT

The focus of this chapter is the development of a sensor for on-line measurement of shaft diameter in bar turning while using a cutting fluid (Shawky and Elbestawi, 1994). The measurement is intended primarily for the assessment of machining errors which result from the cutting process itself and not due to machine tool errors. Therefore, a measurement accuracy of ±5 μm (±0.0002") is considered adequate for most practical situations. The measuring system developed is based on three ultrasonic proximity transducers positioned around the workpiece. The measurement is performed with respect to an extrinsic datum. The datum is taken as the locus formed by the longitudinal motion of the intersection point of the sensors center lines.

The chapter begins with a general description of the measurement technique. This is followed by the details of the sensor design, sensor calibration and overall configuration of the measurement system. Next, an error analysis is presented to resolve the measurement error introduced due to translation of the workpiece axis of rotation. An algorithm is proposed to eliminate this error from radius data and provide an absolute measurement of the workpiece diameter.

4.1 PRINCIPLE OF MEASUREMENT

The measurement principle of the sensor developed is based on using an ultrasonic beam as shown in Fig. 4.1. The ultrasonic transducer is simply a piezoelectric crystal that works as both a transmitter and a receiver. When the piezoelectric crystal is excited by a suitably tuned electric impulse it vibrates mechanically at its natural frequency (*MHz* range). This mechanical ultrasonic wave propagates through the material with the speed of sound. Every material has its own acoustic impedance and its boundary with another material represents an interface of acoustical impedance mismatch. Whenever a sound beam reaches an acoustical impedance mismatch, it divides into two beams; a transmitted and a reflected beam. The latter is referred to as the "echo" because it returns back and is received by the transducer. By measuring the time-of-flight elapsed t_f for one round trip of the sound wave and knowing the speed of sound in the material ξ, the distance traveled P_m can be easily calculated from,

$$P_m = \xi * \frac{1}{2} t_f \qquad (4.1)$$

For example, referring to Fig. 4.1, signals '*1*' and '*2*' are called the front-wall echo and the back-wall echo, respectively. A measurement of the time-of-flight of the former can give the distance between the sensor and the workpiece. While the difference in time between the front-wall and back-wall echoes gives a direct (caliper) measurement of the workpiece diameter.

4.2 THE SQUIRTER SYSTEM

Air results in high attenuation of the power of high frequency sound waves. Therefore, air is usually avoided by coupling the probe directly (in contact) to the material surface using grease, or indirectly (non-contact) by immersing both the transducer and the object in water (immersion technique) as shown in Fig. 4.1. An alternative version of the immersion technique is using a squirter system (DeWalle, et al., 1978), which is basically a nozzle (usually seen in sheet metal rolling mills). The squirter method is an immersion technique whereby only the transducer is immersed in the coupling fluid. The ultrasonic transducer is fixed inside the squirter (coaxially) as shown in Fig. 4.2. The coupling fluid exits from the nozzle tip (which is pointed towards the target) to fill the air gap between the sensor and the workpiece with column of fluid. A relatively resized miniature squirter (compared to the ones normally seen in industry) is used in this application and uses the cutting fluid as its coupling medium to enable incorporating it into a CNC lathe. Care has been taken in resizing the squirter to achieve a smooth uniform flow in the vicinity in front of the transducer (i.e., in chamber '2' as illustrated in Fig. 4.2) to minimize turbulence and eliminate air bubbles which could stop the ultrasonic beam from reaching its target.

4.3 DIRECT VERSUS INDIRECT MEASUREMENT

In the development process of the first sensor prototype, difference in performance using the two measurement techniques illustrated in Fig. 4.1 (namely, "direct" versus "indirect" measurement) has been investigated experimentally. Based on the findings of this study the indirect method using three proximity probes was chosen. Although, using both

the front-wall and back-wall echoes provides a direct "calliper" measurement of the shaft diameter and seems more attractive for a first glance, it suffers accuracy deterioration due to the following limitations:

- Unrecoverable measurement error can result if the ultrasonic beam does not pass through the center of the workpiece due to any sensor/workpiece misalignment which may result during cutting. This represents the situation of measuring a chord of a circle rather than measuring its true diameter.
- The attenuation of the ultrasonic signal in the workpiece material is very high and increases with higher frequencies. (Note that high frequency signals are required for higher dimensional accuracy.) Such attenuation results in low amplitude (and thus, low signal to noise ratio) of the back-wall echo and can even lead to a complete loss of the signal for larger diameters specially in the case of steel workpieces.
- Slight change in the frequency content of the signal from the front-wall to the back-wall, due to filtration within the workpiece material, causes a dissimilarity in the rise-time of both signals. This leads to errors in the time-of-flight measurement of the order of nano-seconds which is intolerable.
- Microstructural variations in steel workpieces from one batch to the next causes slight but also intolerable variation in the speed of sound which would require a different calibration for every material batch.
- Variation of the sound speed in the workpiece material due to temperature changes during cutting.

Accordingly, the proximity (indirect) measurement was chosen because of its independence of the behavior of the ultrasonic signal in the workpiece material, which simplifies the problem.

4.4 SENSOR DESIGN

The normal sound beam from a planar transducer would suffer beam spreading as shown in Fig. 4.3a. The four transducers used in this work are identical; *10 MHz* natural frequency, *10 mm* diameter piezoelectric "self-focusing" element with *30 mm* focal length which results in a focal diameter of *0.370 mm* (according to ASNT, 1991). Focusing is normally used to concentrate energy from an acoustic beam into a small area as shown in Fig. 4.3b. The focal diameter can be further reduced by either increasing the element diameter or decreasing the focal length. The range of the proximity sensor is limited to *10 mm* which corresponds to *20 mm* range of the workpiece diameter. Such limitation is imposed by two aspects: first, the length of the sound beam portion before and after the focal point which has a uniform beam diameter (refer to Fig. 4.3b); and second, the maximum length of the cutting fluid column between the nozzle tip and the workpiece surface which can be kept straight (note that this is most crucial for a nozzle in the horizontal position where gravity can cause the fluid column to bend downwards). Figure 4.4 shows the shift of the front surface signal in the time domain corresponding to changes of *0.0254 mm* (*0.001"*) and *0.1016 mm* (*0.004"*) in the sensor proximity from the workpiece.

4.5 CONFIGURATION OF THE MEASUREMENT SYSTEM

The sensors are incorporated into a LeBlond, *20 hp* CNC lathe, retrofitted with a VME-bus Open Architecture Controller (OAC) hosted on an MC68030. Three sensors are positioned at the same cross section around the workpiece and at the angles shown in Fig. 4.5. A rigid fixture is designed to position the three sensors around the workpiece while being fixed to the carriage and not in contact with the cross-slide, thus, making the sensors independent of the radial position of the tool, but still able to travel with the carriage motion longitudinally along the machine. The fixture of the sensor is designed to enable manual adjustment of each sensor position individually in three rotations and two translations as shown in Fig. 4.6. In addition, coarse manual rotation around the machine axis is possible for setting up each sensor at the required angle as indicated in Fig. 4.5.

The sensors are pointed exactly towards the center line of the machine. This setting is finely adjusted by using a master bar as a target for the sensors. The master bar has a calibrated diameter d_m and has been cut carefully on the same machine tool to minimize workpiece runout. To adjust the sensors in their exact positions, the reflected signal has to be maximized by tilting each squirter finely back and forth as shown in Fig. 4.7. This process has to be performed in both longitudinal and transverse planes. If the proximities of the three sensors from the master bar are P_{m1}, P_{m2}, and P_{m3}, then each of the sensors is away from the center line of the machine by P_{d1}, P_{d2} and P_{d3}, thus

$$P_{d_i} = \frac{d_m}{2} + P_{m_i} \qquad \textbf{(4.2)}$$

where, the suffix 'i' indicates the sensor number. The locus of the longitudinal translation

of the center of the sensors is taken as an extrinsic datum for the measurement throughout this work. This datum may not coincide with the machine axis at some points due to both spindle runout and misalignment in the carriage travel within *1 μm*.

A fourth sensor is used for the calibration of the sound velocity in the cutting fluid. This will be explained further in the next section.

4.6 INFLUENCE OF THE CUTTING FLUID

The cutting fluid plays a major role in transmitting the sound waves to the workpiece surface, and hence, its condition is crucial to the system performance. The velocity of sound in the cutting fluid is calibrated using the mechanism shown in Fig. 4.8. A fourth squirter is used to calibrate the system using a dial gauge (with a resolution of *2 μm/div*). The sound velocity is finely tuned, so that when the sliding block is moved, the measurement indicated by the ultrasonic sensor is identical to that indicated by the dial gauge.

The velocity calibration for the cutting fluid has been monitored for cutting periods of one hour long, and no change was observed within an accuracy of *5 μm*. In addition, an experiment was carried out to check the change in sound velocity corresponding to a variation in the cutting fluid temperature within a range of *20-37 °C*. Such temperature fluctuation can very well occur due to seasonal changes in poorly controlled workshop room temperatures. However, the experiment failed to show any change. This indicated that practically fluctuations in cutting fluid temperature under normal shop floor conditions are insignificant within the sensor accuracy.

An efficient filtering system is also used to maintain the integrity of the cutting fluid

from contamination by metal chips and dust. The pump tank system used has four baffles, to allow settling down of any suspended particles, in addition to a *150*-sieve filter which has a mesh size of *97 μm* and a magnetic core to attract any minute unfiltered metallic particles.

4.7 SIGNAL PROCESSING AND COMPUTER INTERFACING

The signal processing unit is basically a counter which counts the number of clock ticks between the transmission and the reception of a signal. Refer to the block diagram shown in Fig. 4.9. The signal level is checked by a comparator set at a threshold level. The counter circuitry has an oscillator of *400 MHz* and serves three channels. Every ten measurements per channel the counts are averaged to help eliminate the random errors. The average number of counts is converted into dimensional units (*μm*) with a dead band of *5 μm*, representing the sensor accuracy. The data is transferred to the VME-bus system through a double buffered *16-bit* parallel interface. The handshake protocol is handled by a *16 MHz* programmable chip through two handshake lines. The complete cycle time for three channel measurements including handshaking for data transfer and ten averages per channel is *2.16 ms*. Thus, if a workpiece is running at a cutting speed *V*, then the circumferential distance covered per reading is l_{cir} *[mm/measurement]*, where,

$$l_{cir} = \frac{V\ [m/\min] * 0.216\ [ms]}{60} \tag{4.3}$$

i.e., at *V=110 m/min*, l_{cir}*=0.4 mm/measurement* which is averaged ten times to give a reading every *4 mm*. This in effect approximates the act of a low pass filter for the measurements, as it averages out only the high frequency components of the out-of-roundness. It should be

noted that the measurements are inherently digital, and thus the only way to minimize aliasing effects is to sample as fast as possible. The maximum sampled frequency depends on the cutting speed and the workpiece diameter. Considering the example given above, if the workpiece diameter was as small as *30 mm*, then frequencies up to nine lobes (which is relatively high; Wilson, 1992) would not be aliased.

4.8 MISALIGNMENT ERROR ANALYSIS

Having the measurement system based on radius change measurement rather than direct diameter measurement, makes it sensitive to unwanted and uncontrollable workpiece axis motions. Such motion can be caused by spindle runout or workpiece-tool system vibrations resulting in relatively high frequency measurement errors. On the other hand, a more significant measurement error (specially in the case of slender workpieces) is the translation of the axis of rotation due to structural deflection under the effect of cutting forces. The amount of deflection depends on the stiffness of both the machine tool clamping system components and the workpiece. Thus, the magnitude of this translation varies from one cutting tool position to the next along the cutting length. Such effect results in a relatively large misalignment between the sensor and the generated workpiece surface (i.e., axis of rotation) causing a low frequency error in the measurement along the length of the cut. This type of measurement error is unique because it is only encountered in on-line measurements when the workpiece is loaded by the cutting tool. The following error analysis explains the method used to eliminate this error from the measurement .

Ideally, the axis of rotation of the workpiece coincides with the locus of the

intersection point of the sensor centerlines along the cut. This locus forms the datum for the measurement. In such ideal situation one sensor is sufficient for measuring the diameter of the workpiece, as shown in Fig. 4.10, and the absolute diameter d_{wp} is given by,

$$d_{wp} = 2 * P_d - P_m(0) - P_m(180) \tag{4.4}$$

where, P_d is the calibrated distance from the sensor to the measurement datum, $P_m(0)$ and $P_m(180)$ are the sensor proximities from the workpiece measured at $180°$ apart.

In Fig. 4.11, the workpiece cross-section, of radius R_{wp}, is represented by a circle of center 'm' concentric with the center of the sensors (i.e., the measurement datum). The three proximity measurements on circle 'm' would give the true workpiece radius R_{wp} by,

$$R_{wp} = P_{d_i} - P_{m_i} \tag{4.5}$$

However, due to misalignment error the workpiece cross-section of center 'm' is displaced by dx and dy to center 'n'. This results in erroneous measurements r_1, r_2, and r_3 with errors of e_1, e_2, and e_3, respectively. To correct for these errors, the three points Z_1, Z_2 and Z_3 which lie on circle 'n' are considered. The xy-coordinates of these three points are determined from,

$$\begin{aligned} x_i &= r_i * \cos\theta_i \\ y_i &= r_i * \sin\theta_i \end{aligned} \tag{4.6}$$

where, θ_i is the orientation angle of the respective sensor as illustrated in Fig. 4.11, and

$$r_i = P_{d_i} - P_{m_i} \tag{4.7}$$

where, P_d is given from the calibration, and P_m is the measured signal. Hence, the xy-

coordinates of the points Z_1, Z_2 and Z_3 are used to solve the circle equation given by,

$$x^2 + y^2 + ax + by + c = 0 \tag{4.8}$$

and find the constants a, b, and c as follows:

$$A_1 = x_2^2 + y_2^2 - (x_1^2 + y_1^2) \tag{4.9}$$

$$A_2 = \left(\frac{x_1 - x_2}{y_2 - y_1}\right) * (y_3 - y_1) - x_1 + x_3 \tag{4.10}$$

$$A_3 = x_3^2 + y_3^2 - (x_1^2 + y_1^2) + \left(\frac{y1 - y3}{y2 - y1}\right) . A_1 \tag{4.11}$$

$$a = -\frac{A_3}{A_2} \tag{4.12}$$

$$b = -\frac{1}{(y_2 - y_1)} * \left(A_1 + a(x_2 - x_1)\right) \tag{4.13}$$

$$c = -(x_1^2 + y_1^2 + a x_1 + b y_1) \tag{4.14}$$

The workpiece radius is finally determined from,

$$R_{wp} = \sqrt{x_n^2 + y_n^2 - c}$$
$$x_n = -\frac{a}{2} \quad , \quad y_n = -\frac{b}{2} \tag{4.15}$$

where, x_n and y_n are the coordinates of the displaced circle center 'n'.

In this algorithm it is assumed that the misalignment is much larger in amplitude than the out-of-roundness of the workpiece. Therefore, it is suitable for slender workpieces which suffer relatively large translations in their axis of rotation during cutting.

4.9 EXPERIMENTAL RESULTS

The three sensors were positioned in the angular orientations shown in Fig. 4.5 with θ_1, θ_2, and θ_3 equal to *268.5*, *173.32*, and *60.86°*, respectively. The performance of the sensor was first checked for different proximities from the workpiece while it is being rotated at *500 rpm*. The measurements confirmed that the sensor has a stable working range of up to *10 mm* away from the workpiece surface. Beyond this range, the sound beam suffers scattering which weakens the signal and makes it more vulnerable to disturbances in the coupling medium.

All cutting tests were performed with the workpiece held between two centers. The length of cut varied for different experiments, but all the workpieces were AISI 1045 steel, *610 mm* (*24 in*) long. Also, a feed and speed of 151 mm/min and 500 rpm were used in all the experiments. Figure 4.12a, 4.12b, and 4.12c present the proximity results of the three sensors measured during cutting using *1.27 mm* depth of cut. In the figure, two abrupt changes in the signal levels can be noticed at the start and end of the cut. Further examination of these abrupt changes (with respect to their amplitudes and the angular orientations of the sensors) reveals that the workpiece translated in the horizontal plane (inwards) a small distance *dx* and in the vertical plane (upwards) a larger distance *dy*. The resultant of these two translations points roughly in the direction of the resultant cutting force.

In order to demonstrate the effectiveness of the developed algorithm in canceling the effect of workpiece translation and accounting for the measurement errors induced, more experiments were performed. Each experiment includes two measurement passes; one takes place during the cutting pass while the second follows with the same cutting feed and speed

but with the tool retracted away from the workpiece. The proximity data captured is then processed using the algorithm (Eqs. 4.6-4.15) to provide the corrected diameter measurements. The data presented in Figs. 4.13a and 4.13b show the results of two experiments using two different depths of cut, 1.27 and 0.635 mm, respectively. It can be observed that the effect of workpiece misalignment is eliminated and that both measurements during and after the cut are in very good agreement. Figures 4.13a and 4.13b show a total diameter variation of *50* and *35* μm, respectively, over a cutting length of *279 mm* (*11 in*).

Figure 4.14 presents a comparison of the diameter variation measured off-line using a CMM with that measured on-line, using the ultrasonic sensor (with *500 rpm*, *151 mm/min* feed rate and with no cutting). Both results are in good agreement within a tolerance of $5\mu m$. The repeatability of the measurements was tested by running a number of experiments with measurements taken during and after the cut for the same surface profile. The results of the repeatability tests are shown in Fig. 4.15a and 4.15b. Each set of measurements is presented by a best fit (second order) curve for clarity. The curves marked '*a*' were measured during cutting while those marked '*b*' and '*c*' were measured after the cut. It can be seen that the diameter measurements are repeatable within the proposed accuracy.

In addition to diameter measurement, form tolerances are essential for the assessment of geometrical accuracy of the machined surface profile. Specifically, "cylindricity" has always been a very useful geometric parameter because it has the potential for analysis of total form geometry (Dawson, 1992). On-line measurements obtained during cutting using the ultrasonic sensor can be transformed to represent the machined surface in 3-dimensional (3D) coordinates. Fig. 4.16 shows a 3D plot of the workpiece measurements presented in Fig. 4.13b. For improved visual representation, the two axes representing the workpiece

radius are scaled down (actual radius minus *19.3 mm*). The 3D information can be used to evaluate cylindricity tolerance of the workpiece after each cutting path using a mathematical model of the workpiece surface. Modeling of the workpiece surface for such application is usually based on non-linear optimization techniques to fit the data to the minimum tolerance zone. This work is the subject of the next chapter.

4.10 SUMMARY

An on-line ultrasonic multi-probe system was developed for the absolute measurement of workpiece diameter in bar turning while using cutting fluid. The absolute measurement of the diameter is based on an extrinsic datum represented by the center of the sensors. An algorithm was developed and used to account for misalignment error due to the translation of the rotation axis during cutting. The measurement system was tested under real cutting conditions and the results showed good agreement with off-line measurements using a CMM. The sensor diameter measurements were found to be accurate within ± 5 μm and have a stable working range of *20 mm*.

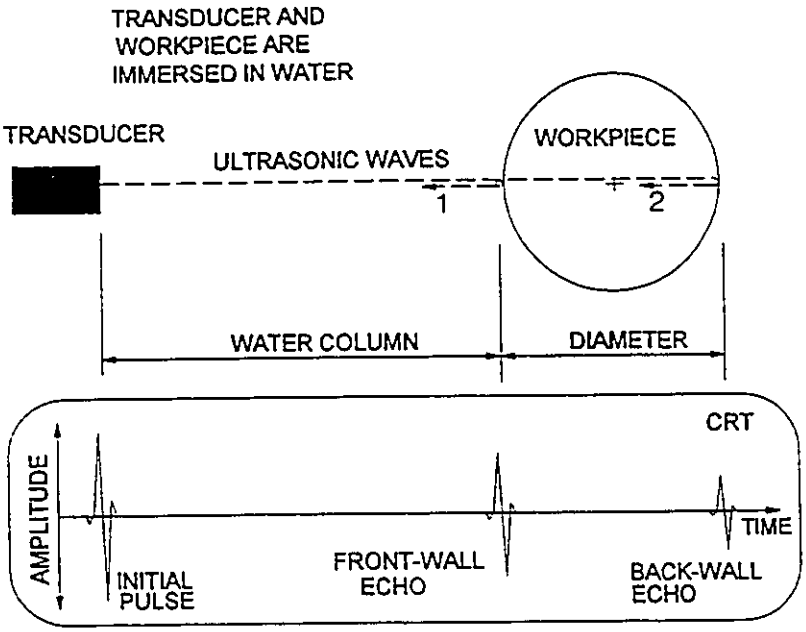

Fig. 4.1 Principle of Measurement Using Ultrasonic Waves.

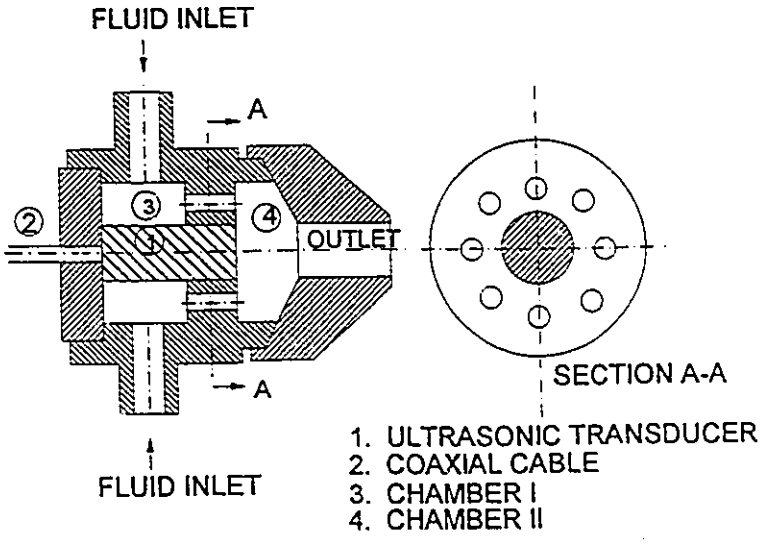

Fig. 4.2 The Squirter Containing the Ultrasonic Transducer.

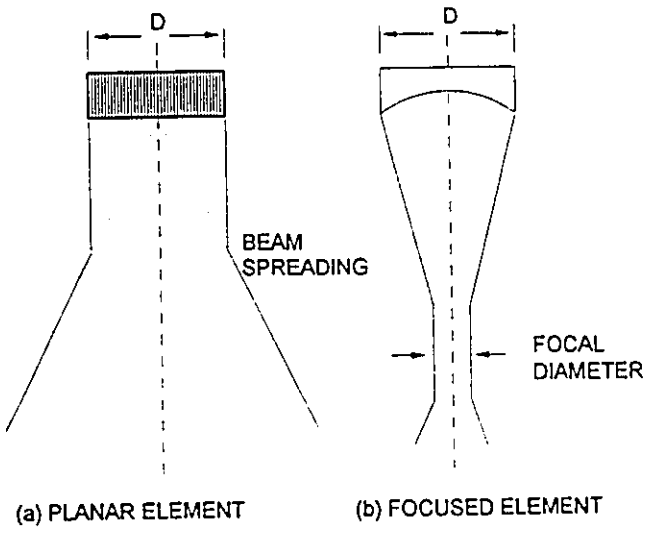

Fig. 4.3 Focusing a Sound Beam to Concentrate its Energy.

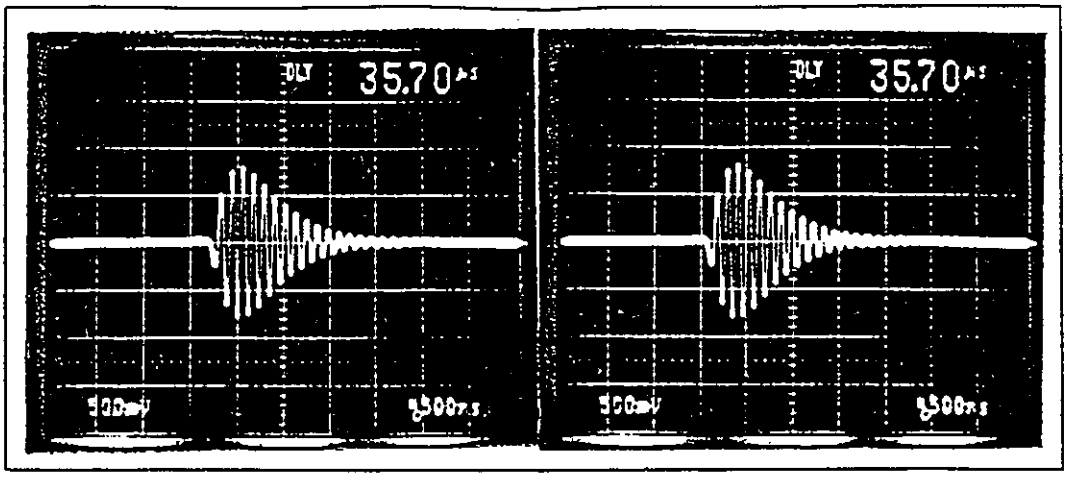

(a)

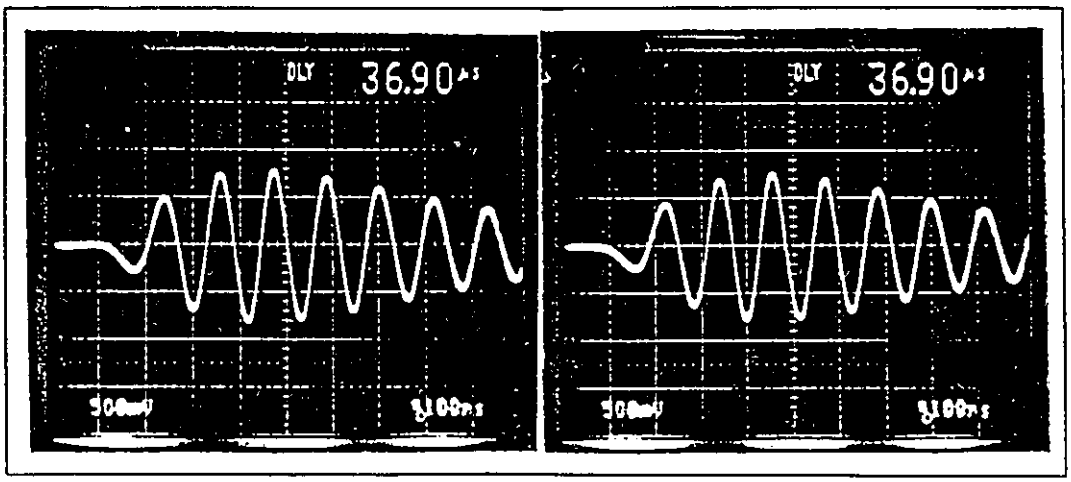

(b)

Fig. 4.4 Shift of the Reflected Signal in the Time Domain
(a) Corresponding to 0.1016 mm (0.004").
(b) Corresponding to 0.0254 mm (0.001").

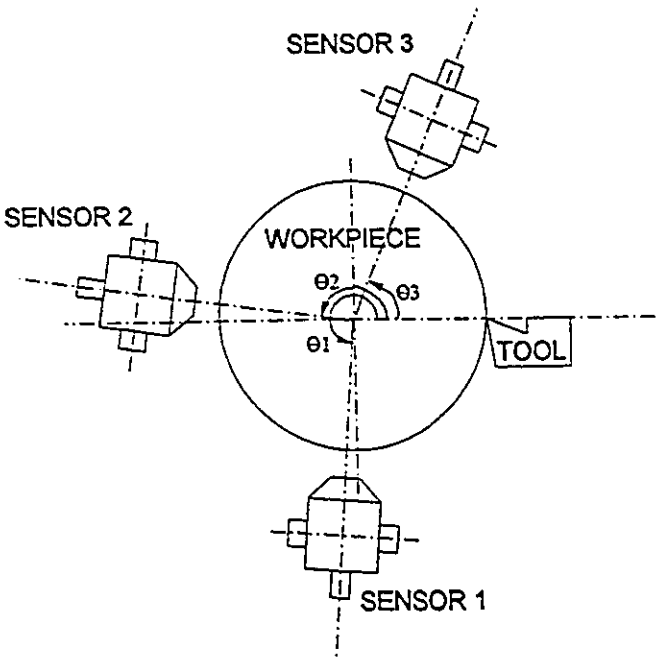

Fig. 4.5 Configuration of the Three Sensors Around the Workpiece.

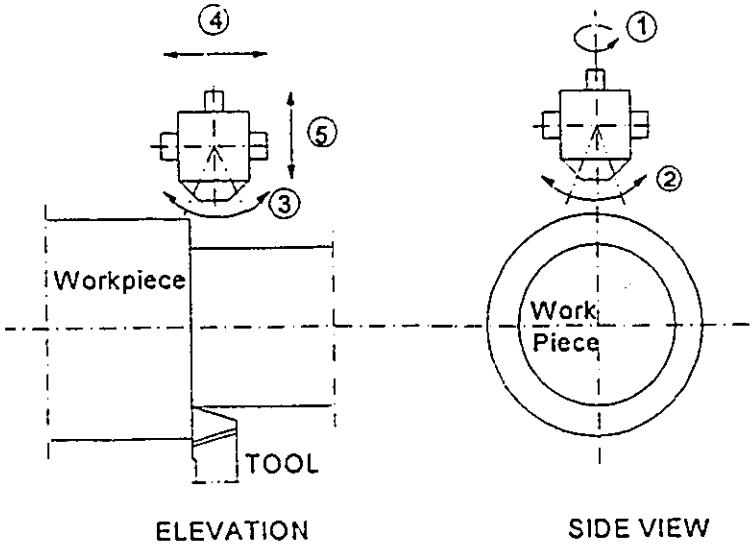

Fig. 4.6 Sensor Location Fixture.

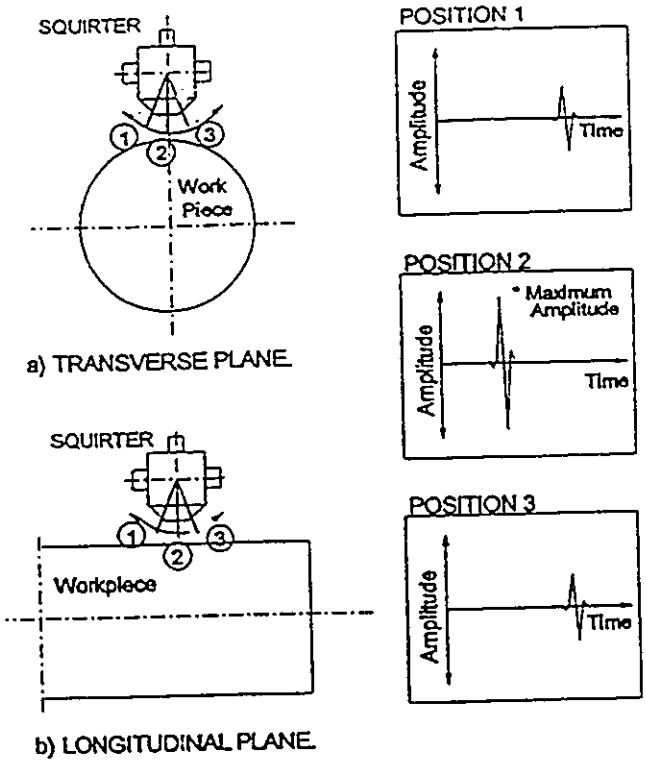

Fig. 4.7 Adjusting the Sensor Position by Maximizing the Reflected Signal.

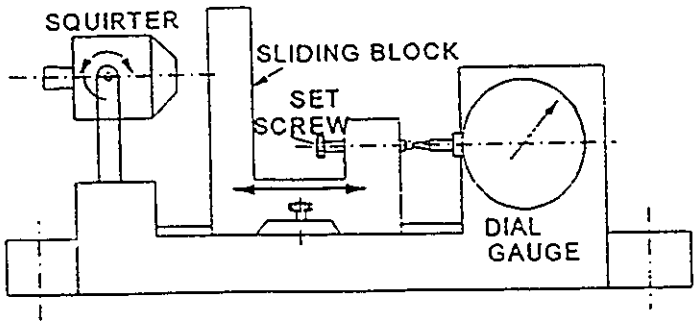

Fig. 4.8 Velocity Calibration System.

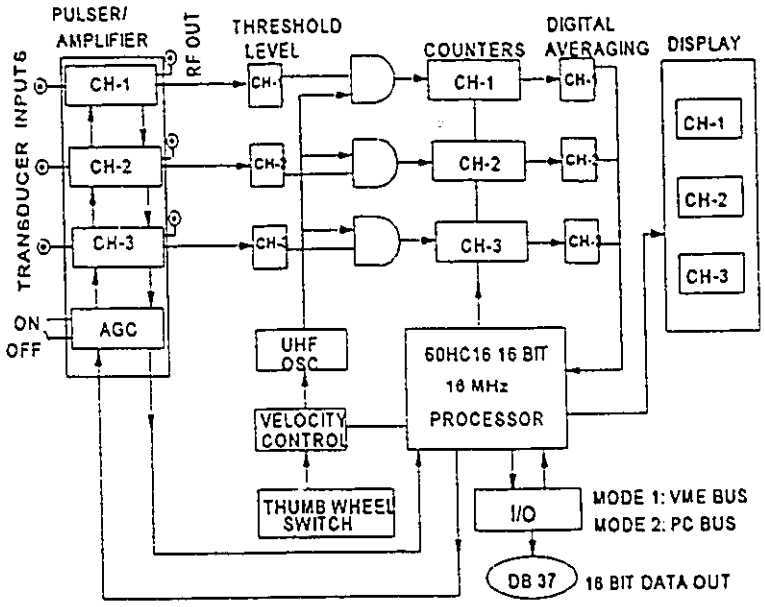

Fig. 4.9 Digital Signal Processing Block Diagram.

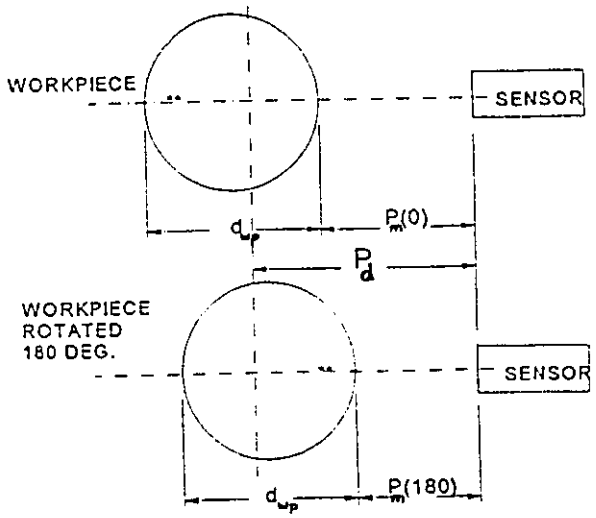

Fig. 4.10 Measurement of Workpiece Diameter in Ideal Rotating Conditions.

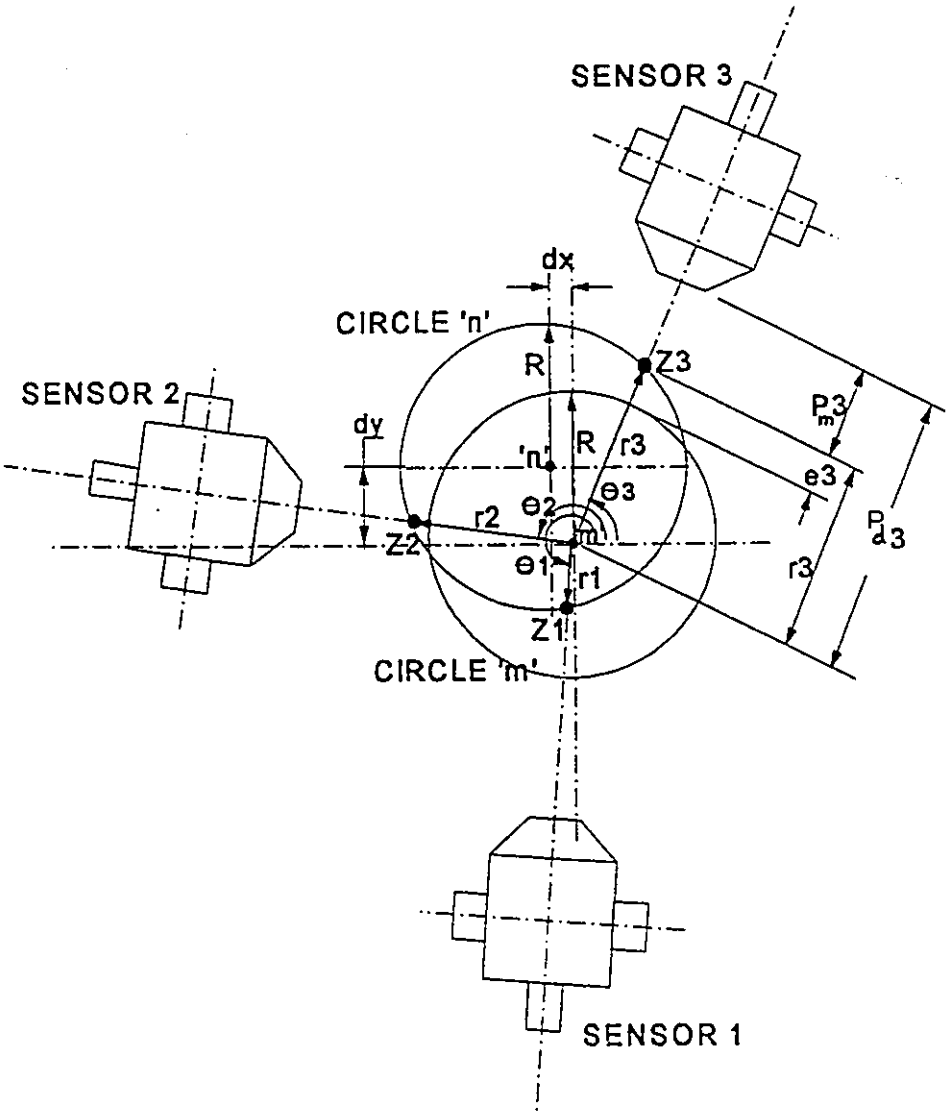

Fig. 4.11 Errors due to Rotation Axis Misalignment.

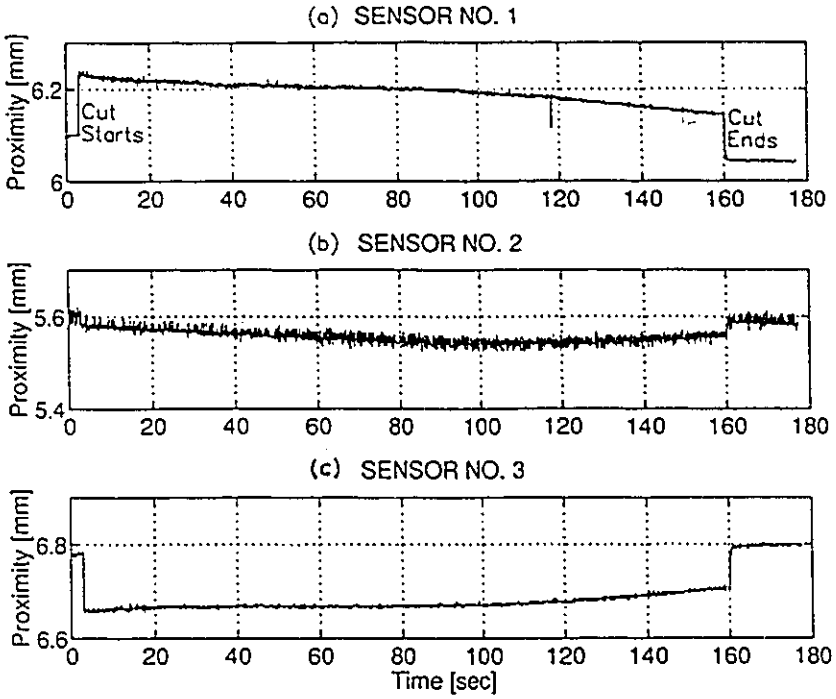

Fig. 4.12 Measured Distance Between Sensor and Workpiece Surface. (Diam=48.6 mm, Doc=1.27 mm, Feed Rate=151 mm/min, N=500 RPM)

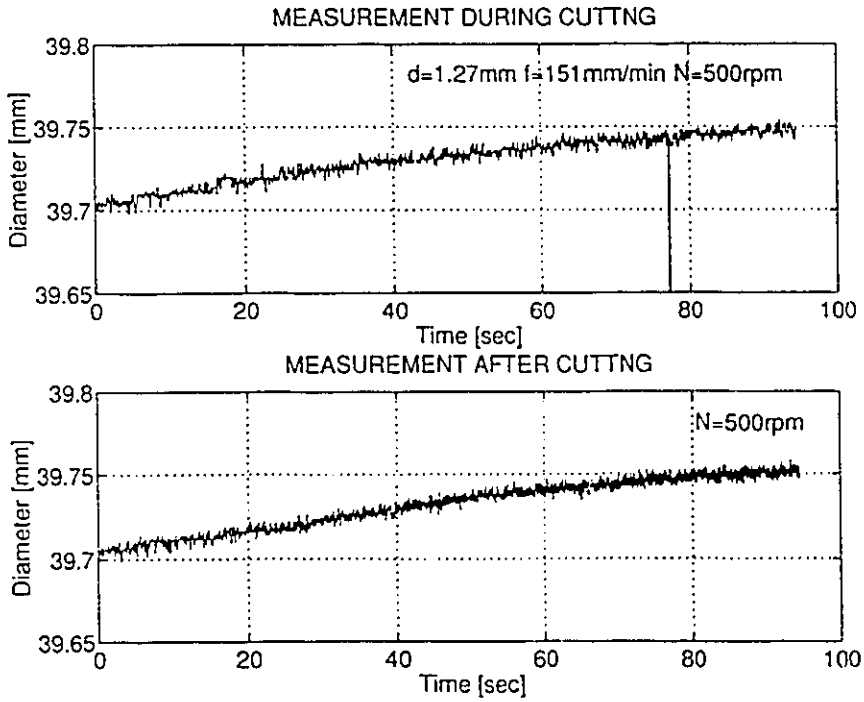

Fig. 4.13a On-Line Diameter Measurement During and After Cutting Using 1.27 mm Depth of Cut.

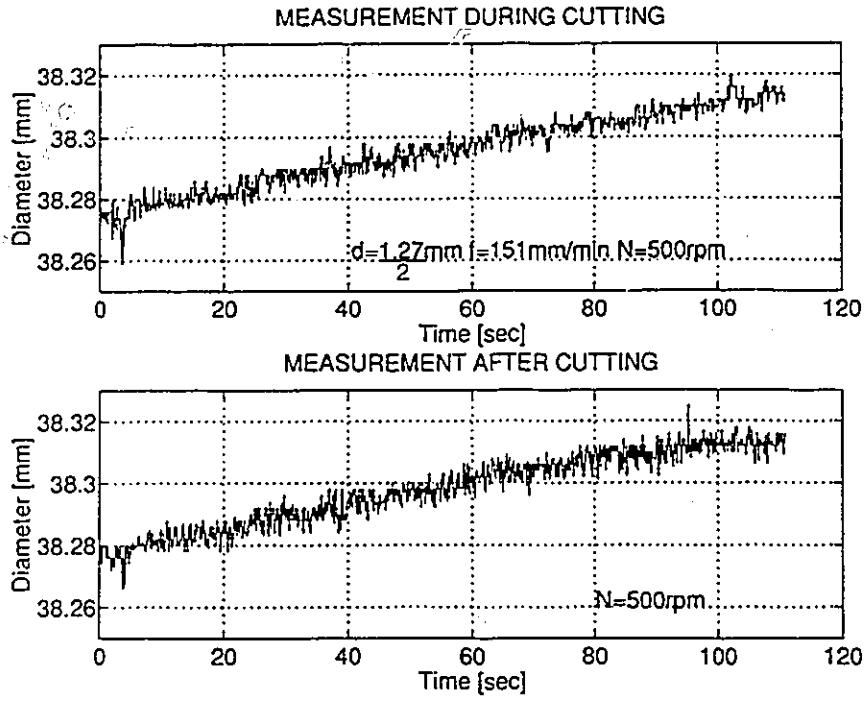

Fig. 4.13b On-Line Diameter Measurement During and After Cutting Using 0.635 mm Depth of Cut.

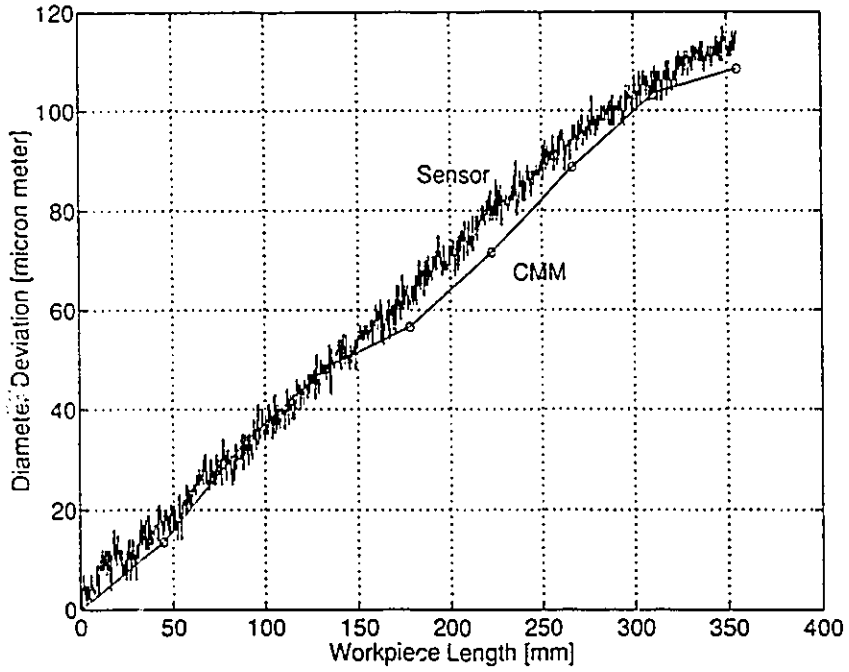

Fig. 4.14 Comparison of Sensor and CMM Measurements.

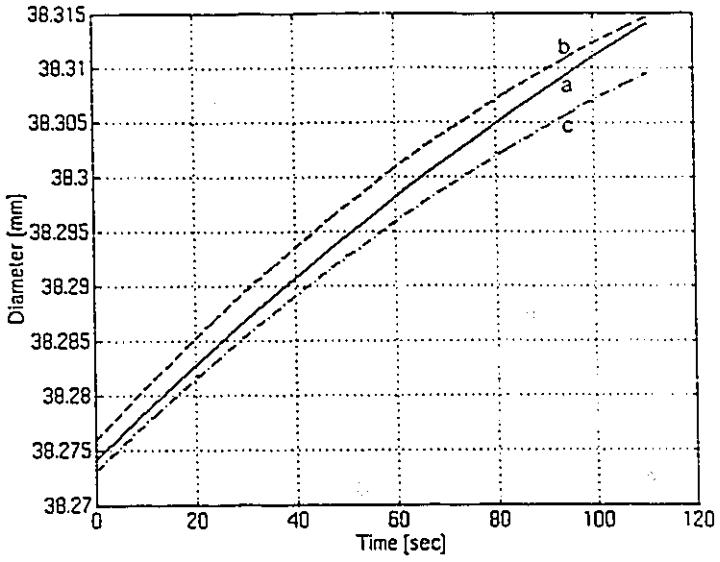

(a)

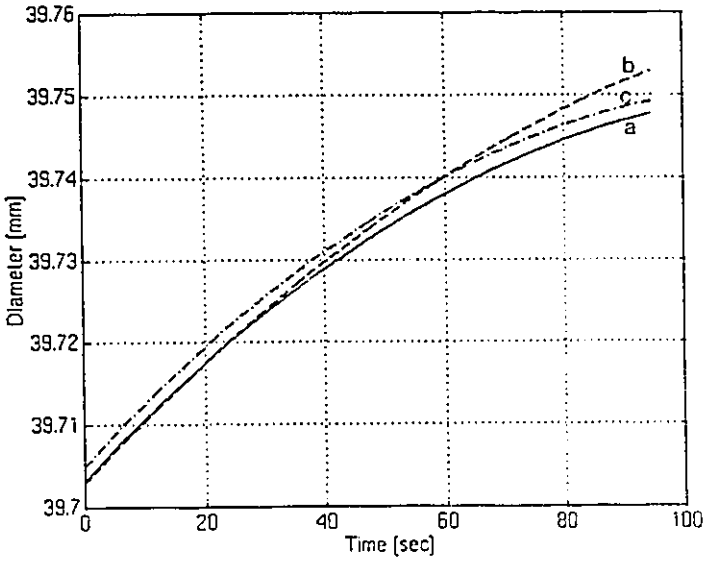

(b)

Fig.4.15 Surface Profile Measurements for Repeatability Tests.

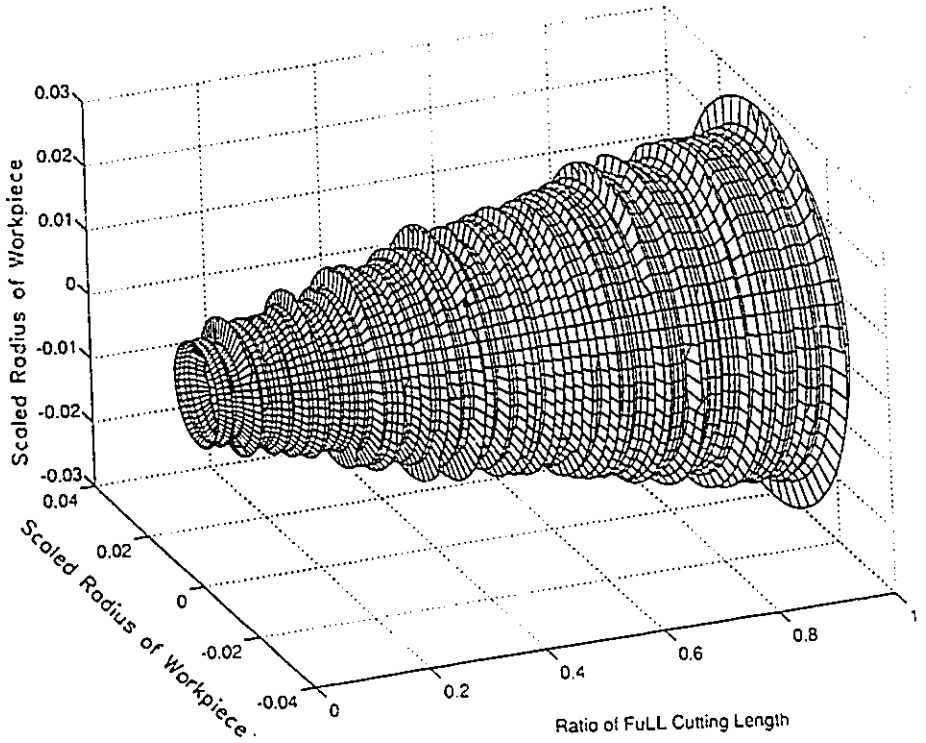

Fig. 4.16 3-Dimensional Representation of On-Line Measurement Data.

CHAPTER 5

IN-PROCESS EVALUATION OF GEOMETRICAL TOLERANCES

The development of an on-line measurement system was presented in the previous chapter. It was shown that the system is capable of reliably measuring the workpiece diameter during cutting while using a cutting fluid. A natural extension to such development is to employ the dimensional measurement gathered by the system in evaluating the geometrical tolerances of the workpiece. Such process is usually based on non-linear optimization techniques to fit the data to a mathematical surface model of the workpiece in a way to provide the minimum tolerance zone. It is the purpose of this chapter to investigate the evaluation of workpiece geometrical tolerances in turning using non-contact on-line measurements with particular emphasis on cylindricity (Shawky and Elbestawi, 1996b). The analytical formulation of cylindricity error is presented in details. The analysis method is based on an unconstrained non-linear numerical optimization approach. Two different fitting functions are compared: the least squares and the minimax fit. The sufficiency of the sampled data set is investigated. Spectral analysis and error separation methods are used to suppress noise and compensate for sensor misalignment due to workpiece deflection during

cutting. The determination of cylindricity tolerance of the workpiece from given experimental data is presented and recommendations for the implementation of such system are given.

5.1 TOLERANCES OF THE CYLINDRICAL FEATURE

A number of publications in the literature were dedicated towards the development and comparison of different methods for the evaluation of tolerances of different geometric features (e.g. Murthy, 1982, and Wang, 1992). The work by ElMaraghy, et al. (1989) was devoted to the cylindrical feature, and a procedure for evaluating geometric tolerances using CMM data was presented based on the minimum zone criterion. The cylindrical feature has, in addition to its size tolerance, several other geometric tolerances. It has form tolerances (roundness, cylindricity, straightness of the longitudinal surface element and straightness of the axis), orientation tolerance (perpendicularity), runout tolerance (circular and total runout), location tolerance (position), and profile tolerance of the longitudinal surface element.

The measurements provided by the non-contact on-line sensor represent radius data of the discretized points uniformly spaced on a spiral trace surrounding the workpiece as shown in Fig. 5.1. The pitch of the spiral is equal to the feed of the cutting tool. For the analysis and evaluation of tolerance the 3-dimensional Cartesian coordinates of the measurement points are extracted from the radius measurements.

The evaluation of runout, position, and profile tolerances is straight forward because it is based on the nominal center (or axis) position of the circle (or cylinder), rather than the actual ones. However, the determination of the remaining geometric tolerances as well as

the size tolerance require non-linear optimization. Optimization is used to achieve the given fitting objective by adjusting the positions and orientations of the centers (or axes) of circles (or cylinders). The complexity and the number of control variables in the optimization problem vary for different types of tolerances. For example, the evaluation of roundness tolerance has two control variables (which are the x- and y- coordinates of the substitute circle), while for cylindricity tolerance the complexity increases and the control variables are four (the x and y coordinates of the start and end points of the substitute cylinder axis). It should be noted that the same optimization problem can be formulated differently by switching from unconstrained to constrained optimization (e.g. Wang, 1992).

As mentioned in section 2.2.2, the most frequently used fitting algorithms are based on the L_p-norm, (Gonin and Money, 1989)

$$L_p = \left[\frac{1}{N} \sum_{i=1}^{N} | \epsilon_i |^p \right]^{\frac{1}{p}} \qquad \textbf{(5.1)}$$

where, $0<p<\infty$, N is the total number of data points, and ϵ_i is the smallest residual (i.e., distance between the i^{th} data point and the considered feature).

In the current work, the cylindricity tolerance objective is based on minimizing the L_p-norm. Two different fits are used; the least square fit ($p=2$) and the minimax fit ($p=\infty$). The next subsection presents the formulation of cylindricity tolerance for both fitting functions in details.

5.2 CYLINDRICITY TOLERANCE FORMULATION

The cylindricity is the tolerance zone bounded by two concentric cylinders with

minimum separation within which all measurements should lie. The axis *AB* of the substitute cylinder shown in Fig. 5.2 can be represented mathematically in the 3-dimensional Cartesian space (x, y, z) by the following set of linear parametric equations:

$$\begin{aligned} x(u) &= x_a + (x_b - x_a)\,u \\ y(u) &= y_a + (y_b - y_a)\,u \\ z(u) &= z_a + (z_b - z_a)\,u \end{aligned} \tag{5.2}$$

where, the parametric variable u is constrained to the parametric interval $u \in [0,1]$, and the suffix 'a' and 'b' denote the coordinates of the start and the end points $\boldsymbol{p}(0)$ and $\boldsymbol{p}(1)$, respectively. In vector form, Eqs. (5.2) can be represented by,

$$\boldsymbol{p}(u) = \boldsymbol{p}_a + u(\boldsymbol{p}_b - \boldsymbol{p}_a) \qquad \forall \quad u \in [0,1] \tag{5.3}$$

where,

$$\begin{aligned} \boldsymbol{p}_n &= x_n\,i + y_n\,j + z_n\,k \\ &= [x_n \;\; y_n \;\; z_n]\;[i \;\; j \;\; k]^T \qquad\qquad \text{for } n = 1,2; \end{aligned} \tag{5.4}$$

while, i, j, and k are unit vectors in the x, y, z directions, respectively. Note that at $u=0$ and $u=1$ the terminology $\boldsymbol{p}(0)=\boldsymbol{p}_0$ and $\boldsymbol{p}(1)=\boldsymbol{p}_1$ is used, respectively.

The minimum distance d_{min} from a given (measured) point $\boldsymbol{q}$ to the line AB is determined by finding a vector $\boldsymbol{p}$-$\boldsymbol{q}$ from the point to the line that is perpendicular to the tangent vector $\boldsymbol{p}'$ at $\boldsymbol{p}$. Mathematically the required conditions for the minimum distance are expressed as,

$$d_{\min} = |\boldsymbol{p} - \boldsymbol{q}| \tag{5.5}$$

when,

$$(\boldsymbol{p} - \boldsymbol{q}) \cdot \boldsymbol{p}^{u} = 0 \tag{5.6}$$

The tangent vector $\boldsymbol{p}^{u}$ is given by,

$$\boldsymbol{p}^{u} = \frac{d\boldsymbol{p}(u)}{du} \tag{5.7}$$

and the vector components are the parametric derivatives:

$$\begin{aligned} x^{u} &= \frac{dx(u)}{du}, \\ y^{u} &= \frac{dy(u)}{du}, \\ z^{u} &= \frac{dz(u)}{du}. \end{aligned} \tag{5.8}$$

Thus by determining $\boldsymbol{p}^{u}$ and substituting in equation (5.6), we get,

$$u = \frac{(x_q - x_a)(x_b - x_a) + (y_q - y_a)(y_b - y_a) + (z_q - z_a)(z_b - z_a)}{(x_b - x_a)^2 + (y_b - y_a)^2 + (z_b - z_a)^2} \tag{5.9}$$

If the four "control variables" x_a, y_a, x_b, and y_b are represented by the vector $\boldsymbol{b}$, then the substitute cylinder changes its location and orientation with the change of $\boldsymbol{b}$. The fitting problem is to minimize some objective function with respect to the control variables $\boldsymbol{b}$. The objective function used is in the form,

$$S_p = \sum_{i=1}^{N} |\epsilon_i|^p \tag{5.10}$$

where, S_p represents the same problem as the L_p-norm given in equation (5.1). The value of $\boldsymbol{b}$ that minimizes L_p (and S_p) is called the "L_p-estimator" of the feature (Gonin and Money, 1989).

For the least square fitting, the sum of the squared distances S_2 can be formulated as,

$$\begin{aligned} S_2 &= \sum_{i=1}^{N} | \epsilon_i |^2 \\ &= \sum_{i=1}^{N} \epsilon_i^2 \end{aligned} \tag{5.11}$$

The objective function can be expressed as,

$$F_{obj} = \min_{b} \left(\sum_{i=1}^{N} \epsilon_i^2 \right) \tag{5.12}$$

where, ϵ_i is a non-linear function of the measured data point $\boldsymbol{q}$ and the point $\boldsymbol{p}$ and is given by,

$$\epsilon_i = \sqrt{(x_u - x_q)^2 + (y_u - y_q)^2 + (z_u - z_q)^2} - R_m \tag{5.13}$$

and R_m is the mean value of the radius measurements.

On the other hand for the two-sided minimax fitting, the value of p approaches ∞, and the norm becomes the max absolute distance. The estimator $\boldsymbol{b}$ is then called the two-sided minimax fit for the feature. The minimax fit for the cylinder can be expressed as,

$$F_{obj} = \min_{b} \left(\max | \epsilon_i | \right) \tag{5.14}$$

and ϵ_i in this case is given by,

$$\epsilon_i = \max (R_i - R_{nom}) - \min (R_i - R_{nom}) \tag{5.15}$$

(where, R_{nom} is the nominal radius) and this form reduces to, (Murthy and Abdin, 1980)

$$\epsilon_i = \max(R_i) - \min(R_i) \qquad \textbf{(5.16)}$$

Similarly, by following the geometric representation presented above, the size tolerance and the other geometric tolerances for a cylinder can be formulated.

5.3 OPTIMIZATION ROUTINES

The minimization of the fitting functions under consideration is performed using two of the unconstrained non-linear optimization routines available in the literature. The Davidon-Fletcher-Powell (DFP) algorithm (Fox, 1980) is used for the least squares minimization function (Eq. 5.14). The algorithm requires the ability of computing the function's gradients, or the first partial derivatives,

$$\frac{\partial F_{obj}}{\partial x_a}, \quad \frac{\partial F_{obj}}{\partial y_a}, \quad \frac{\partial F_{obj}}{\partial x_b}, \quad \frac{\partial F_{obj}}{\partial y_b}$$

As for the minimax fitting function in Eq. 5.16, the derivatives are not defined. Therefore, Powell's method of conjugate directions was chosen, and to avoid the chance of linear dependence buildup the method was modified. This modification is based on discarding the direction of largest decrease (Press, et al., 1990).

The line minimization steps in both routines are performed by means of inverse parabolic interpolation using Brent's method (Brent, 1973). In addition to resolve the problem of having local minima, various starting points are used based on the "random walk" method (Fox, 1980).

5.4 DATA CONDITIONING

In the previous chapter the effect of low frequency misalignment error on diameter measurement (due to workpiece translation) has been analyzed and a method was developed to eliminate it from the measurement. When evaluating geometrical tolerances, measurement errors of relatively higher frequencies (e.g., those due to spindle runout and vibrations) are also of a concern. Based on a knowledge of the process mechanics and its error dynamics, spectral analysis and error separation methods are used to provide the appropriate data conditioning and eliminating the effect of such errors. This is explained in the following paragraphs.

The block diagram presented in Fig. 5.3 shows the different steps used in conditioning the measured signals (P_{m1}, P_{m2} and P_{m3}) in order to eliminate measurement errors. To eliminate the low frequency axis translation error and determine the radius data (R_i), the algorithm developed in the previous chapter is used. This algorithm tracks the axis of rotation of the workpiece continuously and accounts for the misalignment due to curvature of the axis then determines the absolute radius. As explained before, the algorithm is based on the repetitive fitting of circular cross-sections to the multi-sensor data. Thus, the presence of out-of-roundness with appreciable amplitudes in the acquired data may result in erroneous estimation of the axis of rotation. This can be overcome by using two filters: a low pass and a high pass filter, both with the same cut-off-frequency f_c (where, f is set equal to the rotational speed of the workpiece). In effect, this results in separating the measured signal into two groups; group-I and group-II with frequencies lower and higher than f_c, respectively. The data in group-I is processed by the low frequency axis-translation algorithm to give

radius data r_i with the low frequency form error superimposed. In group-II there are three signals of average amplitudes equal to zero and with frequency contents higher than f_c. Those signals represent the change in the radius due to out-of-roundness (i.e., high frequency form error dr_i). Such data could be contaminated with high frequency axis translation errors due to vibrations and spindle runout. The "three point method" by Whitehouse (1976, see Appendix C for more details) can be used to separate the workpiece out-of-roundness from such errors. This method is based on modeling the circular form using Fourier series and orthogonal polynomials expansion with respect to a datum line determined by the method of least squares. The datum line in this case coincides with the zero line due to the high-pass filtering which preceded the analysis. Finally, the out-of-roundness data dr_i is added to r_i to give the total radius measurement R_i. The latter radius data represent the measurement on a spiral trace along the workpiece length (z-axis) as shown in Fig. 5.1.

Knowing the tool feed f, the cutting speed and the sampling frequency, the radius information can be directly converted to cartesian coordinates in the object space as shown in Fig. 5.1. The next step as shown in Fig. 5.3 is sampling the available data by the specified number of cross-sections and points per cross-section. This procedure is carried out based on equidistant sampling for both the cross-sections and the points per cross-section. The sampled coordinates are used to determine the workpiece tolerances. This will be explained in the next section.

5.5 EXPERIMENTAL RESULTS AND DISCUSSION

The data analysis and evaluation of cylindricity tolerance were performed on a SUN SPARC station 4/330. The data was gathered during cutting tests using the same experimental setup explained in Section 4.8. The cutting conditions used were, *151 mm/min* feed, *500 rpm* spindle speed, and *1.27 mm* depth of cut. In this experiment three measurements were performed; one during the cutting path, and the other two in two separate paths while the tool was retracted away from the workpiece. Figure 5.4 shows a sample of the radius results of the three measurements captured for a machining length of *250 mm*. The experimental data captured is used in the following analysis.

The evaluation of the cylindricity tolerance is based on sampled data sets. Several sets of data are sampled from the same measurement using equidistant sampling and each set of data has a different number of points. The total number of points is equal to the product of the number of points per level (i.e., circular cross-section) and the number of levels along the workpiece length. The number of levels considered in this work are *10, 15, 20, 25, 30, 35, 40, 44, 48, 53, 60, 69, 75, 90, 100, 112, 128, 149, 178, 222*. Spectral analysis of the measured data revealed the lack of any frequency content higher than f_c that would correspond to lobbing of the workpiece circular cross-section. Accordingly, all data sets were sampled using the minimum possible number of points per level (i.e., three points).

Figure 5.5 presents a sample of the cylindricity evaluation results for the two fitting functions considered; the least squares and the minimax. The corresponding optimized control variables $\boldsymbol{b}$ for both fittings are shown in Fig. 5.6a and 5.6b, respectively. The results of both methods tend to fluctuate considerably when a small number of levels is used. They

follow an exponentially increasing pattern as shown in Fig. 5.5, until they stabilize at relatively large level numbers. Level numbers such as *150* and *180* may be considered unfeasible if measurements were to be taken off-line and with a touch probe.

The true value of cylindricity is considered to be that determined using the maximum number of levels. A consistent slight over-prediction of less than *2%* of cylindricity tolerance in the least squares results can be recognized in Fig. 5.5. Over-prediction of least squares results compared to minimax results is normal and can reach up to *20%* (Murthy and Abdin, 1980). However, in a noisy measurement environment like the wet cutting application encountered in this work, the presence of data outliers is expected to influence the accuracy of the minimax solution, most likely by increasing the tolerance value predicted. Thus, such over-prediction should not be expected to be consistent and this can be observed in the results shown in Fig. 5.7a, 5.7b and 5.7c. It should be noted that the latter figures represent the results of the data sets extracted from the radius data given in Fig. 5.4.

By examining Fig. 5.7a, 5.7b, and 5.7c individually, it can be recognized that there is an uncertainty $\leq 1\mu m$ for number of levels larger than 150 due to the data analysis strategy used. However, comparing all three results together, it can be seen that there is an uncertainty $\leq 5\mu m$ which is directly related to the accuracy limitation of the sensors used. For the least squares fitting function both algorithms, the DFP and the modified Powell's method, have been used. In spite of the lengthy function derivatives, the DFP algorithm has shown faster convergence to the optimal solution. However, no significant difference has been seen in the results. A comparison of the results is shown in Fig. 5.8.

According to the results presented above, several recommendations can be made for the development and implementation of on-line measurement systems used for the evaluation

of size and geometric tolerances in bar turning applications:

- Spectral analysis of the process errors and error separation methods provide the appropriate data conditioning for on-line multi-probe radius measurements with adequate accuracy.
- Compared with the least squares fit, the minimax fit does not guarantee minimum zone evaluation in the presence of data outliers which is normally present in such applications. No appreciable advantage has been seen of one over the other.
- To minimize the uncertainty in tolerance evaluation due to sample size insufficiency, relatively high number of levels (over one level every 2.5 mm along workpiece length) should be considered.
- The tolerance function derivatives are quite lengthy specially in the case of cylindricity. However, non-linear optimization based on gradient information has shown faster convergence. Thus, if minimax fit is to be used, reformulation of the tolerance function using constrained optimization (Wang, 1992) will be more beneficial.

5.6 SUMMARY

The implementation of an on-line measurement system for the evaluation of size and geometrical tolerances was presented. It was shown that the cylindricity tolerance of the workpiece can be determined successfully within the required accuracy using on-line data, provided that two main conditions are maintained. The first is that appropriate data conditioning procedures are implemented, and the second is that high density sample data

sets are used. Since high speed on-line measurement systems essentially employ non-contact sensing devices, they inherently provide the rich-data environment which fulfills the demand of large data sets. This maintains the advantages provided by on-line assessment of workpiece geometry in reducing quality control costs drastically.

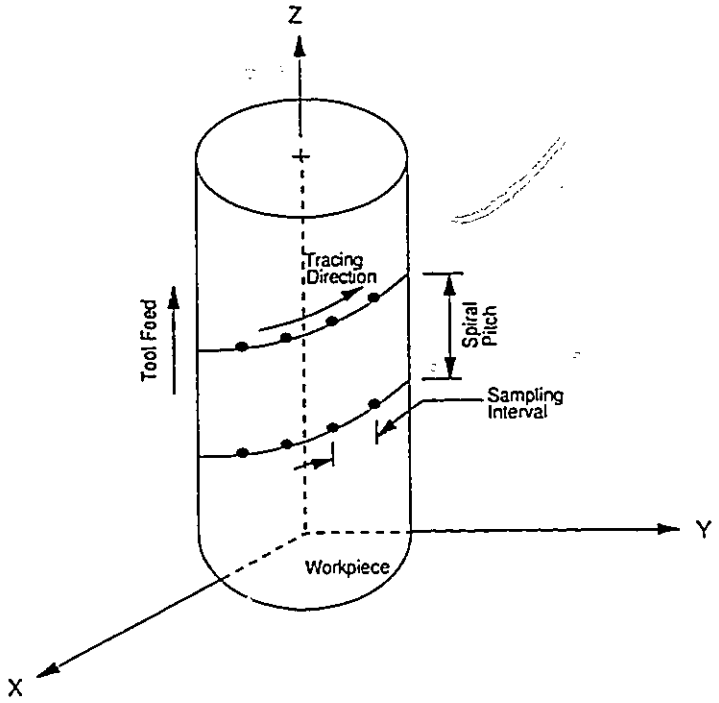

Fig. 5.1 The Spiral Trace of Uniformly Spaced Measurement Points Surrounding the Workpiece.

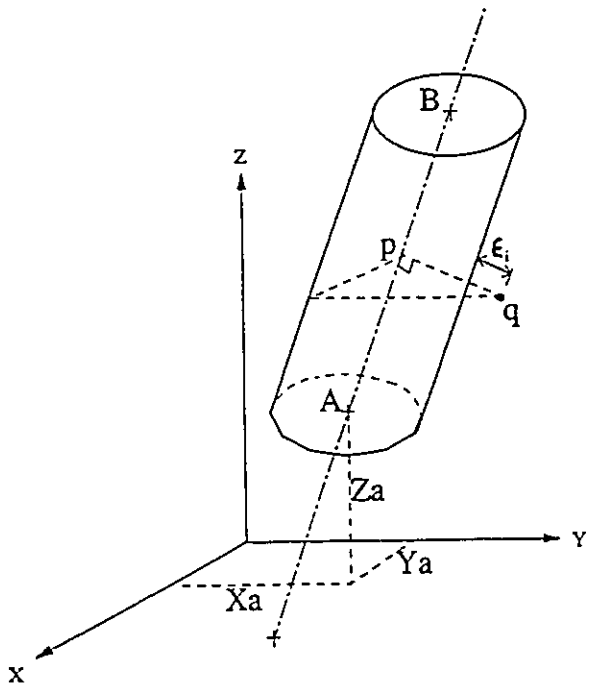

Fig. 5.2 Deviation of a Data Point from the Substitute Geometry of the Cylinder.

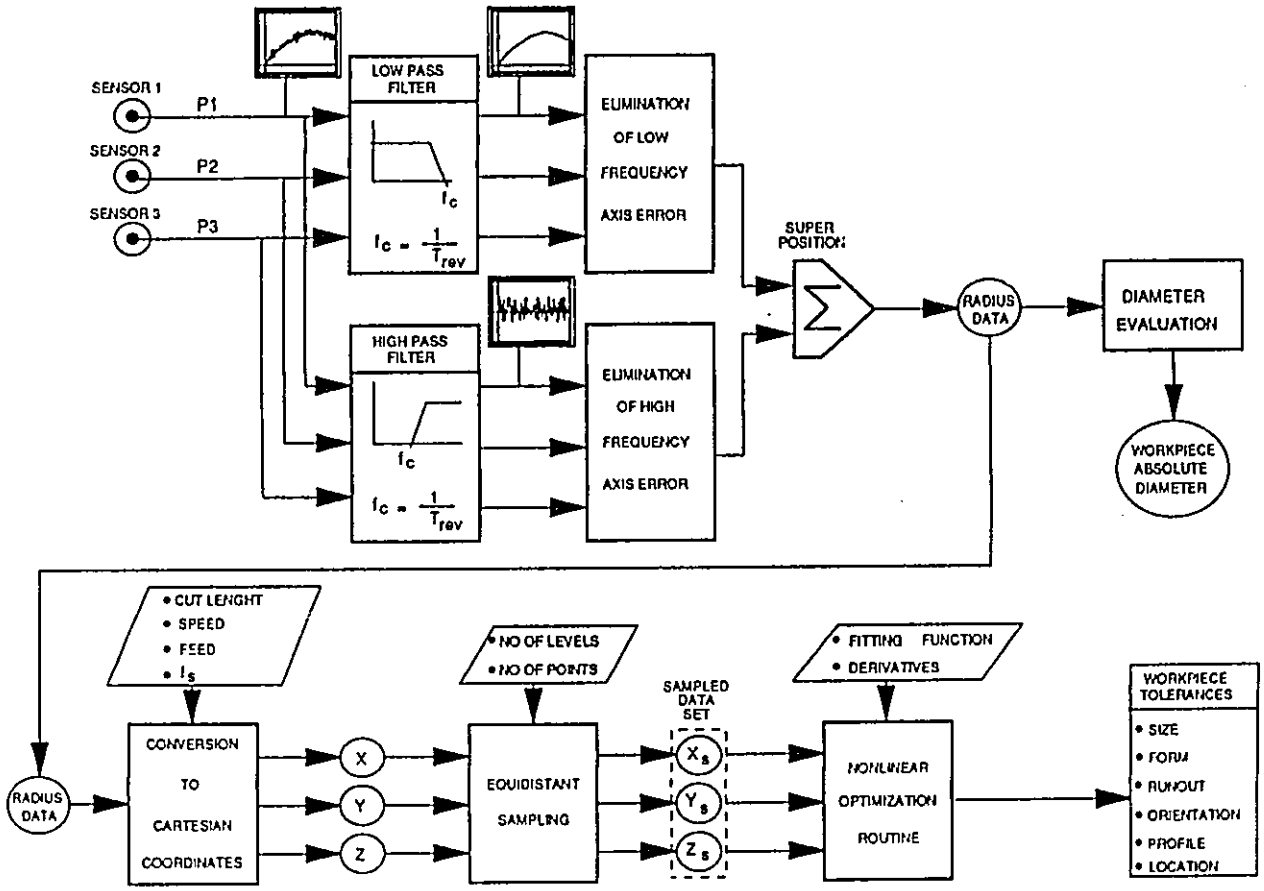

Fig. 5.3 Data Conditioning Block Diagram.

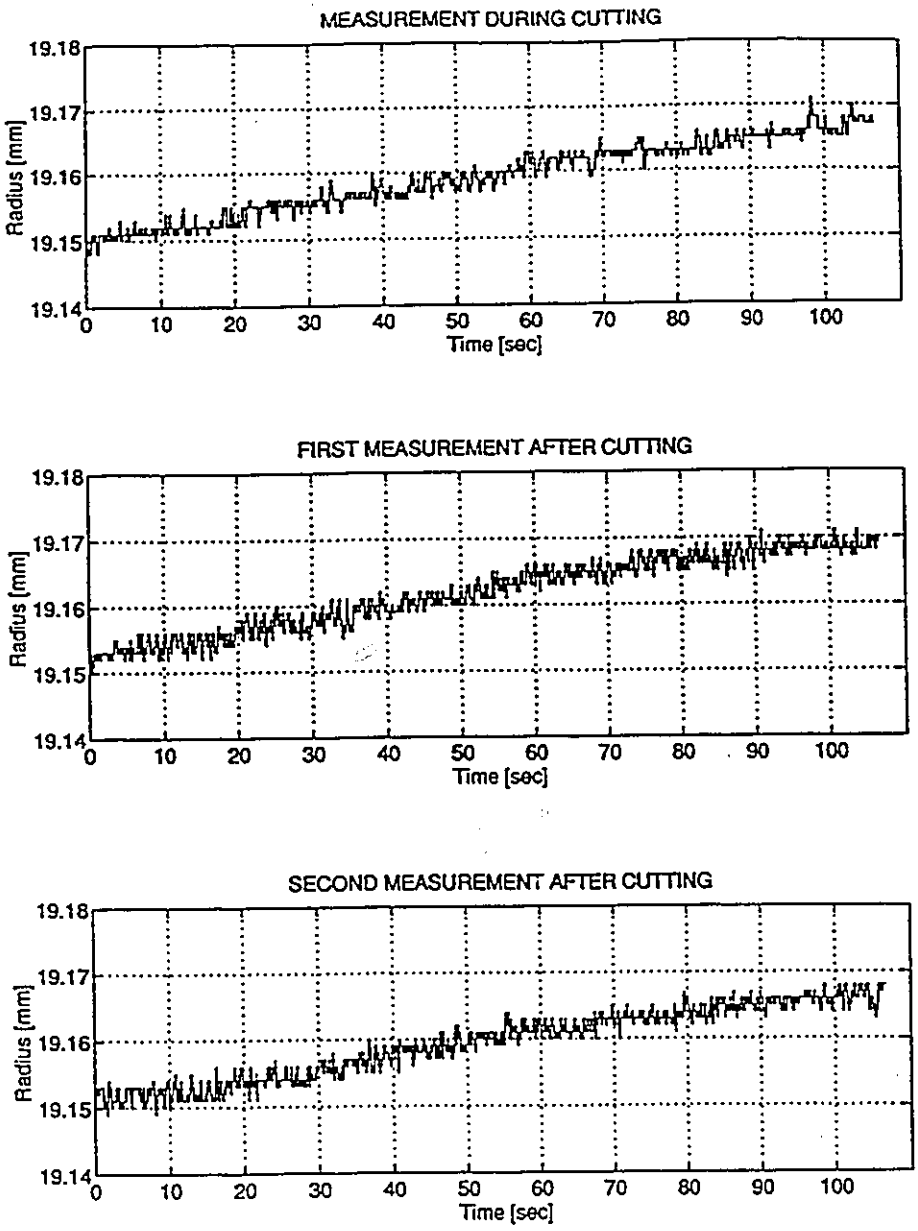

Fig. 5.4 On-Line Radius Measurements. (Length of Cur 250 mm, Depth of Cut 0.635 mm, Feed 151 mm/min, and Cutting Speed 500 rpm).

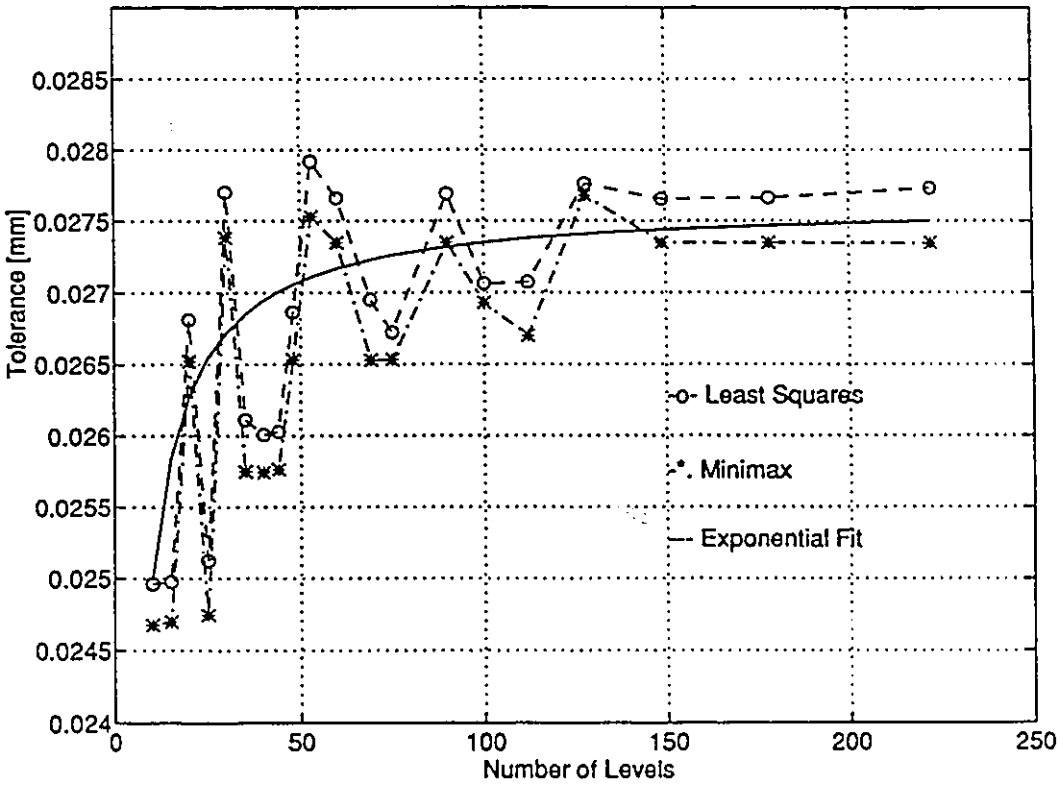

Fig. 5.5 Cylindrical Tolerances Computed for Increasing Number of Levels.

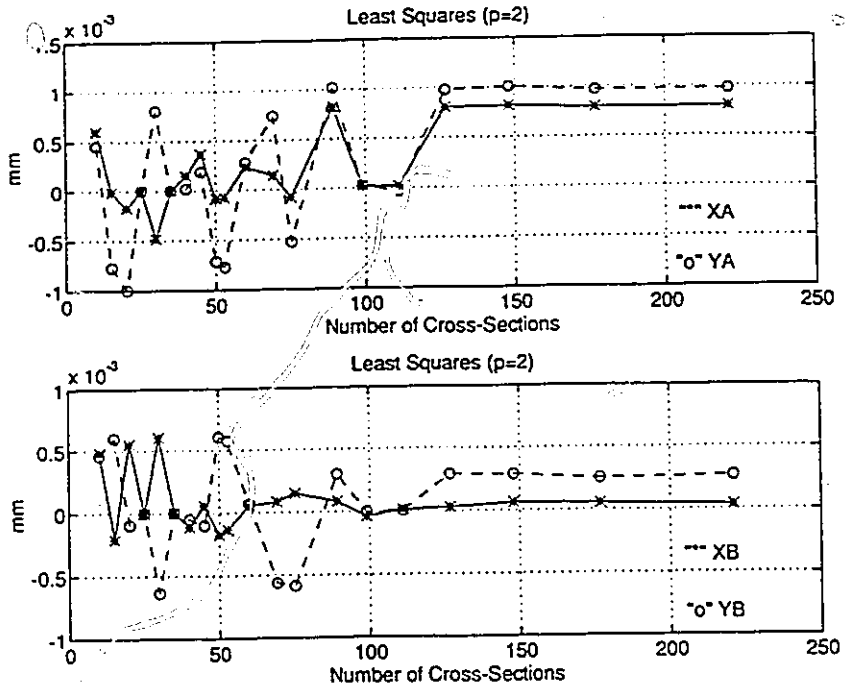

Fig. 5.6a The Optimized Control Variables for the Least Squares Fit Results Shown in Fig. 5.5.

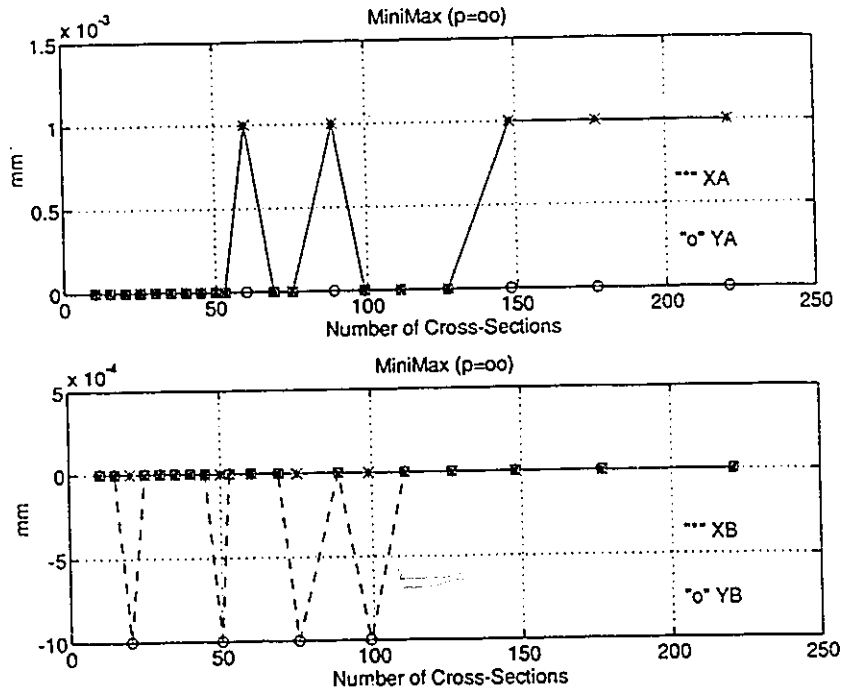

Fig. 5.6b The Optimized Control Variables for the Minimax Fit Results Shown in Fig. 5.5.

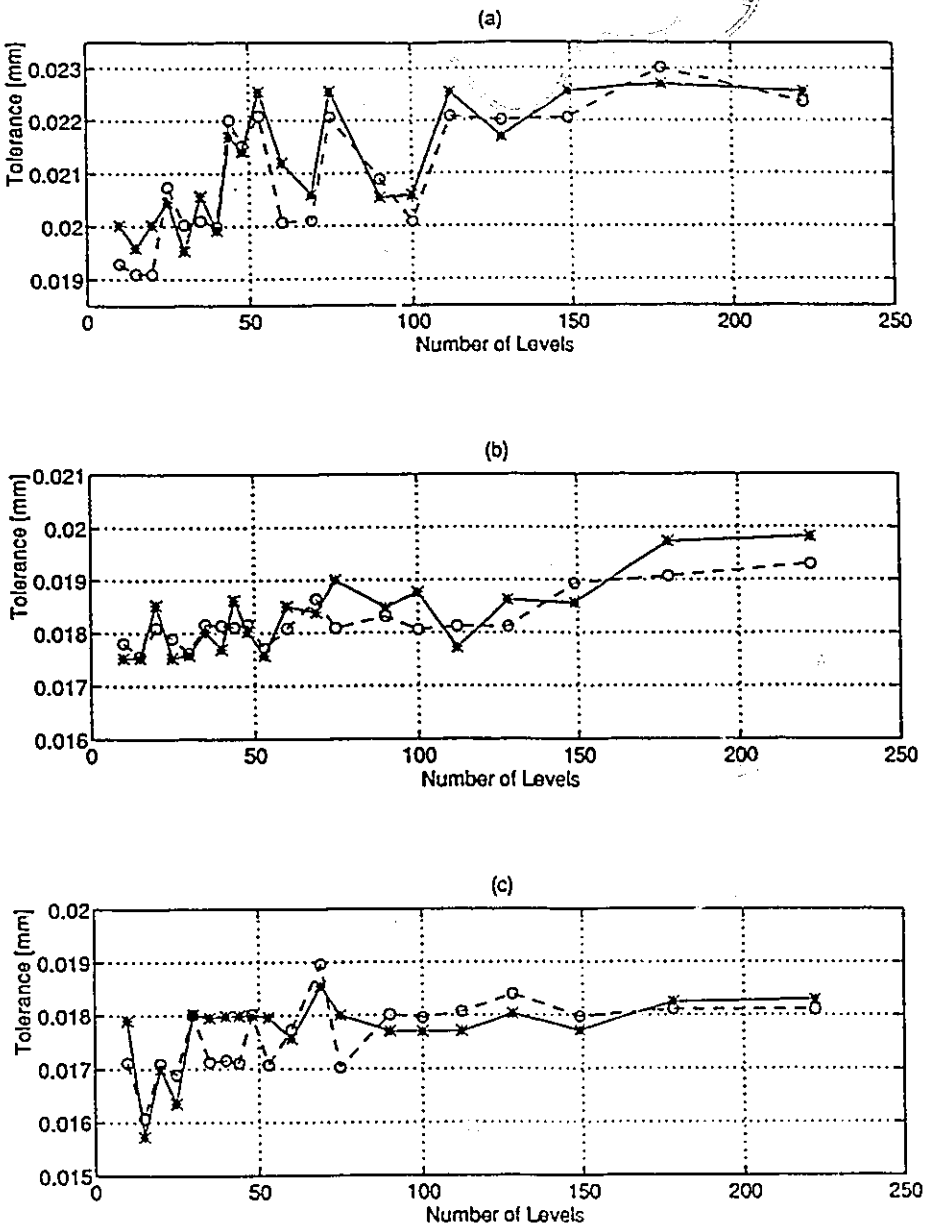

Fig. 5.7a, b, and c The Cylindrical Tolerances Determined from the Data Presented in Fig. 5.4a, b, and c, Respectively.

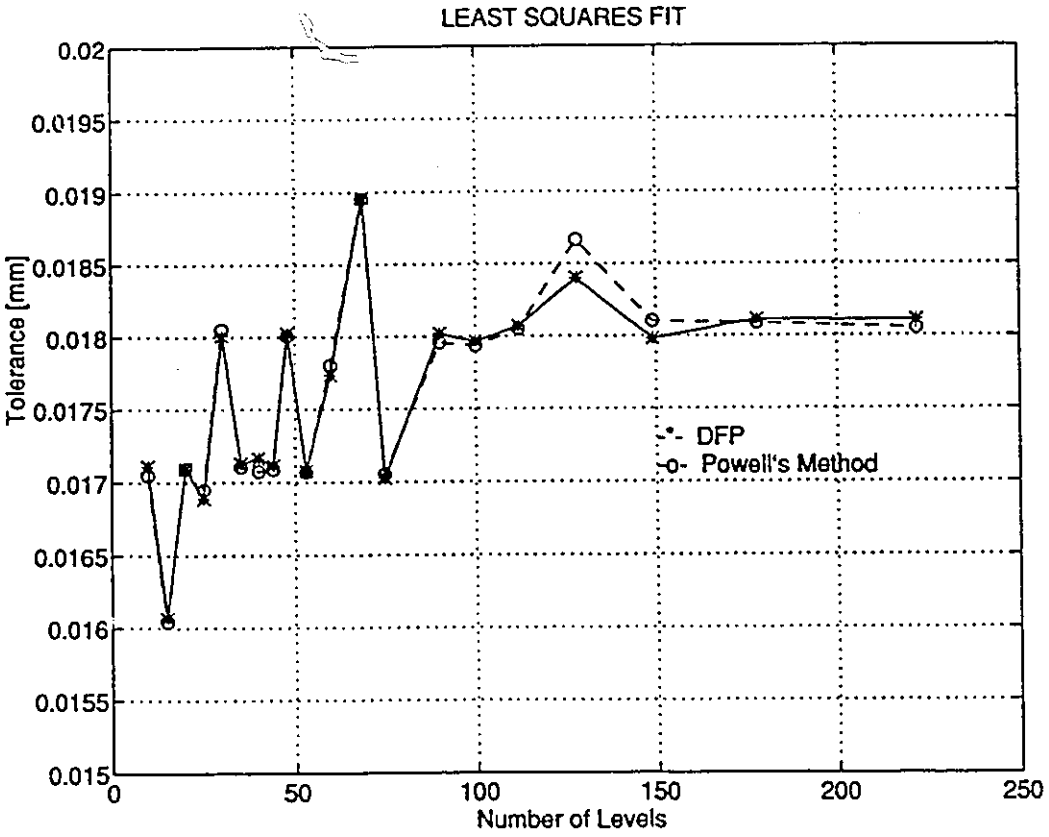

Fig. 5.8 Comparison Between Evaluation of Cylindricity Tolerance Using DFP Algorithm and Powell's Method.

CHAPTER 6

MODEL-BASED PREDICTIVE CONTROL

The previous chapters have discussed the model predictions and on-line measurements of the machined surface accuracy in bar turning. Both the predictions and the measurements can be used in a feedback control loop to improve the geometric accuracy of the workpiece (Shawky and Elbestawi, 1996c). This task is the focus of the current chapter. The control strategy used is based on modern control theory which makes it customary to formulate the process model in the state space. The schematic diagram shown in Fig. 6.1 represents the overall configuration of the system. The sensor physically trails the cutting edge by a distance δ. This lag manifests itself as a time delay in the dimensional measurement. The mechanistic process model is used to predict ahead in time in order to overcome the time delay in the feedback loop. A Kalman filter is used in a predictor/corrector fashion based on the dimensional measurement to correct the model predictions and to update them with the effect of unmodeled process disturbances such as tool wear and thermal deflections of the tooling system. A Linear Quadratic Gaussian (LQG) feedback controller with an integral action is designed to regulate the depth of cut. The controller output is used to govern the position of the tool tip in real-time by commanding

the same servo motor which is driven by the preprogrammed G-code. This represents a very important concern for the real-time implementation of a GAC system and will be explained further in this chapter.

6.1 STATE SPACE FORMULATION

The state space formulation of the process model is essential for both the design of the control system off-line and the prediction of the process states and outputs in real-time. Accordingly, a lower order model is desirable and becomes more suitable for the real-time implementation of such control system. The comprehensive dynamic model developed in Chapter 3 permits the prediction of machined surface errors in bar turning, however, it was intended primarily for off-line computer simulations. In this section, the model is simplified and reformulated in the state space to suit the design and implementation of the control system. The block diagram shown in Fig. 6.2 represents the structure of the machining system considered. Based on the physical understanding of the process, the function for which the model is intended, as well as the insight provided by the original simulation model, the following assumptions are made without sacrificing the accuracy of model predictions:

a. The contribution of the tangential force to the form error printed on the workpiece surface is insignificant. Computer simulations using different cutting conditions showed that this error is less than *10%* (refer to Fig. 6.3).

b. The cutting speed V is a constant value. This assumption is valid for most practical situations because, in addition to the small effect that speed has on the cutting force,

normally large change in the cutting speed is not required in bar turning for the same cutting pass.

c. The cutting forces are given by a linear function of both actual chip thickness h_a and actual depth of cut d_a (within a small working range) given by,

$$\begin{aligned} F_L &= g_{oy} + g_{hy}\, h_a + g_{by} d_a \\ F_R &= g_{ox} + g_{hx}\, h_a + g_{bx} d_a \end{aligned} \qquad \textbf{(6.1)}$$

where, F_L and F_R are the longitudinal and radial cutting forces, respectively, while the g's are regression constants. These constants are determined from simulation runs by using the original model for different feeds and depths of cut within the required ranges. The simulation results are then introduced to a multi-variable linear regression routine which determines the constants.

d. Higher modes of both tool and workpiece are associated with negligible displacement values.

e. The time delay term, e^{-T*s}, of one workpiece revolution, T, which is required for the regenerative feedback loop in the feed direction is adequately given by the second order Padé approximation, (Shiraishi, 1991)

$$\begin{aligned} \frac{y_{ty_d}(s)}{y_{ty}(s)} &= \frac{1 - a_0\, s + b_0\, s^2}{1 + a_0\, s + b_0\, s^2} \\ a_0 &= \frac{T}{2}\,, \qquad b_0 = \frac{T^2}{12} \end{aligned} \qquad \textbf{(6.2)}$$

where, s is the Laplace operator and y_{ty} is the tool displacement in feed direction. The structural dynamics of the tool and workpiece are represented by a lumped mass

system and a distributed parameter system, respectively, where:

the tool displacement in the radial (depth of cut) direction y_{tx} is given by,

$$m_{tx}\,\ddot{y}_{tx} + C_{tx}\,\dot{y}_{tx} + K_{tx}\,y_{tx} = F_R \tag{6.3}$$

tool displacement in the feed (longitudinal) direction y_{ty} is given by,

$$m_{ty}\,\ddot{y}_{ty} + C_{ty}\,\dot{y}_{ty} + K_{ty}\,y_{ty} = F_L \tag{6.4}$$

and the workpiece displacement in the radial direction $y_{wx}(l,t)$ is given by,

$$\begin{aligned} y_{wx}(l,t) &= \sum_{i=1}^{r} \eta_{x_i}(t)\,.\,Y_{x_i}(l) \\ \ddot{\eta}_{x_i} + 2\,\zeta_{wx_i}\,\omega_{wx_i}\,\dot{\eta}_{x_i} + \omega_{wx_i}{}^2\,\eta_{x_i} &= Y_{x_i}(l_0)\,.\,F_R \end{aligned} \tag{6.5}$$

η_{xi} is the workpiece displacement of the *ith* mode in the normal coordinates, $Y_{xi}(l)$ is the *ith* mode shape and l is the spatial variable along the workpiece length. (l_o is the position of the cutting edge). In the current study only the first mode of the workpiece is considered, thus $r=1$. However, notice that the dependency of y_{wx} on the tool position along the cutting length will result in a system matrix that is continuously changing along the cut.

The relationship between the nominal chip thickness h_{nom} and the feed f is given by a first order model. Figure 6.4 shows a comparison of the actual chip thickness build up (during one revolution T) and the step response of the first order model using several time constants. The model with a time constant of $T/2$ provides the most acceptable response. Accordingly, the change in chip thickness is given by,

$$\dot{h}_{nom} = 2\left(\frac{f - h_{nom}}{T}\right) \tag{6.6}$$

In the current work, the tool actuation is performed using the same servo motors commanded by the preprogrammed G-code (this is explained further in Section 6.5). The servo motor in the feed (longitudinal) direction was identified as a second order system,

$$\ddot{f} + 2\,\zeta_f\,\omega_f\,\dot{f} + \omega_f^2\,f = k_f\,\omega_f^2\,f_{com} \tag{6.7}$$

where, f_{com} is the commanded feed (*mm/rev*), while the servo motor in the depth of cut (radial) direction was identified as a second order system with delay T_d, and represented by,

$$\begin{aligned} &\ddot{d}_o + 2\,\zeta_d\,\omega_d\,\dot{d}_o + \omega_d^2\,d_o = k_d\,\omega_d^2\,d_c \\ &\frac{d_d(s)}{d_o(s)} = \frac{1 - a_{0_1}\,s}{1 + a_{0_1}\,s}, \qquad a_{0_1} = \frac{T_d}{2} \end{aligned} \tag{6.8}$$

where, d_c is the commanded depth of cut (*mm*).

Both, the primary and regenerative feedback loops are incorporated in the model by making the following substitutions into Eq. (6.1),

$$\begin{aligned} d_a &= d_d(t) - y_{tx}(t) - y_{wx}(l,t) \\ h_a &= h_{nom} - y_{ty}(t) + \mu\,y_{ty_d}(t) \end{aligned} \tag{6.9}$$

Let $\boldsymbol{x}$ be the state vector,

$$\boldsymbol{x} = \left[x_1\ x_2\ x_3\ x_4\ x_5\ x_6\ x_7\ x_8\ x_9\ x_{10}\ x_{11}\ x_{12}\ x_{13}\ x_{14}\right]' \tag{6.10}$$

where, ($'$) stands for transpose, and the state equations are given by,

$$
\begin{aligned}
x_1 &= f && [\,mm/rev\,] \\
x_2 &= \dot{x}_1 = \dot{f} && \\
x_3 &= d_o && [\,mm\,] \\
x_4 &= \dot{x}_3 = \dot{d}_o && \\
x_5 &= d_d && [\,mm\,] \\
x_6 &= h_{nom} && [\,mm\,] \\
x_7 &= y_{tx} && [\,m\,] \\
x_8 &= \dot{x}_7 = \dot{y}_{tx} && \\
x_9 &= y_{ty} && \\
x_{10} &= \dot{x}_9 = \dot{y}_{ty} && \\
x_{11} &= y_{wx}(l,t) && [\,m\,] \\
x_{12} &= \dot{x}_{11} = \dot{y}_{wx}(l,t) && \\
x_{13} &= y_{ty_d} && [\,m\,] \\
x_{14} &= \dot{x}_{13} = \dot{y}_{ty_d} &&
\end{aligned}
\tag{6.11}
$$

This results in the Multi-Input-Multi-Output (MIMO) state space process model of the form,

$$
\begin{aligned}
\dot{x} &= A_c\, x + B_c\, u \\
y &= C_c\, x + D_c\, u
\end{aligned}
\tag{6.12}
$$

where, u is a four-element input vector and y is a five-element output vector given by,

$$
\begin{aligned}
u &= \left[f_{com} \;\; \Delta d_c \;\; 1 \;\; d_c \right]' \\
y &= \left[F_R \;\; F_L \;\; R_{wp} \;\; h_a \;\; \Delta d \right]'
\end{aligned}
\tag{6.13}
$$

while Δd_c represents the commanded change in depth of cut (tool offset). The matrices A_c, B_c, C_c, and D_c are given by,

$$A_c = \begin{bmatrix}
0 & 1 & 0 & 0 & 0 & 0 & 0 & 0 & 0 & 0 & 0 & 0 & 0 & 0 \\
-\omega_f^2 & -2\zeta_f\omega_f & 0 & 0 & 0 & 0 & 0 & 0 & 0 & 0 & 0 & 0 & 0 & 0 \\
0 & 0 & 0 & 1 & 0 & 0 & 0 & 0 & 0 & 0 & 0 & 0 & 0 & 0 \\
0 & 0 & -\omega_d^2 & -2\zeta_d\omega_d & 0 & 0 & 0 & 0 & 0 & 0 & 0 & 0 & 0 & 0 \\
0 & 0 & \frac{1}{a_{o_1}} & -1 & \frac{-1}{a_{o_1}} & 0 & 0 & 0 & 0 & 0 & 0 & 0 & 0 & 0 \\
\frac{2}{T} & 0 & 0 & 0 & 0 & \frac{-2}{T} & 0 & 0 & 0 & 0 & 0 & 0 & 0 & 0 \\
0 & 0 & 0 & 0 & 0 & 0 & 0 & 1 & 0 & 0 & 0 & 0 & 0 & 0 \\
0 & 0 & 0 & 0 & \frac{g_{bx}}{m_{tx}} & \frac{g_{hx}}{m_{tx}} & \frac{-K_{tx} - 1000g_{bx}}{m_{tx}} & -\frac{C_{tx}}{m_{tx}} & -1000\frac{g_{hx}}{m_{tx}} & 0 & -1000\frac{g_{bx}}{m_{tx}}Y_x(l) & 0 & 1000\mu\frac{g_{hx}}{m_{tx}} & 0 \\
0 & 0 & 0 & 0 & 0 & 0 & 0 & 0 & 0 & 1 & 0 & 0 & 0 & 0 \\
0 & 0 & 0 & 0 & \frac{g_{by}}{m_{ty}} & \frac{g_{hy}}{m_{ty}} & -1000\frac{g_{by}}{m_{ty}} & 0 & \frac{-K_{ty}-1000g_{hy}}{m_{ty}} & -\frac{C_{ty}}{m_{ty}} & -1000\frac{g_{by}}{m_{ty}}Y_x(l) & 0 & 1000\mu\frac{g_{hy}}{m_{ty}} & 0 \\
0 & 0 & 0 & 0 & 0 & 0 & 0 & 0 & 0 & 0 & 0 & 1 & 0 & 0 \\
0 & 0 & 0 & 0 & g_{bx}Y_x(l_o) & g_{hx}Y_x(l_o) & -1000g_{bx}Y_x(l_o) & 0 & -1000g_{hx}Y_x(l_o) & 0 & -1000g_{bx}Yx(l)Y_x(l_o)-\omega_{wx}^2 & -2\zeta_{wx}\omega_{wx} & 1000\mu g_{hx}Y_x(l_o) & 0 \\
0 & 0 & 0 & 0 & 0 & 0 & 0 & 0 & 0 & 0 & 0 & 0 & 0 & 1 \\
0 & 0 & 0 & 0 & \frac{g_{by}}{m_{ty}} & \frac{g_{hy}}{m_{ty}} & -1000\frac{g_{by}}{m_{ty}} & 0 & \frac{1}{b_0}-\frac{k_{ty}+1000g_{hy}}{m_{ty}} & -\frac{a_o}{b_o}-\frac{C_{ty}}{m_{ty}} & -1000\frac{g_{by}}{m_{ty}}Y_x(l) & 0 & -\frac{1}{b_o}+1000\mu\frac{g_{hy}}{m_{ty}} & -\frac{a_o}{b_o}
\end{bmatrix} \quad \textbf{(6.14)}$$

$$B_c = \begin{bmatrix} 0 & 0 & 0 & 0 \\ k_f\omega_f^2 & 0 & 0 & 0 \\ 0 & 0 & 0 & 0 \\ 0 & k_d\omega_d^2 & 0 & 0 \\ 0 & 0 & 0 & 0 \\ 0 & 0 & 0 & 0 \\ 0 & 0 & 0 & 0 \\ 0 & 0 & \frac{g_{ax}}{m_{tx}} & \frac{g_{bx}}{m_{tx}} \\ 0 & 0 & 0 & 0 \\ 0 & 0 & \frac{g_{ay}}{m_{ty}} & \frac{g_{by}}{m_{ty}} \\ 0 & 0 & 0 & 0 \\ 0 & 0 & g_{ax}Y_x(l_a) & g_{bx}Y_x(l_a) \\ 0 & 0 & 0 & 0 \\ 0 & 0 & \frac{g_{ay}}{m_{ty}} & \frac{g_{by}}{m_{ty}} \end{bmatrix} \qquad \textbf{(6.15)}$$

$$C_c = \begin{bmatrix} 0 & 0 & 0 & 0 & g_{bx} & g_{bx} & 1000\ g_{bx} & 0 & -1000\ g_{bx} & 0 & -1000\ g_{bx}Y_x(l) & 0 & 1000\ \mu\ g_{bx} & 0 \\ 0 & 0 & 0 & 0 & g_{by} & g_{by} & 1000\ g_{by} & 0 & -1000\ g_{by} & 0 & -1000\ g_{by}Y_x(l) & 0 & -1000\ \mu\ g_{by} & 0 \\ 0 & 0 & 0 & 0 & -1 & 0 & 1000 & 0 & 0 & 0 & 1000\ Y_x(l) & 0 & 0 & 0 \\ 0 & 0 & 0 & 0 & 0 & 1 & 0 & 0 & -1000 & 0 & 0 & 0 & 1000\ \mu & 0 \\ 0 & 0 & 0 & 0 & 1 & 0 & -1000 & 0 & 0 & 0 & -1000\ Y_x(l) & 0 & 0 & 0 \end{bmatrix}$$

(6.16)

$$D_c = \begin{bmatrix} 0 & 0 & g_{ax} & g_{bx} \\ 0 & 0 & g_{ay} & g_{by} \\ 0 & 0 & R_w & 0 \\ 0 & 0 & 0 & 0 \\ 0 & 0 & 0 & 0 \end{bmatrix} \qquad \textbf{(6.17)}$$

It can be noticed that Δd_c is added to the input vector $\boldsymbol{u}$ and used as the control variable rather than using d_c directly. The reason for this is to permit the construction of the control design problem in the standard regulator form rather than being a tracking (servo) problem. By examining the model matrices, it can be noticed that some of their elements are functions of the longitudinal tool position. This is due to change in workpiece flexibility along the cutting length and the dependence of this behavior on the workpiece fixtures (i.e., boundary conditions at both ends of the workpiece). Figure 6.5 shows the form error profile predicted for a workpiece supported between two centers.

The state-space formulation presented above shows that in addition to using the depth of cut, the feed can be used as well for geometric control. However, in the current setup the lead angle of the cutting edge is zero, thus, resulting in a very low dc-gain between the feed and the form error. Figure 6.6 shows a comparison of the change in workpiece radius (at mid span) corresponding to step inputs of *0.1 mm* and *0.1 mm/rev* in the depth of cut and feed, respectively, for a workpiece fixed between two centers. It is clear that using the depth of cut offset Δd_c as the control variable provides less control effort.

Since we are dealing with measurements taken at discrete equispaced intervals of time T_s, it is convenient to discretize the state equation (Eq. 6.12a). By integrating the state equation (Eq. 6.12a) over the sampling interval kT_s to $(k+1)T_s$ assuming a zero-order hold on the inputs and that the elements of $\boldsymbol{A}_c$ and $\boldsymbol{B}_c$ are constant over the interval, we get the matrix difference equation,

$$x_{k+1} = \Phi x_k + \Gamma u$$

$$\text{where,} \quad \Phi = e^{A_c T_s} \qquad \Gamma = B_c \int_0^{T_s} e^{A_c (T_s - \tau)} d\tau \tag{6.18}$$

6.2 THE KALMAN FILTER AND STATE PREDICTION

The Kalman Filter (Kalman, 1960) is an optimal statistical procedure for combining noisy process measurements with on-line process dynamic models in order to keep the models tracking the actual process. Given the state and measurement equations by,

$$\begin{aligned} x_{k+1} &= \Phi x_k + \Gamma u_k + G w_k \\ y_k &= C x_k + D u_K + v_k \end{aligned} \tag{6.19}$$

where, w_k and v_k are Gaussian white noise vectors with zero mean and with diagonal covariances R_w and R_v, respectively. The matrix G is taken equal to Γ, thus, assuming that the process noise is introduced to the system through the process inputs; namely feed, depth of cut and material cutting resistance. For convenience the matrices C_c (5x14) and D_c (5x4) are reduced in size to C (1x14) and D (1x4), respectively, to represent one output only; that is the change in depth of cut Δd_c.

When the new measurement ym_{k+1} becomes available at time t_{k+1} the state estimates can be updated via the Kalman Filter given by, (refer to Fig. 6.7)

$$\hat{x}_{k+1/k+1} = x_{k+1/k} + K_{k+1} (ym_{k+1} - y_k) \tag{6.20}$$

where, K_{k+1} is the steady state Kalman gain computed off-line by solving the recursive matrix

Riccati equation,

$$\begin{aligned} K_{k+1} &= P_{k+1/k}\, C'\, (C P_{k+1/k} C' + R_v)^{-1} \\ P_{k+1/k} &= \Phi\, P_{k/k}\, \Phi' + G\, R_w\, G' \\ P_{k+1/k+1} &= [\, I - K_{k+1}\, C\,]\, P_{k+1/k} \end{aligned} \tag{6.21}$$

The Kalman filter provides optimal estimates of the states in a least square sense. When the state estimate $x_{k/k}$ at time kT_s is available, the prediction for the states at a future point m-steps ahead, $(k+m)T_s$, is given by,

$$\begin{aligned} x_{k+m/k} = \Phi^m \hat{x}_{k/k} + \Phi^{m-1}\, \Gamma\, u_k + \Phi^{m-2}\, \Gamma\, u_{k+1} \\ + \ \ldots \ + \Phi\, \Gamma\, u_{k+m-2} + \Gamma\, u_{k+m-1} \end{aligned} \tag{6.22}$$

The main tuning parameters of the Kalman Filter are the diagonal elements of the covariance matrices R_w and R_v. In the current case, R_v is scaler and represents the variance of the sensor measurements. Therefore, an average value for R_v was determined from the experimental results of the sensor. The diagonal elements of R_w were tuned to filter out the high frequency measurement noise and provide a rather conservative slow filter. To decrease the state estimate bias due to slowly changing form errors, the Kalman gain matrix K was then increased by artificially decreasing the magnitude of the sensor noise covariance R_v until the bias in the predicted output was within the sensor accuracy of 5 μm. Another possible way of removing the offset error is by augmenting the states by a stochastic state to add an integral action to the filter. Figure 6.8 shows the response of the predicted output to deterministic disturbances predicted by the model and stochastic disturbances captured by the measurement system. It can be seen that the output prediction tracks the actual process

through both disturbances rather closely.

6.3 CONTROLLER DESIGN

The workpiece form error is compensated by regulating the tool position using the depth of cut offset Δd_c. The controller design is based on full state feedback as illustrated in Fig. 6.9. In order to remove the tracking error between desired and actual tool position, an integral action is required in the closed control loop. Thus, the state vector given by Eq. (6.10) is augmented by a new state variable g where,

$$g = \int_0^t (y - y_{ref})\, dt \tag{6.23}$$

This results in a reformulated system of the form,

$$\begin{aligned} \dot{z} &= \hat{A}\, z + \hat{B}\, v \quad , \quad \hat{A} = \begin{bmatrix} A & 0 \\ C & 0 \end{bmatrix} \quad , \quad \hat{B} = \begin{bmatrix} B \\ D \end{bmatrix} \\ \text{where, } z &= \begin{bmatrix} z_1 \\ z_2 \end{bmatrix} = \begin{bmatrix} x - x_s \\ g - g_s \end{bmatrix} \quad , \quad v = u - u_s \end{aligned} \tag{6.24}$$

and x_s, g_s and u_s are the steady state solution. By discretizing the above state equation (Eq. 6.24), we get,

$$z_{k+1} = \hat{\Phi}\, z_k + \hat{\Gamma}\, v \tag{6.25}$$

Using full state feedback the control law is,

$$v = -L\, z \tag{6.26}$$

where, L is the state feed back gain matrix. Partitioning L appropriately yields,

$$\begin{aligned} L &= [L_1 \quad L_2] \quad , \quad v = -L_1 z_1 - L_2 z_2 \\ u - u_s &= -L_1 (x - x_s) - L_2 (g - g_s) \end{aligned} \tag{6.27}$$

The steady state terms must balance each other. Therefore, by replacing g, we get the control input u_k equals,

$$u_k = -L_1 x_k - L_2 g_k = -L_1 x_k - L_2 [\, g_{k-1} + (y_k - y_{ref}) \,] \tag{6.28}$$

This shows that the control consists of proportional state feedback and integral control of output error. The optimal state feedback gain matrix L is that which minimizes the quadratic cost function given by,

$$J = \Sigma (y' Q y + v' R v) \tag{6.29}$$

where, Q and R are positive semi-definite weighing matrices. The solution to this problem is given by the equation, (e.g. Takahashi, 1970)

$$L_\infty = (R + \hat{\Gamma}' S_\infty \hat{\Gamma})^{-1} \hat{\Gamma}' S_\infty \hat{\Phi} \tag{6.30}$$

where, S_∞ is the steady state unique positive definite solution of the associated discrete matrix Riccati equation,

$$S_t = \hat{\Phi}' S_{t-1} \hat{\Phi} + Q - \Phi' S_{t-1} \hat{\Gamma} (R + \hat{\Gamma}' S_{t-1} \hat{\Gamma})^{-1} \hat{\Gamma}' S_{t-1} \hat{\Phi} \tag{6.31}$$

For the current model, there is one control input which is the depth of cut offset thus, both Q and R are scalars. It is desired to design a controller which would minimize the

workpiece form errors subject to a reasonable constraint on the depth of cut offset. The weight on the output variance Q was assigned a value of *1*. A suitable choice for the constraining weight R was then derived in the following manner. Optimal stochastic controllers were designed for a number of different values of R, and the resulting step responses were compared. The value of R and the corresponding controller was chosen as a rather slow controller. Moreover, this controller is adequate for the form errors encountered. Figure 6.10 shows the step response of the closed loop. It has the benefit of integral control in eliminating steady state errors. In addition, the controller has a detuned transient response to provide more robustness and prevent any overshoot which would directly cause undercutting.

6.4 TOOL ACTUATION SYSTEM

The geometric controller developed above was implemented on a CNC turret lathe (Leblond Knight *20 hp*). The physical realization of such control system requires two subsystems: an on-line measurement system and a tool actuation system. The ultrasonic measurement system developed in Chapter 4 is used to provide an on-line measurement of the workpiece diameter. The tool actuation system is described in this section.

The CNC lathe used for the implementation of the developed GAC system is retrofitted with an Open Architecture Controller (OAC), (Teltz, et al., 1994). The OAC provides a very powerful platform for the implementation of the GAC system specially with respect to two main aspects. First, synchronization and update of the model-based control algorithm with change in the longitudinal position of the tool. This update is necessary for both feedback and Kalman gain matrices to follow the continuous change in the system

matrices due to change in workpiece flexibility along the cut. Second, the ability to change the tool position in real-time using the same CNC servo motor (commanded by the G-code) rather than using an external actuating device.

The OAC is based on a VME Bus system hosted on an MC68030 with a real-time multi-task operating system (VxWorks). The motion control is performed using a Programmable Multi-Axis Controller (PMAC) based on Motorola's DSP56001. PMAC has a dual ported RAM (DPRAM) of *8 Kbytes* which allows access to specific memory locations, thus providing the real-time control algorithm with the ability to read or change the different variables at these locations in real-time (i.e., while running CNC programs). Obviously, such capability is not possible using conventional machine tool controllers, since it involves interference with the motion program being executed during the cut.

Consequently, by using the OAC, tool position in the radial (x-) direction can be manipulated by changing the next *x-word* in real-time. However, this would require breaking down the G-code into smaller steps. Also, it should be noted that the G-code is normally executed by interpreting every two successive lines of the code together in order to perform blended motion. This makes it customary to account for such effects before issuing the control commands, and thus, complicates both the model and the control algorithm. Therefore, in the current work, a simpler approach is followed. It is based on manipulating an offset value for the depth of cut direction of the tool. This is performed by accessing the specific register to which the manual hand wheel override of the machine control panel writes. The values in this register are recognized by the PID controller (which closes the position feedback control loop) as changes in the reference (position) signal. Thus, these changes are performed as offsets to the values assigned by the preprogrammed

motion program (G-code). The block diagram shown in Fig. 6.11 illustrates this position offset mechanism. Such position offsets can be updated every *0.8 ms*. However, manipulating the tool position is physically limited by the bandwidth of the cross-slide servo of *5Hz*.

6.5 EVALUATION OF SYSTEM PERFORMANCE

The performance of the proposed GAC system is evaluated using real-time cutting control experiments. First, identification experiments were performed to determine the different parameters of the model. These included calibration of the force model, modal analysis of the machine/tool workpiece structure, and identification of the servo system dynamics using step response tests. The identified model parameters are summarized in Table 6.1. The experimental conditions used in the real-time control tests are explained in the next subsection, followed by a presentation and discussion of the experimental results.

Table 6.1 The Parameters of the Model Identified Experimentally

Parameter	Value	Parameter	Value	Parameter	Value
g_{ox}	2.2 N	K_{tx}	34.6 MN/m	ζ_d	0.87
g_{hx}	963.7 N/mm	m_{ty}	98.9 Kg	ω_d	40 rad/sec
g_{bx}	56.1 N/mm	C_{ty}	4651 N.s/m	K_d	1
g_{oy}	-459.04 N	K_{ty}	95.0 MN/m	T_d	0.01 sec
g_{hy}	1718.7 N/mm	ω_{wx}	999 rad/sec	ζ_f	0.7
g_{by}	439.53 N/mm	ζ_{wx}	0.025	ω_f	30 rad/sec
m_{tx}	91.2 Kg	K_c	24 MN/m	K_f	1
C_{tx}	4493 N.s/m	K_l	4.3 MN/m		

6.5.1 EXPERIMENTAL CONDITIONS

All cutting experiments have been performed with carbide inserts, while using a cutting fluid and at a cutting speed of *55 m/min*. Slender AISI *1045* steel shaft workpieces of *75 mm* in diameter and *508 mm* long have been used. The workpieces have been fixed between two centers. The model matrices have been updated in a discrete fashion every *5 mm* of the workpiece length. Consequently, the corresponding Kalman gains $\boldsymbol{K}$ and state feedback gains $\boldsymbol{L}$ have been determined off-line and saved in a soft form. The longitudinal position of the cutting edge along the cutting length has been used as an auxiliary measurement to update both the model and controller using the prescheduled gains. The distance δ between the tool and the vertical plane passing through the center lines of the sensors was set to a minimum value equal to *0.27 mm*. The real-time code has been optimized for speed. The measurements have been taken at a sampling interval of *8 ms*. A control time step of *40 ms* allowed the averaging of five measurements for more robustness.

In order to ensure the accuracy of the time step and synchronization of both control and measurement on such real-time multi-task operating system, an interrupt service routine (ISR) has been used. The ISR runs at a high priority level and uses a dedicated auxiliary system clock to monitor the specified real-time tasks and give the starting signals (i.e., semaphores) for each task at the designated times. A summary of the experimental conditions is given in Table 6.2.

Table 6.2 Conditions of the Control Cutting Experiments.

Workpiece:	AISI 1045 Steel
	508 mm Length
	75 mm Diameter
Tool:	P40 Carbide Insert
	0° Approach Angle
	-6° Back Rake Angle
	0.8 mm Nose Radius
Cutting Speed:	55 m/min
Tool Feed:	0.2 / 0.3 mm/rev
Depth of Cut:	1.905 - 3.175 mm
Sampling Time Step:	8 ms
Control Time Step:	40 ms
Parameters Update:	Every 5 mm of workpiece length

6.5.2 EXPERIMENTAL RESULTS AND DISCUSSION

Several bar turning experiments were designed and carried out for straight cuts, taper turning, and other cuts including sudden changes in the depth of cut. The measured form error after control and the real-time control action of the tool position are presented for each cutting experiment. The tool compensatory control action also shows the amount of form error removed using the proposed control system. A closeup photograph showing the cutting tool and the measurement system during operation is presented in Fig. 6.12.

Figure 6.13 present the performance of the system in straight bar turning for a depth of cut and feed of *1.905 mm* and *0.3 mm/rev*, respectively. A total form error of

approximately *140 μm*, over a machined length of *190 mm*, is reduced to within *10 μm* accuracy. The figure also shows a continuous decrease in the tool compensatory control action as the cutting edge travels from the tail stock side to the chuck side. The same trend is observed in Fig. 6.14 which demonstrates the performance of the system in a similar experiment while using a different feed of *0.2 mm/rev*. A total form error of approximately *70 μm* over a machining length of *97 mm* is reduced without any undercut errors.

Figures 6.15 and 6.16 demonstrate the performance of the GAC system during step changes in the depth of cut. The tool path was planned to create a stepped shaft from a straight workpiece. In Fig. 6.15, there is one step of *0.762 mm* and the feed and exit depth of cut used were *0.3 mm/rev* and *1.905 mm*, respectively. While in Fig. 6.16 there are three steps; two of *0.381mm* and a third one of *0.254 mm*. Since the GAC controller is designed only for the purpose of regulating the error and not for performing the gross motion of the tool, the steps were included in the CNC motion program. In other words, the tool tip trajectory required to create the steps is the responsibility of the machine tool motion control board. On the other hand, information on changing the set point (reference diameter) for the control algorithm (at each of the steps) is captured from the G-code while monitoring the longitudinal tool position. The performances of the system presented in Figs. 6.15 and 6.16 exhibit rather smooth transients at the steps while maintaining the accuracy within the required limits. Although the first and second steps in Fig. 6.16 are of the same magnitude, it can be noticed that the second transient is slightly smaller. This is attributed to the decrease in workpiece flexibility.

Figure 6.17 demonstrates the results of a taper turning experiment (for a *2 °* included angle taper). The starting depth of cut of *3.175 mm* was continuously changed as interpolated

by the motion control board. By feeding the G-code information to the model, this situation represented a cut with a deterministic disturbance. A rather smooth performance of the control system can be observed in the results shown. Notice that the continuous decrease in the depth of cut acted in favor of reducing the form error along the machined length.

Figures 6.18 and 6.19 present the results of two straight cuts for a workpiece with an originally tapered surface. Such situation represents a stochastic disturbance to the system since it is only seen by the on-line measurement and not accounted for in the model. In both experiments the depth of cuts at both the start and end of the cutting path were *1.905* and *3.301 mm* over a machined length of *80 mm* while using a feed of *0.3 mm/rev*. The results in Fig. 6.19 show the system performance with induced sensor noise. In order to investigate the system robustness and reliability in the case of noisy measurement, sensor noise was induced during this experiment by lowering the level of the cutting fluid in the reservoir, which results in generating bubbles in the fluid stream. It can be observed in Fig. 6.19 that in spite of the noise the output accuracy is still maintained within *10 μm*.

In order to demonstrate the significance of using the process model predictions to account for the measurement delay, a control cutting experiment was designed and performed based on sensor feedback only. The controller used is a simple PID which has a step response (when no delay is encountered) similar to that of the model based controller (shown in Fig. 6.10). The results presented in Fig. 6.20 show the performance of the PID controller in a straight cut experiment for a depth of cut of *1.905 mm* and feed of *0.3 mm/rev*. The oscillatory behavior of this controller is clearly due to the feedback delay and it is expected that the presence of any measured disturbances can easily threaten the stability of the system.

It should be noted that the success of the control experiments is largely due to the

measurement system developed. However further improvement in enhancing the quality of the measurement and bringing the sensor closer to the cutting point can certainly help increasing the bandwidth of the system. On the other hand the model stabilizes the control system effectively by accounting for the lag in the feedback loop. It is also believed that utilizing the servo loop of the machine tool in performing the control actions provides the system with more practicality and less external hardware as long as it does not limit the speed of the system response.

6.6 SUMMARY

A model-based GAC system was developed for bar turning. A mechanistic state space model of the machining system was formulated and used in the design and implementation of the control system. The model accounts for the machine tool servo dynamics, tool/workpiece structural dynamics and permits prediction of the cutting forces and workpiece form error. A Kalman Filter was designed and used to update the model predictions using on-line measurement of the workpiece diameter. This is essential to compensate for model missmatch or the occurance of unmodelled disturbances such as thermal deformation and tool wear. An LQG controller with an integral action was designed to regulate the depth of cut. The system was implemented on a CNC lathe retrofitted with an OAC. The robustness of the control system was evaluated experimentally using different cutting conditions. It can be concluded from the presented results that the proposed system is capable of improving the diameteral accuracy of the workpiece by more than 90%.

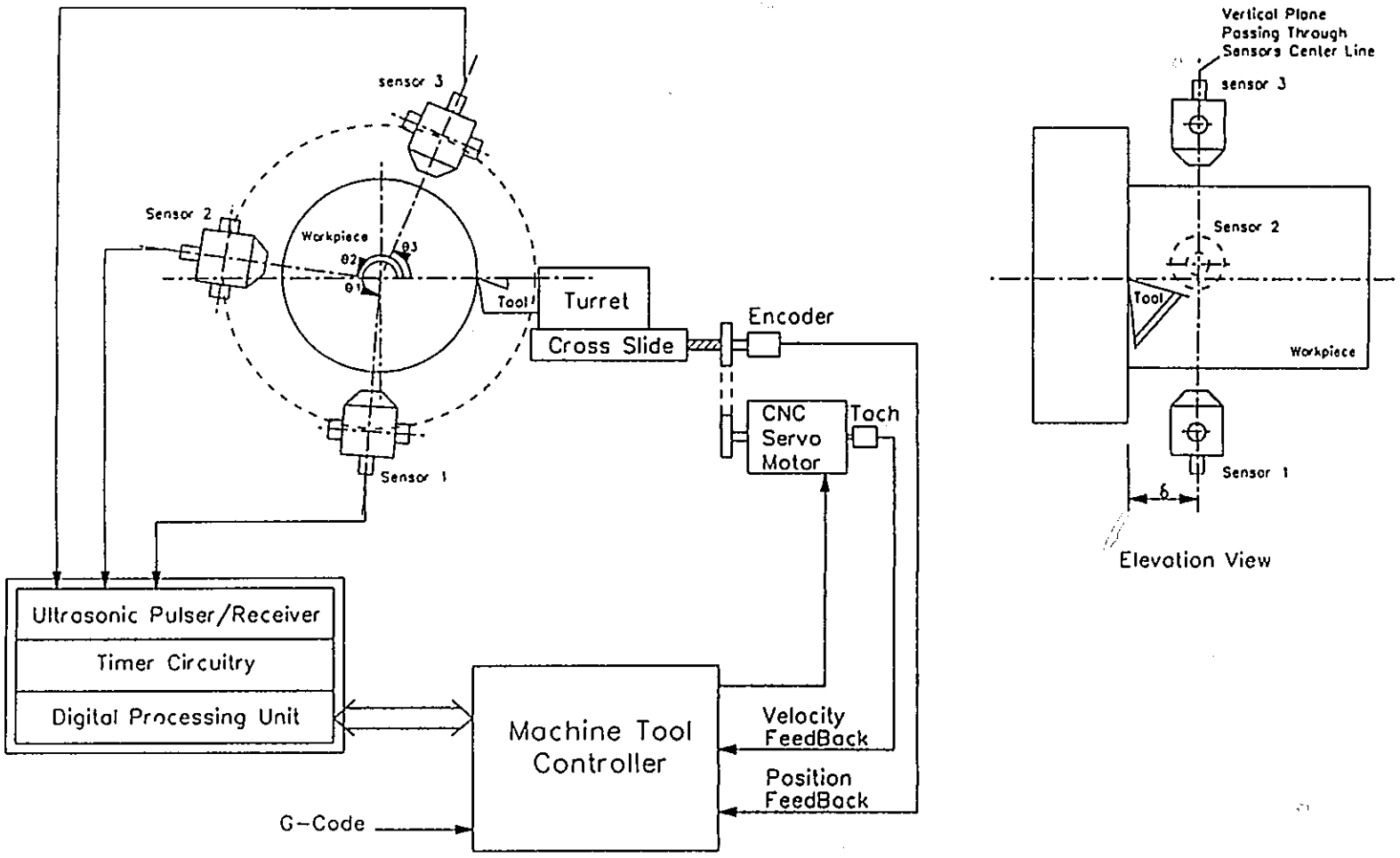

Fig. 6.1 Schematic Arrangement of the Proposed GAC System.

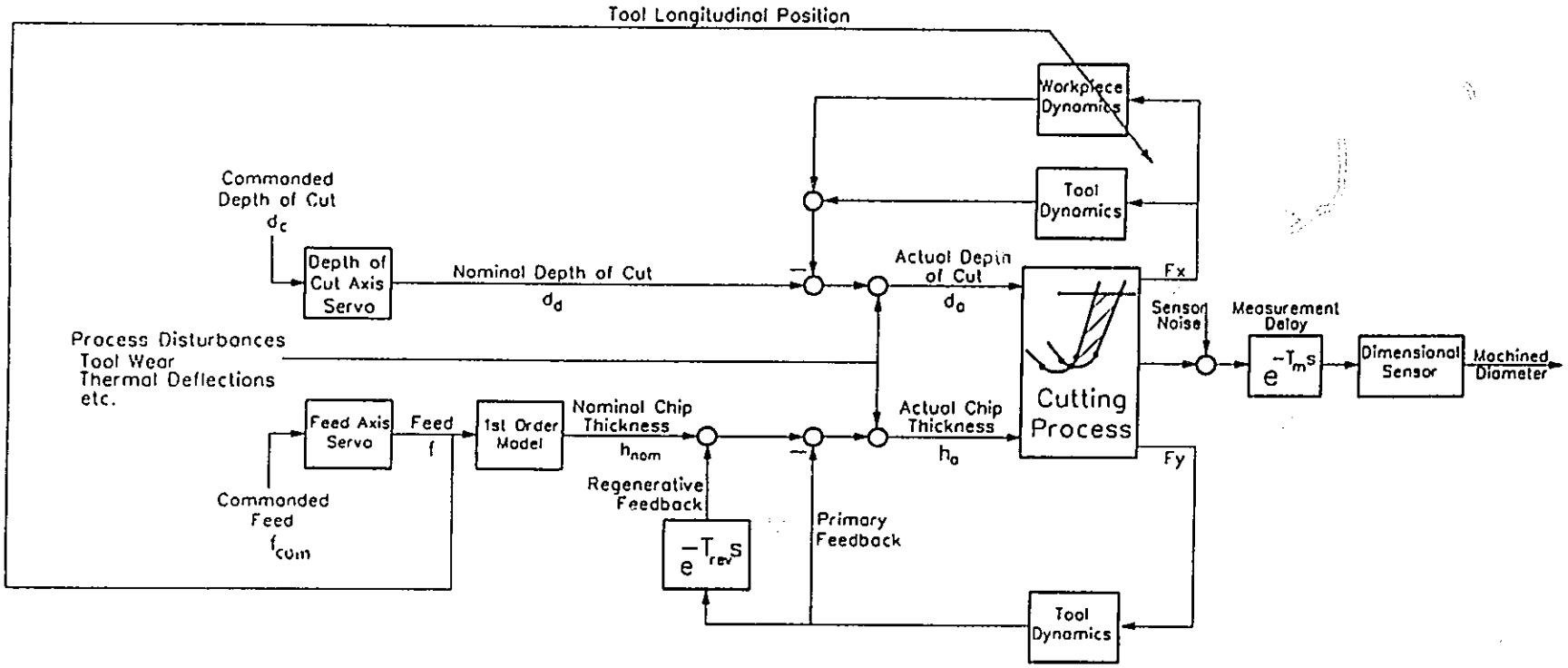

Fig. 6.2 Structure of the Machining System in Bar Turning.

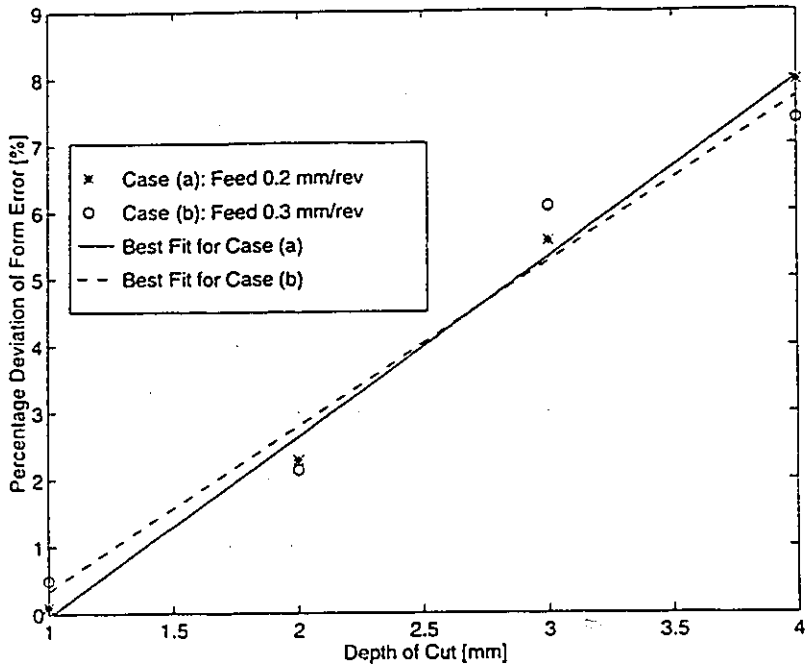

Fig. 6.3 The effect of neglecting the Tangential Cutting Force on Model Predictions of the Workpiece Form Error.

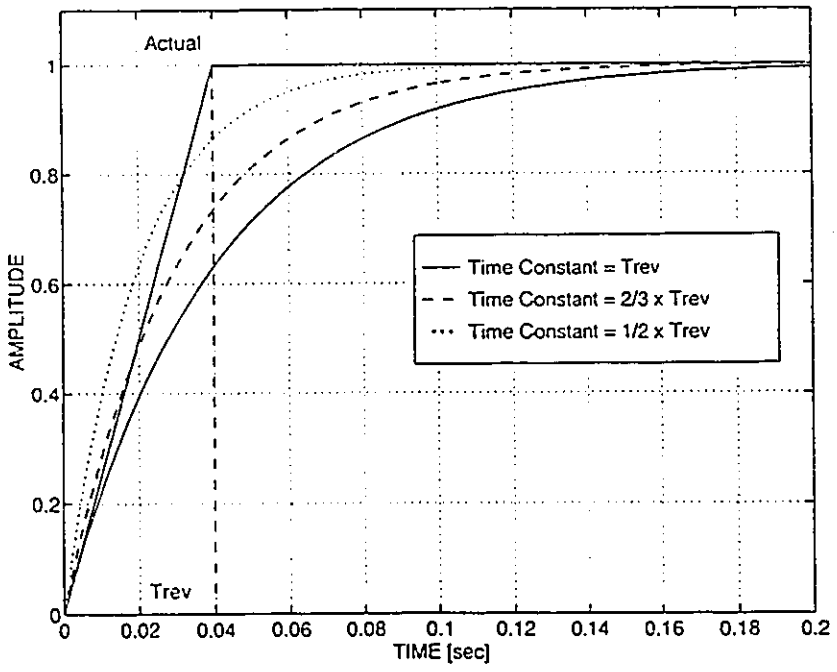

Fig. 6.4 Modeling of the Actual Chip Thickness Development over One Workpiece Revolution using a First Order Model.

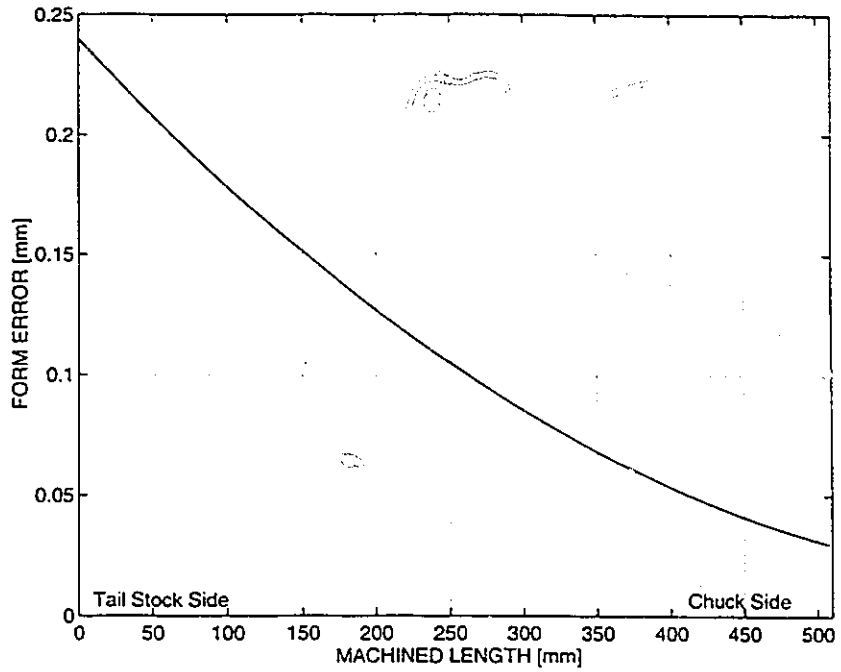

Fig. 6.5 Predicted Form Error Profile of a Workpiece Supported Between Two Centers. (Depth of Cut=2.0 mm, Feed=0.3 mm/rev, Cutting Speed=55 m/min.)

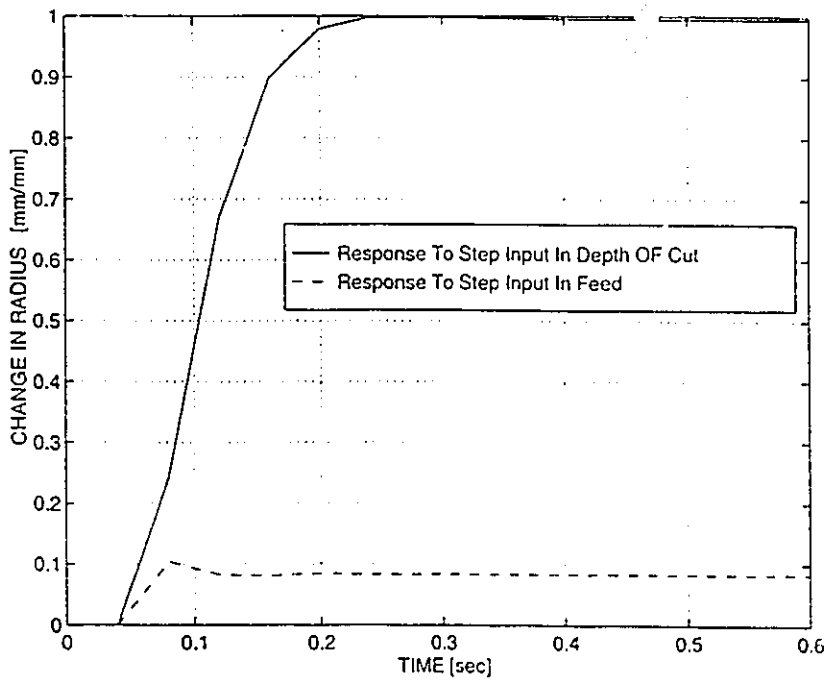

Fig. 6.6 Change in Workpiece Radius for Step Inputs in Depth of Cut and Feed of 0.1 mm and 0.1 mm/rev, respectively.

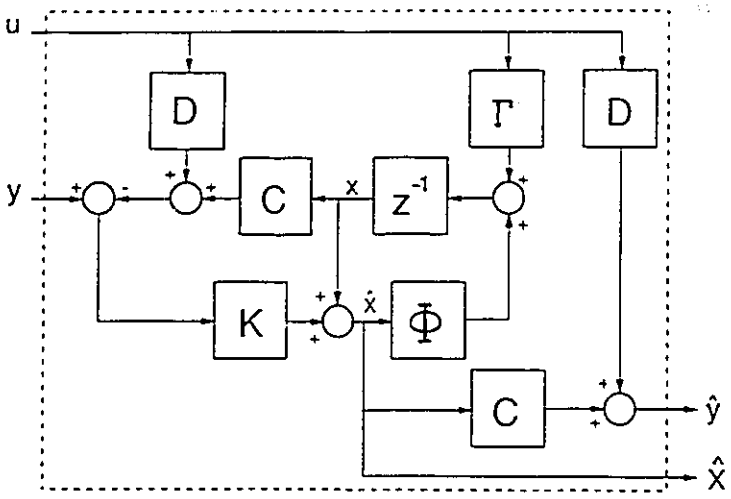

Fig. 6.7 Discrete Kalman Estimator Filter.

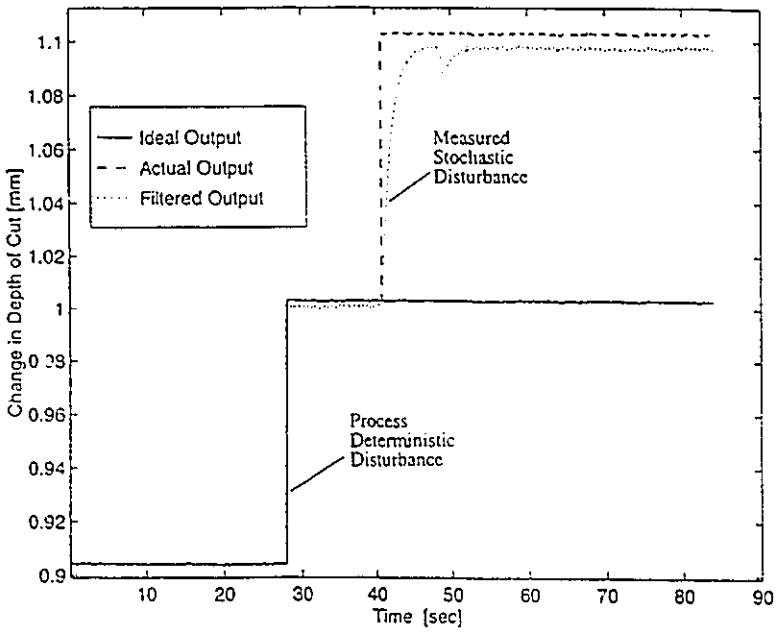

Fig. 6.8 Response of Kalman Filter and Output Prediction of Both Deterministic and Stochastic Disturbances.

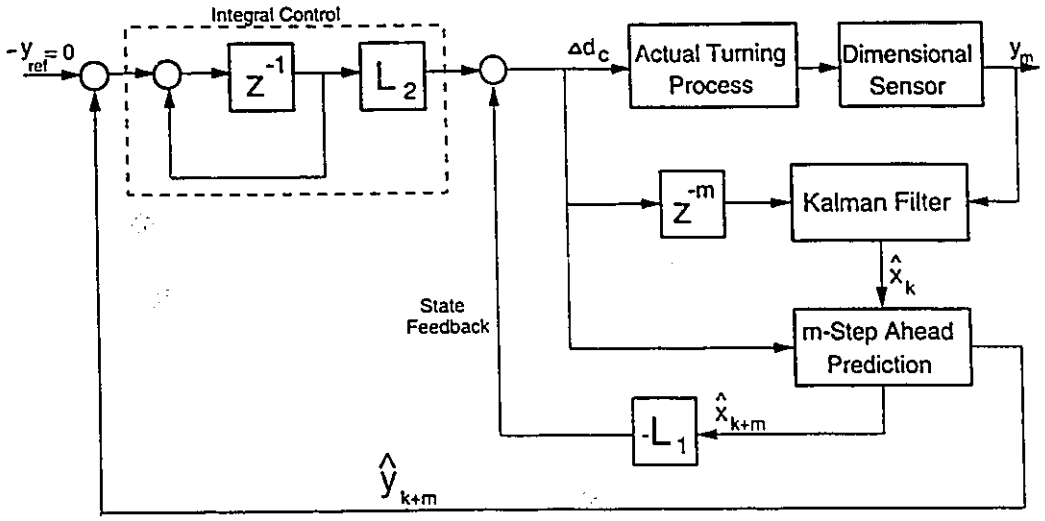

Fig. 6.9 The Structure of the Model-Based Predictive Controller.

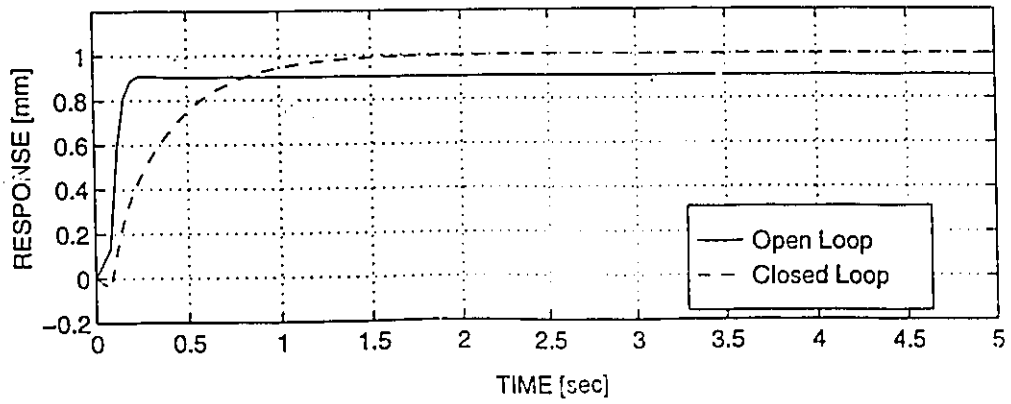

Fig. 6.10 Step Response of the Simulated Closed Loop.

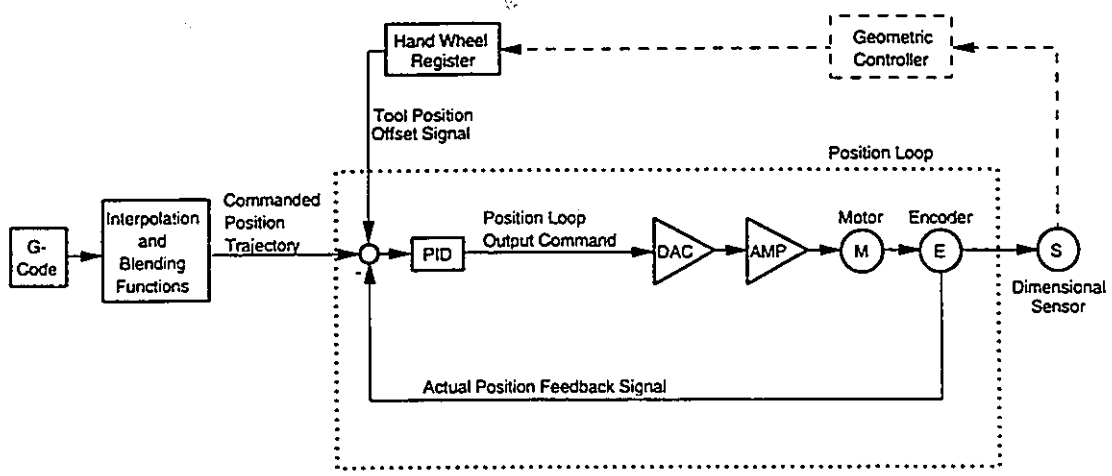

Fig. 6.11 The Machine Tool Position Control Loop with an Additional Control Offset Signal.

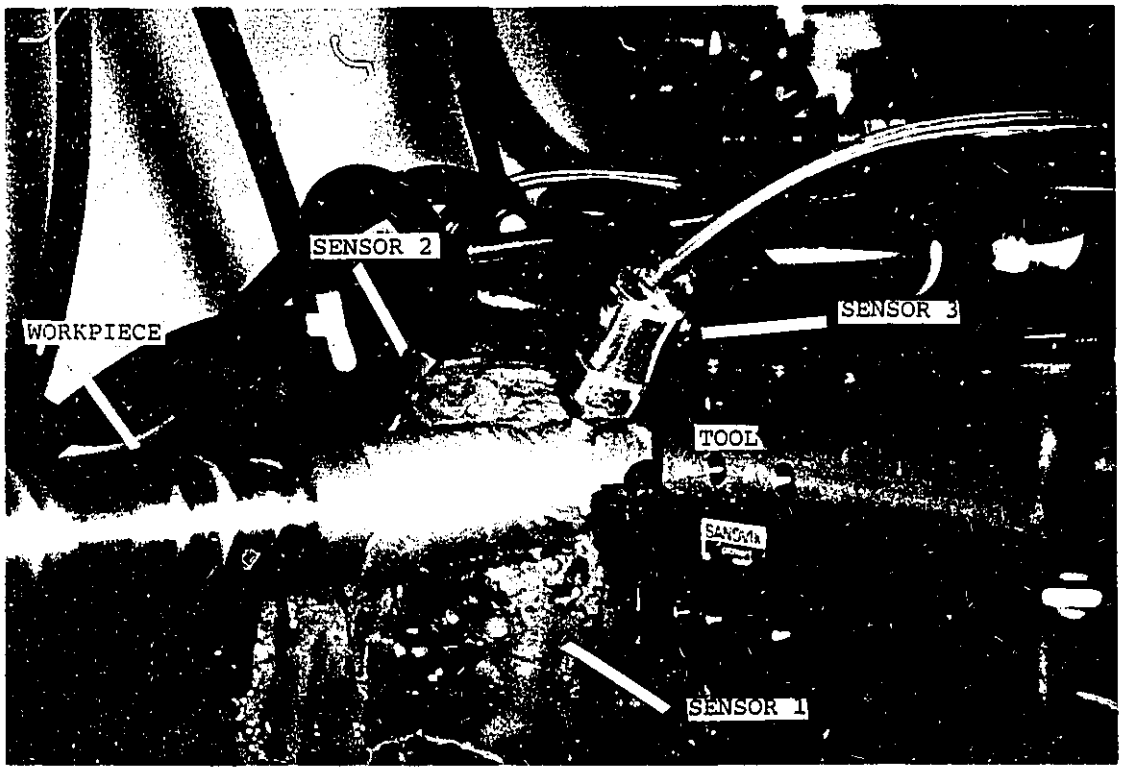

Fig. 6.12 A Close-Up Photograph Showing the Tool and the Measurement System during Operation.

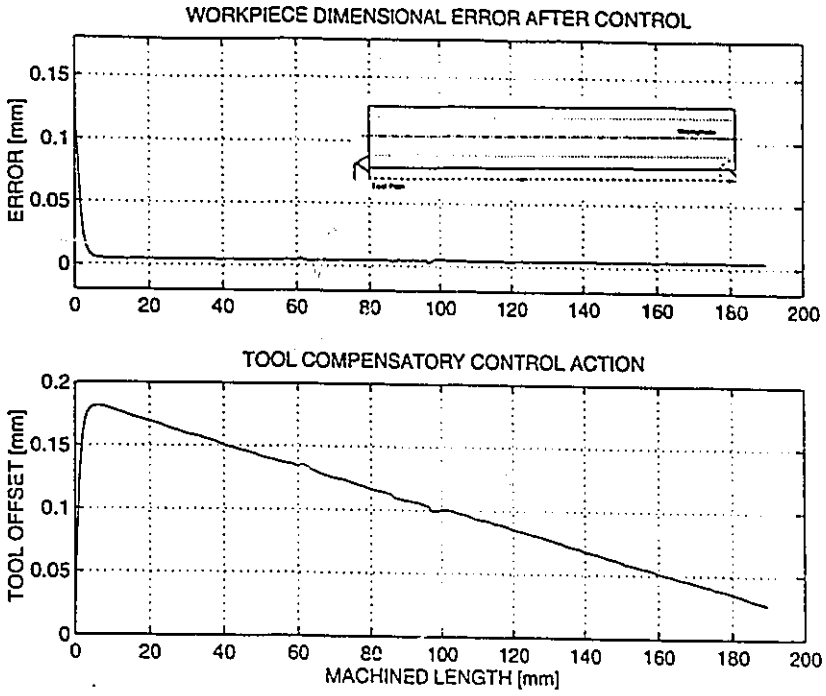

Fig. 6.13 Control System Performance in Straight Bar Turning. (Depth of Cut = 1.905 mm, feed = 0.3 mm/rev, Cutting Speed = 55 m/min)

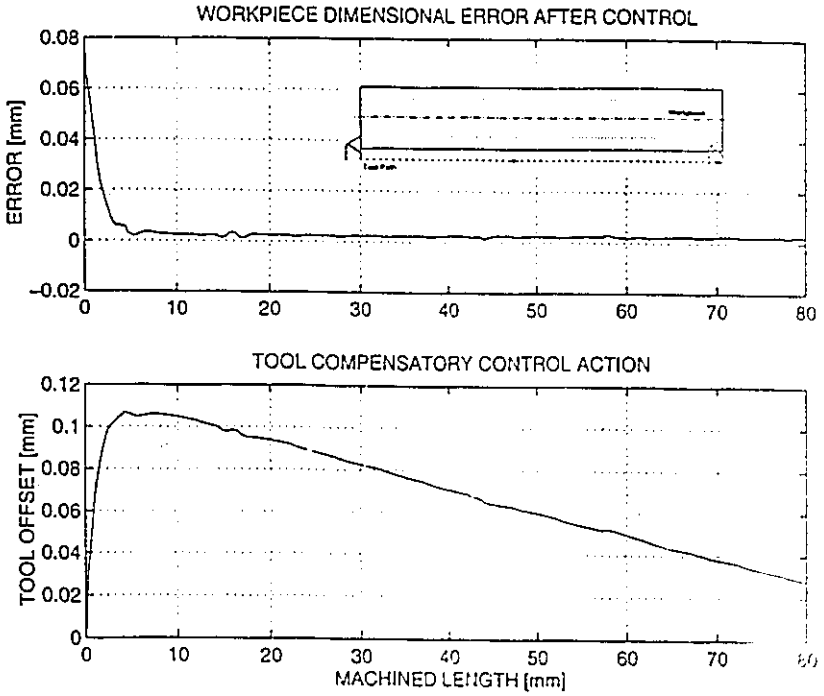

Fig. 6.14 Control System Performance in Straight Bar Turning. (Depth of Cut = 1.905 mm, feed = 0.2 mm/rev, Cutting Speed = 55 m/min)

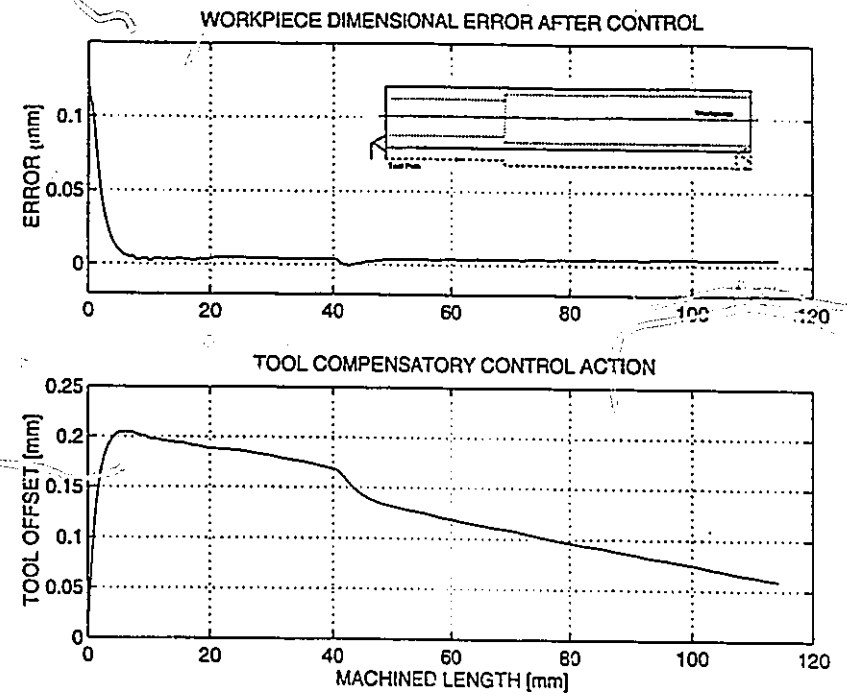

Fig. 6.15 Performance of the Control System during a Step Change of 0.762 mm in the Depth of Cut.

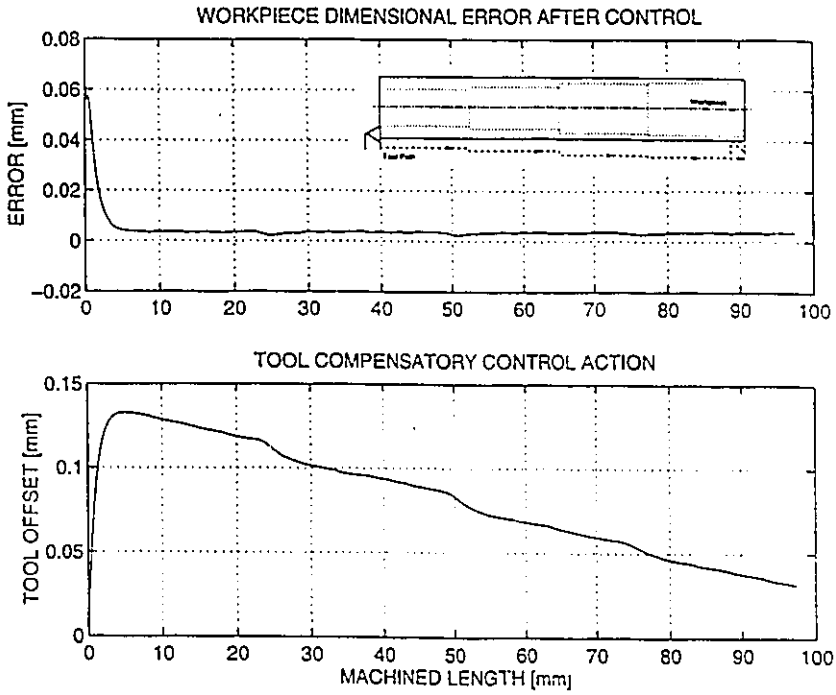

Fig. 6.16 Performance of the Control System during Three Step Changes of 0.381, 0.381, and 0.254 mm in the Depth of Cut.

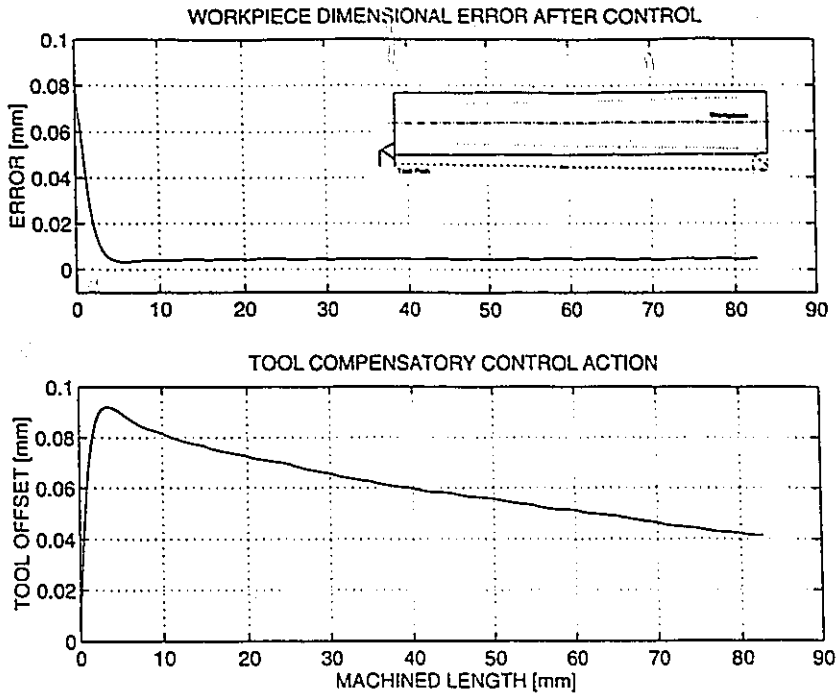

Fig. 6.17 Control System Performance in Taper Turning.

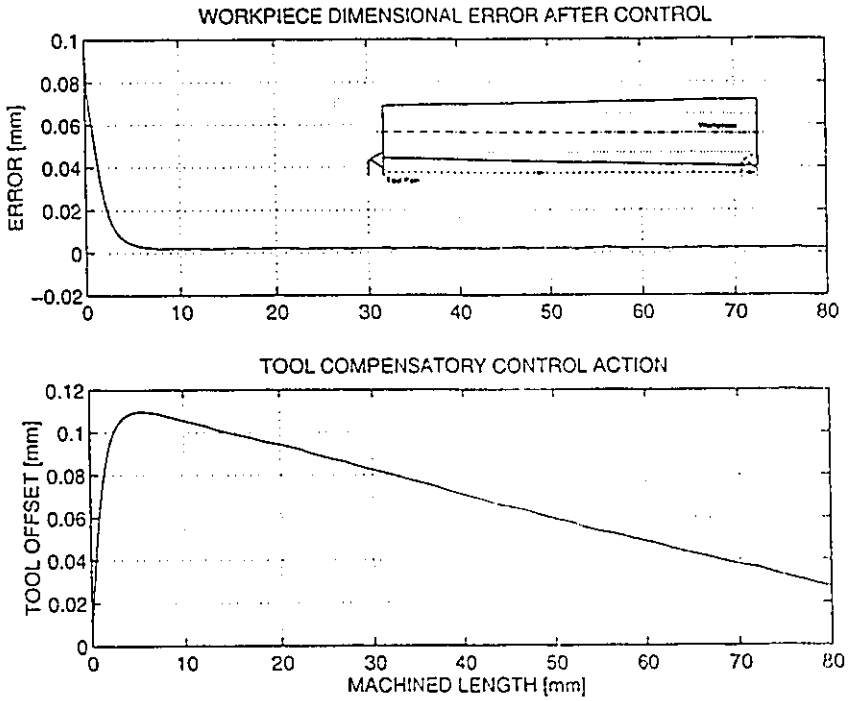

Fig. 6.18 Control System Performance in Straight Bar Turning Using a Tapered Workpiece.

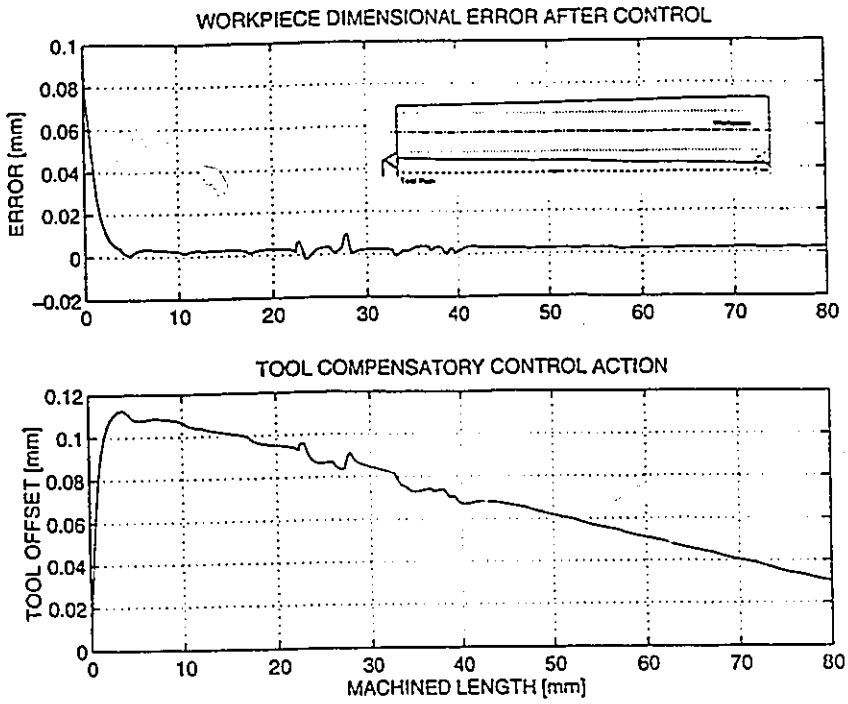

Fig. 6.19 Control System Performance in Straight Bar Turning Using a Tapered Workpiece and Measurements with Induced Sensor Noise.

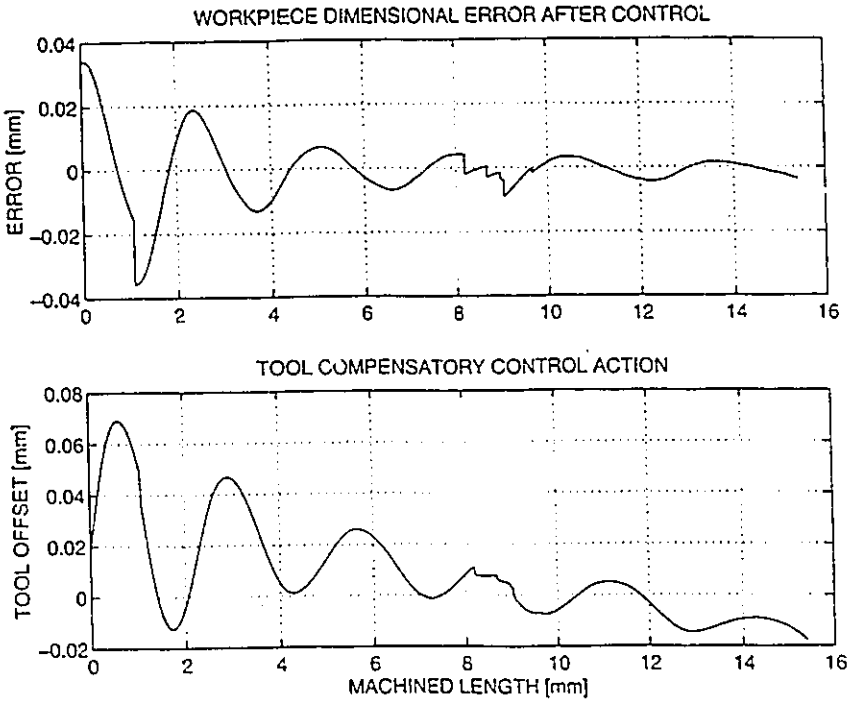

Fig. 6.20 Control System Performance Using Sensor Only without Model Contribution.

CHAPTER 7

CONCLUSIONS AND RECOMMENDATIONS FOR FUTURE WORK

The research presented in this dissertation described the development and integration of the different subsystems required to implement GAC in bar turning. These subsystems are: modeling of the machining system, on-line measurement of the workpiece geometry, tool actuation and predictive control design. This chapter begins with a summary of the work completed in this study and the main conclusions. Next, an outline of the primary contributions of the research is presented. Finally, the chapter concludes with recommendations for future work.

7.1 CONCLUSIONS

A mechanistic model of the machining system in bar turning was developed in Chapter 3. The simulation of machining dynamics is significantly enhanced by incorporating a mechanistic ploughing force model which permits the prediction of cutting process damping. The ploughing forces at the clearance face were decomposed into static and dynamic components. The static component is due to tool edge radius and tool feed while the dynamic component is due to machined surface undulations. The dynamic component

is responsible for the process damping and is considered proportional to the dynamic change in the volume of ploughed work material. The volume calculations were developed for a multi-edged cutting tool where both radial and longitudinal vibrations have to be considered. Such vibrations are the resulting superposition of both the workpiece and tool displacements. Experimental modal analysis techniques were used for the identification of the structural dynamics. The model was further expanded by adding a surface topography generation module to construct the predicted machined surface. The model was used to predict the cutting forces, surface topography and form error in slender bar turning. Experimental results for turning hardened steel with ceramic inserts were used for model verification.

Next, a novel non-contact system was developed in Chapter 4 which allows on-line high speed monitoring of the workpiece diameter. It employs three ultrasonic transducers and provides an absolute diameter measurement. The measurement system has a compact design and uses the cutting fluid as the coupling medium for transmitting the ultrasonic waves. The system was incorporated into a CNC lathe. Proximity measurements performed during real cutting experiments revealed a significant translation in the workpiece axis of rotation as a result of the dynamic cutting forces. This causes misalignment between the sensors and the axis of rotation and leads to measurement errors. An algorithm based on multi-probe measurements was developed to process the radius data and simultaneously compensate for sensor misalignment by tracking the center-line of the workpiece. Sensor measurements were compared with those obtained from a CMM. The accuracy and repeatability of the measuring system were tested experimentally under realistic cutting conditions.

In Chapter 5, the on-line measurements were employed to evaluate size and geometrical tolerances of the workpiece. It was shown that the cylindricity tolerance of the workpiece can be determined successfully within the required accuracy using on-line data, provided that two main conditions are maintained. The first is that appropriate data conditioning procedures based on knowledge of the process error dynamics are implemented, and the second is that high density sample data sets are used. Since the on-line measurement system essentially employs non-contact/high speed sensors, it inherently provides the rich-data environment to fulfill the demand of large data sets. This extends the applicability of the measurement system to provide complete on-line assessment of workpiece geometry and reduces quality control costs drastically.

In Chapter 6, a model-based predictive controller was designed and implemented to minimize the form error of the workpiece in bar turning. The mechanistic model of the machining system was simplified and reformulated into the state space to permit design and real-time implementation of the control system. The measurement system was set as close as possible to the cutting edge (at a distance of 0.27 mm). An optimal regulator with a Kalman Filter was designed. The on-line measurement of the workpiece diameter is used through the Kalman Filter to update the model predictions with unmodeled process disturbances such as tool wear and thermal deflections of the tooling system. The system was implemented on a CNC lathe retrofitted with an OAC. The output of the geometric controller was used to govern the position of the tool tip in real-time by commanding the same servo motor which is driven by the preprogrammed G-code. The control system was tested experimentally under different cutting conditions.

In summary, from the work presented the following conclusions have been made:

1. Application of the developed mechanistic model in bar turning using a multi-edged oblique cutting tool provides good predictions of the instantaneous chip load, cutting forces, workpiece form error and machined surface topography for a wide range of cutting conditions with minimal model calibration effort.
2. Incorporation of the mechanistic tool/workpiece interference model significantly enhances the prediction of machining dynamics. Including the ploughing forces to account for process damping is not only important for stability prediction but also necessary for surface roughness predictions specially in low feed finishing pass scenarios.
3. Decomposition of the workpiece indented volume into static and dynamic components showed the correlation between the static volume and the normal measured cutting force and the possibility of using this correlation in calibrating the ploughing force model mechanistically.
4. The contribution of process damping to the machining system is governed by the nature of surface undulations. It varies with the level of excitation as well as the dynamic response of the structure.
5. Experimental identification of the dynamic characteristics of the tool/workpiece dynamic system resulted into more realistic boundary conditions for the workpiece model and a reduced order model for the tool.
6. In hard turning the ratio of deterministic *Ra* to random *Ra* can reach *1:10* for relatively small feeds. This greatly emphasizes the importance of the random excitation mechanism due to material inhomogeneity in predicting the machined

surface topography.

7. Although the indirect ultrasonic technique for on-line measurement of workpiece diameter requires a multi-probe setup, it is more applicable and provides more accuracy than the direct (caliper) measurement.

8. Slender workpieces exhibit a significant translation in their axis of rotation under the effect of the cutting forces. This causes sensor misalignment that varies in both magnitude and direction for different cutting conditions and along the cutting length. Such effect can greatly degrade the accuracy of an on-line measuring system leading to serious measurement errors.

9. Based on multi-probe measurement, sensor misalignment can be compensated. The algorithm developed works effectively in eliminating this error and determining the diameter of the workpiece from three proximity measurements.

10. Testing the ultrasonic on-line measurement system during realistic cutting conditions showed the diameter measurements to have an accuracy and working range of ± 5 μm and 20 mm, respectively. The measurement has a cycle time of 2.3 ms.

10. Evaluation of workpiece geometrical tolerances based on on-line dimensional measurement requires appropriate data conditioning and high density sample data sets. Although, data conditioning based on process knowledge is inconsistent with the tolerancing standard, it provides the appropriate conditioning for on-line measurements.

11. The tolerance function derivatives are quite lengthy specially in the case of cylindricity tolerance. However, non-linear optimization based on gradient information results in faster convergence. Thus, if minimax fit is to be used,

reformulation of the tolerance function using constrained optimization will be more beneficial.

12. The influence of neglecting the tangential cutting force on model predictions of the workpiece form error is less than 10%.

13. Application of the model-based predictive controller to compensate workpiece form error in bar turning improves the diametral accuracy of the workpiece by more than 90%. Although the success of the control system is greatly due to the sensor developed, the predictive ability of the controller using the model is essential to stabilize the system by compensating for the delay in the feedback loop.

14. The OAC is an essential platform for the practical implementation of a GAC system. It effectively permits the controller to read and change the different parameters of the machine tool positioning servo loops in real-time.

7.2 CONTRIBUTIONS OF THIS RESEARCH

The contributions of this research effort lie primarily in the improvement and better understanding of the machining system accuracy in bar turning gained through the modeling, on-line measurement and control of the process. It also provides a useful basis for further development in the area of "Intelligent Machining Systems". Based on the conclusions above, the contributions of this research effort can be summarized as follows:

1. A mechanistic dynamic process model for bar turning has been developed and enhanced by incorporating the effect of ploughing forces as a source of process damping through the implementation of a decomposition concept of the ploughing

forces into static and dynamic components. The model is used as a computer simulation to predict cutting forces, workpiece form error and machined surface topography.

2. A novel ultrasonic on-line measurement system has been developed and implemented to measure the workpiece absolute diameter while turning using a cutting fluid. The measurement system operates reliably during wet cutting and thus has a great industrial potential. The system can be extended to provide a complete on-line assessment of the workpiece accuracy and reduce quality control costs significantly.

3. A new approach of GAC has been proposed using a model-based predictive control strategy in which on-line measurements are integrated with the predictions of the mechanistic model using a Kalman filter. The system has been designed and implemented to improve the geometric accuracy of the workpiece in bar turning by regulating the tool position in real-time.

7.3 RECOMMENDATIONS FOR FUTURE WORK

Numerous doors for future research have been opened with this research effort involving both modeling and experimental work. Future work should be directed towards the following:

1. Investigation of the proposed method for calibrating the ploughing force model mechanistically using the correlation between the static ploughed volume and the normal cutting force in roughing cut scenarios with larger depths of cut.

2. Extending the developed chip load geometry model to handle the tool edge profile using more than three geometric elements. This would easily allow the model to

account for nose wear of the cutting tool.

3. The addition of flank wear and tool thermal deformation modules to the mechanistic model structure would certainly extend the accuracy of the model predictions to the more practical situations where the ideal conditions of tool sharpness and thermal stability cannot be safely assumed. This would also contribute to a better design and more robust performance of the GAC system with smaller Kalman gain and less reliance on the measurement system. However, care should be taken in such development not to use "difficult-to-obtain-parameters" which could complicate the calibration of the model and decrease its practicality.

4. Applying the proposed GAC system to compensate for out of roundness errors which are seen more significantly in machining less rigid workpieces such as hollow shafts.

5. Using the developed mechanistic model off-line for tool path planning and cutting condition optimization for the objective of minimizing machining time and surface errors. This can be beneficial for setups where the implementation of real time control is not possible.

6. Extending the application of the proposed GAC system to contoured workpieces and surfaces with large taper angles, either by modifying the sensor design or actuating the measurement system.

7. Extending the application of the proposed GAC system to other machining processes such as boring, milling and grinding.

8. Modification of the sensor design to allow on-line measurement of the machined surface roughness.

BIBLIOGRAPHY

Albrecht, P., 1965, "Dynamics of the Metal-Cutting Process", Trans. ASME, *J. of Eng. for Ind.*, Vol. 87, Nov., pp. 429-441.

Albrecht, P., 1960, "New Developments in the Theory of the Metal-Cutting Process, Part I. The Ploughing Process in Metal Cutting", Trans. ASME, *J. of Eng. for Ind.*, Vol. 82, pp. 348-358.

Albrecht, P., and McCabe, J. T., et al., 1985, "In-Process Control of Machining", *Precision Engineering*, Vol. 7, No. 2, pp. 77-85.

Alverio, J., 1984, "*An Investigation on the Effect of Tool Geometry and Cutting Conditions on Machining Forces and a Model for Force Prediction in Oblique Machining*", M.Sc. Thesis, Polytechnic Institute, Troy, NY.

Andrew, C., 1964, "Chatter in Horizontal Milling", *Proceedings, Inst. Mech. Engr.*, Vol. 179, part 1, No. 28, pp. 877-906.

ANSI Y14.5M-1982, *Dimensioning and Tolerancing*, American Society of Mechanical Engineers, New York, NY.

Armarego, E. J. A., 1970, "Metal Cutting Analysis for Turning Operations", *J. Mach. Tool. Des. Res.*, Vol. 10, pp. 361-379.

Armarego, E. J. A., 1977, "A General Cutting Analysis for Machining Operations with Plane Rake Face Tools", *Proceedings, Australian Conference on Manufacturing Engineering*, pp. 42-46.

Armarego, E. J. A. and Uthaichaya, M., 1977, "A Mechanics of Cutting Approach for Force Prediction in Turning Operations", *J. of Eng. Prod.*, Vol. 1, pp. 1-18.

Asao, T., Mizugaki, Y., and Sakamoto, M., 1992, "Precision Turning by Means of a Simplified Prediction Function of Machining Error", *Annals CIRP*, 41(1), 447-450, France.

ASNT, 1991, "*Non Destructive Testing Handbook*," American Society for Non-Destructive Testing , Vol. 7, Ultrasonic Testing, Chapter 8.

Babin, T. S., J. M. Lee, J. W. Sutherland, and S. G. Kapoor, 1995, "A Model for the End Milled Surface Topography," *Proceedings, NAMRC 13*, pp. 362-368.

Babu, U., Raja, J., and Hocken, R. J., 1993,"Sampling Methods and Substitute Geometry Algorithms for Measuring Cylindricity in Coordinate Measuring Machines", *Proceedings, Annual Meeting of the ASPE*, Seattle, WA, 103.

Badiv, K., Rall, K., and Mattle, H. P., 1980, "Automatic Dimensional Control with Machine Integrated Gauging on NC Lathes," *Industrial and Production Eng.*, Vol. 1, pp. 61-68.

Bailey, J. A., 1975, "Friction in Metal Machining - Mechanical Aspects", *Wear*, Vol. 31, pp. 243.

Bajpai, S., 1972, "Optimization of Workpiece Size for Turning Accurate Cylindrical Parts", *J. Mach. Tool. Des. Res.*, Vol. 12, No. 3, pp. 221-228.

Bath, M., and Sharp, R., 1972, "In-Process Control of Lathes Improves Accuracy and Productivity," *Proceedings, 9th Int. MTDR Conf.*, pp.1209-1221.

Bisacre, F. F. P. and Bisacre, G. H., 1948, "The Life of Carbide - Tipped Turning Tools", *Proceedings, Inst. Mech. Engr.*, Vol. 157, pp. 452-469.

Boothroyd G., 1975, "*Fundamentals of Metal Machining and Machine Tool*", Scripta Book Co., Washington, D.C.

Brent, R. P., 1973, "*Algorithms for Minimization Without Derivatives*", Englewood Cliffs, NJ, Prentice Hall, Chapter 5.

Brown, D. L., 1976, "*Grinding Dynamics*", Ph. D. Thesis, University of Cincinati.

Brown, R. H. and Armarego, E. J. A., 1964, "Oblique Machining with a Single Cutting Edge", *Int. J. Mach. Tool. Des. Res.*, Vol. 4, pp. 9-25.

Chao, B. T. and Bisacre, G. H., 1951, "The Effect of Speed and Feed on the Mechanics of Metal Cutting", *Proceedings, Inst. Mech. Engr.*, Vol. 165, pp. 1-9.

Chao, B. T., Trigger, K. J., Zysltra, L. B., 1952, "Thermo-physical Aspects of Metal Cutting", *Transaction of ASME*, Vol. 74, pp. 1039-1054.

Colwell, L. V., 1954, "Predicting the Angle of Chip Flow for Single-Point Cutting Tools", *Transaction of ASME*, Vol. 76, pp. 199-204.

Cook, N. H., 1966, "*Manufacturing Analysis*", Addison-Wesley Publishing Co. Inc., Reading, Massachusetts.

Das, M. K. and Tobias, S. A., 1967, "The Relation between the Static and the Dynamic Cutting of Metals", *J. Mach. Tool. Des. Res.*, Vol. 7, pp. 63-89.

Dawson, J. W., 1992, "Cylindricity and its Measurement", *Int. J. Mach. Tools Manufact.*, Vol. 32, No., 1/2. pp. 247-253.

DeVor, R. E., Kline, W. A., and Zdeblick, W. J., 1980, "A Mechanistic Model for the Force System in End Milling with Application to Machining Airframe Structures," *Proceedings, NAMRC 8*, pp. 297-303.

DeWalle, S., Hamoen, D., and Boyd, J., 1983, "Apparatus and Method for Ultrasonic Inspection", US. Patent 4403510, Sept. 13.

Doi, S., and Kato, S., 1956, "Chatter Vibration of Lathe Tools", *Transaction of ASME*, Vol. 78, pp. 1127-1134.

Elbestawi, M. A., Ismail, F., Du, R. X., and Ullagaddi, B. C., 1991, "Modeling Machining Dynamics Including Damping in the Tool-Workpiece Interface", *Proceedings, ASME WAM*, PED-vol. 54/TRIB -vol. 2, pp. 253-263, Atlanta.

ElMaraghy, W. H., Wu, Z., and ElMaraghy, H. A., 1989, "Evaluation of Actual Geometric Tolerances Using Coordinate Measuring Machine Data", *Proceedings, 15th Design Automation Conference, ASME Des Eng Div*, Montreal, Quebec, Canada, p.197.

Elwardani T., Elbestawi M., Attia M. H., and Mohamed E., 1992, "Surface Finish in Turning of Hardened Steel", *Proceedings, ASME WAM*, PED- vol. 62, Engineered Surfaces, pp. 141-159.

Endres, W. J., Sutherland, J. W., DeVor, R. E., Kapoor, S. G., 1990, "A Dynamic Model of the Cutting Force System in the Turning Process", *Proceedings, ASME WAM*, PED-Vol. 44, pp. 193-212, Texas.

Feng, S. C., and Hopp, T. H., 1991, "A Review of Current Geometric Tolerancing Theories and Inspection Data Analysis Algorithms", Technical Report NISTIR-4509, National Institute of Technology and Standards, Gaithersburg, MD.

Field, M., Merchant, M. E., 1949, "Mechanics of Formation of the Discontinuous Chip in Metal Cutting," *Transaction of ASME*, Vol. 71, pp. 412-428.

Fox, R. L., 1971, "*Optimization Methods for Engineering Design*", Addison-Wesley, Publishing Co. Inc., Reading, Massachusetts.

Fu. H. J., DeVor, R. E., Kapoor, S. G., 1984a, "A Mechanistic Model for the Prediction of the Force System in the Face Milling Operations", Trans. ASME, *J. of Eng. for Ind.*, Vol. 106, p. 81-88.

Fu, H. J., DeVor, R. E., and Kapoor, S. G., 1984b, "The Optimal Design of Tooth Spacing in Face Milling Via a Dynamic Force Model," *Procedings, NAMRC 12*, pp. 291-297.

Gonin, R., and Monew, A., 1989, *Non-Linear L_p-Norm Estimation*, Marcel Dekker, NY.

Gurney, J. P., and Tobias, S. A., Tobias, 1962, "A graphical Analysis of Regenrative Machine Tool-Instability", Trans. ASME, *J. of Eng. for Ind.*, Series B84(1), pp. 103-112.

Gustafson, D. A., 1990, "*The Effects of Tool Geometry and Wear on the Cutting Force System in Turning*", M.Sc. Thesis, University of Illinois at Urbana-Champaign.

Hahn, R. S., 1953, "Metal Cutting Chatter and its elimination", *Transaction of ASME*, Vol. 75, pp. 1073-1080.

Haibao, L., Xinmin, Q., Li, D., and Jiadong, S., 1990, "Approach for the On-Line Equipment for Measuring Variation in a Turning Size Using Laser", *Proceedings, SPIE*, International Conference on Optoelectronic Science and Engineering, Vol. 1230, pp. 231-234.

Hanna, N. H., and Tobias, S. A., 1969, "The Non-Linear Dynamic Behavior of a Machine Tool Structure", *J. Mach. Tool. Des. Res.*, Vol. 9, pp. 293-307.

Hocken, R., Raja, J., and Babu,U., 1993, "Sampling Issues in Coordinate Metrology", *Manufacturing Review*, 6(4), pp. 282-294.

Hopp,T. H.,1993, "Computational Metrology", *Manufacturing Review*, 6(4), pp. 295-304.

Jona, M. G., 1971, "Scope and Possibilities of Geometrical Adaptive Control in Turning", *CIRP Annals*, Vol. 19, pp. 305-309.

Kakino, Y., and Kitazawa, J., 1978, "In-Situ Measurement of Cylindricity," *CIRP Annals*, Vol. 27.

Kalman R. E., 1960, "A New Approach to Linear Filtering and Prediction Problems", *J. Basic Eng.* Trans. ASME, Series D, 82, pp. 33-45.

Kegg, R. L., 1965, "Cutting Dynamics in Machine Tool Chatter: Contribution to Machine-Tool Chatter Research - 3", Trans. ASME, *J. of Eng. for Ind.*, Vol. 87, pp. 464-470.

Kim, K., Eman, K. F., and Wu, S. M., 1987, "In-process Control of Cylindricity in Boring Operations," *J. Eng. for Ind.*, Trans. ASME, Vol.109, pp. 291-296.

Kim, K. H., Eman, K. F. and Wu, S. M., 1986, "Feasibility of Form Accuracy identification and Control in Cylindrical Grinding", *Int. J. Mach. Tool Des. Res.*, Vol. 26, No. 3, pp. 259-266.

Kim, K. J., Eman, K. F., and Wu, S. M., 1984, "Identification of Natural Frequency and Damping Ratios of Machine Tool Structures by the Dynamic Data System Approach", *J. Mach. Tool. Des. Res.*, Vol. 24, No. 3, pp. 161-169.

Koenigsberger, I., and Tlusty, J., 1971, "*Structures of Machine Tools*", Pergamon Press.

Kohno, T., Okazaki, Y., Ozawa, N., Mitui, K., and Omoda, M., 1989, "In-Process Measurement and a Workpiece-referred from Accuracy Control System (WORFAC): Concept of the Method and Preliminary Experiment," *Precision Engineering*, Vol. 11, No. 1, pp. 9-14.

Kuhl, M. J., 1987, "*The Prediction of Cutting Forces and Surface Accuracy for the Turning Process*", M.Sc. Thesis, University of Illinois at Urbana-Champaign.

Kwiatkowski, A. W., and Al-Samarai, H. M., 1968, "Identification of Milling Machine Reseptances from Random Signals During Cutting", *CIRP Annals*, Vol. 16, pp. 137-144.

Lau, W. S., and Rubenstein, C., 1983, "The Mechanics of Continuous Chip Formation in Oblique Cutting: Part II. Comparison of Experimental Data with Deductions from Theory", Vol. 23, pp. 21-37.

Lee, H. E., and Shaeffer, W. B., 1951, "The Theory of Plasticity Applied to a Problem of Machining", Trans. ASME, Journal of Applied Mechanics, Vol. 73.

Lemon, J. R., and Ackermann, P. C., 1965, "Applications of Self-Excited Machine Tool Chatter Theory: Contribution to Machine-Tool Chatter Research - 4", Trans. ASME, *J. of Eng. for Ind.*, Vol. 87, Nov., pp. 471-479.

Lin, G. C. I., Mathew, P., Oxley, P.L.B., and Watson, A.R., 1982, "Predicting Cutting Forces for Oblique Machining Conditions", *Proceedings, Inst. Mech. Engr.*, Vol. 196(11), pp. 141-148.

Lin, G. C. I., 1978, "Prediction of Cutting Forces and Chip Geometry in Oblique Machining from Flow Stress Properties and Cutting Conditions", *J. Mach. Tool. Des. Res.*, Vol. 18, pp. 117-130.

Lin, G. C. I., and Oxley, P. L. B., 1972, "Mechanics of Oblique Machining: Predicting Chip Geometry and Cutting Forces from Work Material Properties and Cutting Conditions", *Proceedings, Inst. Mech. Engr.*, Vol. 186, pp. 813-820.

Lin, Y. T., 1985, "*Geometric Adaptive Control for Accuracy and Stability in Machining Cylindrical Workpieces*", Ph.D. Thesis, Purdue University, West Lafayette.

Long, G. W., and Lemon, J. R., 1965, "Structural Dynamics in Machine Tool Chatter: Contribution to Machine-Tool Chatter Research - 2", Trans. ASME, *J. of Eng. for Ind.*, Vol.

87, pp. 455-463.

Lu Wen, F., and Klamecki B., 1988, "Prediction of Chatter onset in Turning with a Modified Chatter Model", *Proceedings, ASME WAM*, PED-Vol. 49, pp. 237-252.

Luk, W. K., 1969a, "The Mechanics of Symmetrical Vee Form Tool Cutting", *J. Mach. Tool. Des. Res.*, Vol. 9, pp. 17-38.

Luk, W. K., 1969b, "The Direction of Chip Flow for a Single Point Lathe Tool with Zero Nose Radius", *J. Mach. Tool. Des. Res.*, Vol. 9, pp. 391-399.

Meirovitch, L., 1986, *"Elements of Vibration Analysis"*, McGraw-Hill, NY.

Merchant, M. E., 1944, "Basic Mechanics of the Metal Cutting Process", *Journal of Applied Mechanics*, Sept., pp. A168-A175.

Merchant, M. E., 1945a, "Mechanics of the Metal Cutting Process. I. Orthogonal Cutting and a Type 2 Chip", *Journal of Applied Physics*, Vol. 16(5), pp. 267-275.

Merchant, M. E., 1945b, "Mechanics of the Metal Cutting Process. II. Plasticity Conditions in Orthogonal Cutting", *Journal of Applied Physics*, Vol. 16(6), pp. 318-324.

Merrit, H. E., 1965, "Theory of Self-Excited Machine-Tool Chatter: Contribution to Machine Tool Chatter Research - 1", Trans. ASME, *J. of Eng. for Ind.*, Vol. 87, Nov., pp. 447-454.

Merwin, J. E. and Johnson, K. L., 1963, "An Analysis of Plastic Deformation in Rolling Contact," *Proceedings, Inst. Mech. Engr.*, Vol. 177, No. 25, pp. 676-690.

Minis, I. E., Magrab, E. B., Pandelidis, I. O., 1990, "Improved Methods for the Prediction of Chatter in Turning: Part I. Determination of Structural Response Parameters", Trans. ASME, *J. of Eng. for Ind.*, Vol. 112, pp. 12-20.

Mohamed, E., 1994, "Cutting Performance and Tool Failure Characteristics during Machining of Difficult-to-Cut Materials Using Ceramic Tools", Master Thesis, McMaster University, Hamilton, Ontario.

Morcos, W. A., 1980, "A Slip Line Field Solution of the Free Oblique Continuous Cutting Problem in Conditions of Light Friction at Chip-Tool Interface", Trans. ASME, *J. of Eng. for Ind.*, Vol. 102, Nov., pp. 310-314.

Morcos, W. A., 1972a, "Contribution to the Mechanics of Free Oblique Continuous Cutting", Int. J. of Prod. Res., Vol. 10(4), pp. 365-377.

Morcos, W. A., 1972b, "On the Mechanics of Rectilinear Continuous Cutting with a Single Point Tool", Trans. ASME, *J. of Eng. for Ind.*, Nov., pp. 1045-1052.

Moriwaki, T., Zhao, C., and Nishiuchi, M., 1990, "A Study on Machining Error in Turning due to Thermal Deformation of Tool", *Mem. Grad. School Sci. and Technol. Kobe Univ.*, 8(A), pp. 81-90.

Moriwaki, T., and Iwata, K., 1976, "In-Process Analysis of Machine Tool Structure Dynamics and Prediction of Machining Chatter", Trans. ASME, *J. of Eng. for Ind.*, Feb, pp. 301-305.

Murthy, T. S. R., 1982, "A Comparison of Different Agorithms for Cylindricity Evaluation", *Int. J. Mach. Tool Des. Res.*, **22**(4), pp. 283-292.

Murthy, T. S. R., and Abdin, S. Z., 1980, "Minimum Zone Evaluation of Surfaces", *Int. J. Mach. Tool Des. Res.*, **20**, pp. 123-136.

Nakayama, K., and Arai, M., 1983, "Semi-Empirical Equations for Three Components of Resultant Cutting Forces", *CIRP Annals*, Vol. 32(1), pp. 33-35.

Nakayama, K., and Arai, M., 1976, "On the Storage of Data on Metal Cutting", *CIRP Annals*, Vol. 25(1), pp. 13-18.

Newman, D. R., 1972, "Ultrasonic Thickness Measurement for Control of Machine Tools", *British J. NdT*, 5, pp. 73-79.

Nigm, M. M., 1981, "A Method for the Analysis of Machine Tool Chatter", *J. Mach. Tool. Des. Res.*, Vol. 21, pp. 251-261.

Nigm, M. M., Sadek, M. M., and Tobias, S. A., 1972, "Predictionn of Dynamic Cutting Coefficients from Steady State Cutting Data", *Proceedings, 13th MTDR Conf.*, Birmingham, pp. 3-12.

Novak, A., 1981, "Sensing of Workpiece Diameter, Vibration and Out of Roundness by Laser-Way to Automatic Quality Control," *CIRP Annals*, Vol. 30, No.1, pp.473-476.

Odayappan, O., 1992, *Development of Methodologies for Measurement of Circles on a Coordinate Measuring Machine*, Master Thesis, University of North Carolina at Charlotte, Charlotte, NC.

Pal, A. K., and Koeningsberger, F., 1968, "Some Aspects of the Oblique Cutting Process", *J. Mach. Tool. Des. Res.*, Vol. 8, pp. 45-47.

Peklinik, J., 1970, "Geometrical Adaptive Control of Manufacturing Systems," *CIRP Annals*, Vol. 18, pp. 265-272.

Peters, J., Vanhereck, P., and Van Brussel, H., 1972, "The Measurement of the Dynamic Cutting Coefficient," *Annals CIRP*, Vol. 20, pp. 129-136.

Press, W. H., Flannery, B. P., Teukolsky S. A., and Vetterling, W. P., 1990, *Numerical Recipes In C*, Cambridge University Press, Cambridge, U.K.

Rahman, M., and Ito, Y., 1979, "Machining Accuracy of a Cylindrical Workpiece Held by a Three-Jaw Chuck", *Bulletin of Japan Society of Precision Engng*, **13** (1), pp.7-12.

Rao, S. B. and Wu, S. M., 1982, "Compensatory Control of Roundness Error in Cylindrical Chuck Grinding", *J. of Eng. for Ind.*, Trans. ASME, Vol. 104, Feb. pp. 23-28.

Rubenstein C., 1983, "The Mechanics of Continuous Chip Formation in Oblique Cutting: Part I. Theory", *J. Mach. Tool. Des. Res.*, Vol. 23, pp. 11-20.

Russell, J. K., and Brown, R. H., 1966, "The Measurement of Chip Flow Direction", *J. Mach. Tool. Des. Res.*, Vol. 6, pp. 129-183.

Sabberwal, A. J. P., 1960, "Chip Section and Cutting Force During the Milling Operation", *CIRP Annals*, Vol. 8, pp. 197-203.

Sadek, M. M., and Knight, W. A., 1975, "Dynamic Acceptance Tests Applied to a Center-Type Lathe", *J. of Eng. for Ind.*, Trans. ASME, pp. 203-210.

Shaw, M. C., Cook, N. H., and Smith, P. A., 1952, "The Mechanics of Three-Dimensional Cutting Operations", *Transaction of ASME*, Vol. 74, pp. 1055-1064.

Shaw, M. C., and DeSalvo, G. J., 1970, "A New Approach to Plasticity and Its Application to Blunt Two Dimensional Indenters", Trans. ASME, *J. of Eng. for Ind.*, Vol. 92, 283-292.

Shawky, A. M., and Elbestawi, M. A., 1994, "Development of an Ultrasonic Sensor for In-Process Measurement of Workpiece Diameter in Bar Turning", *Proceedings, ASME WAM*, PED-Vol. 68-1, Chicago, pp. 193-202.

Shawky, A. M., and Elbestawi, M. A., 1996a, "An Enhanced Dynamic Model in Turning Including the Effect of Ploughing Forces", Trans. ASME, *J. of Eng. for Ind.*, (Accepted - to appear).

Shawky, A. M., and Elbestawi, M. A., 1996b, "In-Process Evaluation of Workpiece Geometrical Tolerances in Bar Turning", *Int. J. of Mach. Tools Manufact.*, Vol. 36, No. 1, pp. 33-46.

Shawky, A. M., and Elbestawi, M. A., 1996c, "Model-based Predictive Control of Workpiece Accuracy in Bar Turning", Trans. ASME, *J. of Eng. for Ind.*, (Submitted).

Shiraishi, M., and Uehara, K., 1979, "In-Process Control of Workpiece Dimension in Turning," *CIRP Annals*, Vol. 28, No. 1, p. 333.

Shiraishi, M. and Sato, S., 1990, "Dimensional and Surface Roughness Controls in a Turning Operation," *J. of Eng. for Ind.*, Trans. ASME, Vol. 112, pp. 78-83.

Shiraishi, M., 1991, "Optimal Control of Chatter in Turning", *Int. J. of Mach. Tools Manufact.*, Vol. 31, No. 1, pp.31-43.

Shiraishi, M., 1984, "Geometric Adaptive Control in NC Turning Operation," Trans. ASME, *J. of Eng. for Ind.*, Vol. 106, pp.75-80.

Smith, J.D., and Tobias, S.A., 1961, "The Dynamic Cutting of Metals", *J. Mach. Tool. Des. Res.*, Vol. 1, pp. 283-292.

Spaans, C., 1967b, "The Extra Forces near the Cutting Edge and Their Implications", *Proceedings*, International Conference on Manufacturing Technology, University of Michigan, Ann Arbor, Michigan, pp. 533-552.

Spaans, C., 1967a, "An Exact Method to Determine the Forces on the Clearance Plane", *CIRP Annals*, Vol. 15, pp. 463-469.

Spaans, C., 1970, "The Mechanics of Oblique Cutting, Taking Into Account the Forces on the Clearance Face", *J. Mach. Tool. Des. Res.*, Vol. 10, pp. 213-220.

Stabler, G. V., 1951, "The Fundamental Geometry of Cutting Tools", *Proceedings, Inst. Mech. Engr.*, Vol. 165, pp. 14-26.

Subramani, G., Kapoor, S. G., DeVor, R. E., and Hayashida, R., 1987a, "An Enhanced Model for the Simulation of Face Milling Operations," *Proceedings, 2nd Int. Conf. on Computer-Aided Production Engr.*, pp. 171-178.

Subramani, G., Suvada, R., Kapoor, S. G., DeVor, R. E., and Meingast, W., 1987b, "A Model for the Prediction of Force System for Cylindrical Boring Process", *Proceedings, 15th NAMRC*, April, pp. 439-446.

Sutherland, J. W., 1988a, "A Dynamic Model of the Cutting Force System in the End Milling Process," Proc., ASME Symposium on Sensors and Controls for Manufacturing, PED-Vol. 33, pp. 53-62.

Sutherland, J. W., Subramani, G., Kuhl, M. J., DeVor, R. E., Kapoor, S. G., 1988b, "An Investigation into the Effect of Tool and Cut Geometry on Cutting Force System Prediction Models", *Proceedings, 16th NAMRC*, pp. 264-272.

Takahashi, 1970, "*Control and Dynamic Systems*", Addison-Wesley, NY.

Taylor, H. R., 1977, "A Comparison of Methods for Measuring the Frequency Response of Mechanical Structures with Particular Reference to Machine Tools", *Proceedings, Inst.*

Mech. Engr., Vol. 191, pp. 257-270.

Teltz, R., Keith, U. and Elbestawi, M. A., 1994, "Intelligent Open Architecture Control for Machining Systems", *Proceedings, ASME WAM*, PED-Vol. 68-1, Chicago, p. 851.

Thomsen, E. G., Macdonald, and A. G., Kobayashi, S., 1962, "Flank Friction Studies With Carbide Tools Reveal Sublayer Plastic Flow", Trans. ASME, *J. of Eng. for Ind.*, Vol. 84, pp. 53-62;

Tillen, R., 1964, "Controlling Workpiece Accuracy", *Production Engineer*, 43, pp. 499-575.

Tlusty, J., 1965, "A Method of Analysis of Machine-Tool Stability," *Proceedings, 6th International MTDR Conf.*, Manchester College of Science and Technology, Manchester, England, Sept. 13-15.

Tlusty, J., and Heczko, O., 1980, "Improving Tests of Damping in the Cutting Process," *Proceedings, NAMRC 8*, pp. 372-376.

Tlusty, J., and Ismail, F., 1981, "Basic Non-Linearity in Machining Chatter", *CIRP Annals*, Vol.30, pp.299-304.

Tlusty, J., Moriwaki, T., and Goel, G. S., 1976, "The Dynamic Cutting Force Coefficient for some Carbon Steels", *Proceedings, 4th NAMRC*, Columbus, Ohio, pp. 287-294.

Tlusty, J., and Polacek, M., 1963, "The Stability of the Machine Tool Against Self-Excited Vibrations in Machining", *Proceedings, ASME Production Engineering Research Conference*, Pittsburgh, pp. 454-465.

Tlusty, J., 1978, "Analysis of the State of Research in Cutting Dynamics", *CIRP Annals*, Vol. 27(2), pp. 583-589.

Tobias, S. A., and Fishwick, W., 1958, "The Chatter of Lathe Tools Under Orthogonal Cutting Conditions", *Transactions of ASME*, Vol. 80, pp. 1079-1088.

Tobias, S. A., 1965, "Machine Tool Vibration", John Wiley and Sons Inc., New York.

Usui, E., and Hirota, A., 1978b, "Analytical Prediction of Three Dimensional Cutting Process: Part II. Chip Formation and Cutting Force With Comventional Single Point Tool", Trans. ASME, *J. of Eng. for Ind.*, Vol. 100, pp. 229-235.

Usui, E., Hirota, A., and Masuko, M., 1978a, "Analytical Prediction of Three Dimensional Cutting Process: Part I. Basic Cutting Model and Energy Approach", Trans. ASME, *J. of Eng. for Ind.*, Vol. 100, pp. 222-228.

Walker, R., 1988, *GIDEP Alert No. X1-A-88-01*, Government-Industry Data Exchange

Program, Washington, DC.

Wang, Y., 1992, "Minimum Zone Evaluation of Form Tolerances," *Manufacturing Review*, Vol. No. 3, pp. 213-220.

Watanabe, T., and Iwai, S., 1983, "A Control System to Improve the Accuracy of Finished Surfaces in Milling", Trans. ASME, *J. of Dyn. Sys., Meas. and Cont.*, Vol. 105, pp. 192-199.

Whitehouse, D. J., 1976, "Some Theoretical Aspects of Error Separation Techniques in surface Metrology," *J. of Physics (E)*, Vol. 9, pp. 531-536.

Wilson, H. R., 1992, "*Form Errors of Cylindrical Features for Specific Manufacturing Processes*", Master Thesis, University of North Carolina at Charlotte, Charlotte, NC.

Wu, C. L., Haboush, R. K., Lymburner, D. R., and Smith, G. H., 1986, "Closed-loop Machining Control for Cylindrical Turning", *Proceedings, ASME WAM*, Modeling Sensing and Control of Manufacturing Systems, New York, pp. 189-204.

Wu, D. W., 1988, "Application of a Comprehensive Dynamic Cutting Force Model to Orthogonal Wave-Generating Process", *Int. J. Mechanical Sciences*, Vol. 30, No. 8, pp. 581-600.

Wu, D. W., 1989, "A New Approach of Formulating the Transfer Function for Dynamic Cutting Processes", Trans. ASME, *J. of Eng. for Ind.*, Vol. 111, pp. 37-47.

Wu, S. M., and Ni, J., 1989, "Precision Machining without Precise Machinery", *CIRP Annals*, Vol. 38(1), pp. 533-536.

Zhang, G., and S. G. Kapoor, 1985, "Dynamic Modeling and Analysis of the Boring Machining System," Proc., ASME Symposium on Sensors and Controls for Manufacturing, PED-Vol. 18, pp. 11-20.

Zhang, G. M., and Kapoor, S.G., 1991a, "Dynamic Generation of Machined Surfaces: Part 1. Description of a Random Excitation System", Trans ASME, *J. of Eng. for Ind.*, Vol. 113, p. 137.

Zhang, G. M., and Kapoor, S. G., 1991b, "Dynamic Generation of Machined Surfaces: Part 2. Construction of Surface Topography", Trans. ASME, *J. of Eng. for Ind.*, Vol. 113, p. 145.

Zorev, N. N., 1966, "*Metal Cutting Mechanics*", Pergamon Press, Oxford, England.

APPENDIX A

RAKE ANGLES IN OBLIQUE CUTTING

In oblique cutting the cutting edge is not normal to the tool direction of motion (as it is the case in orthogonal cutting). However, it has an inclination angle i, which causes the chip to flow at an angle η relative to the cutting edge as shown in Fig. 2.1b. The inclination angle i is defined as the angle formed by the cutting edge and a normal to the cutting velocity vector V as shown in Fig. A.1. The inclination angle is given by,

$$i = \tan^{-1} (\tan \alpha_b \cos la - \tan \alpha_s \sin la) \qquad \textbf{(A.1)}$$

where α_b and α_s are the back rake and side rake angles of the cutting tool, respectively, as shown in Fig. A.1.

In orthogonal cutting, the rake angle is measured from the tool rake face to a line perpendicular to the cutting velocity vector. In oblique machining, the problem arises in choosing the plane in which to measure the rake angle. There are thus three different rake angles defined for oblique cutting. The velocity rake angle α_v is measured in a plane parallel to the cutting velocity vector and normal to the machined work surface. The normal rake angle α_n is measured in a plane normal to the cutting edge of the tool. The effective rake angle α_e is measured in a plane containing the cutting velocity vector and the chip flow

vector. The three angles are shown in Figs. A.2, A.3 and A.4. The equations for the three angles are as follows:

$$\alpha_v = \tan^{-1} (\tan \alpha_s \cos la + \tan \alpha_b \sin la) \quad \textbf{(A.2)}$$

$$\alpha_n = \tan^{-1} [(\tan \alpha_s \cos la + \tan \alpha_b \sin la) \cos i] \quad \textbf{(A.3)}$$

$$\alpha_e = \sin^{-1} (\sin i \sin \eta + \cos i \cos \eta \sin \alpha_n) \quad \textbf{(A.4)}$$

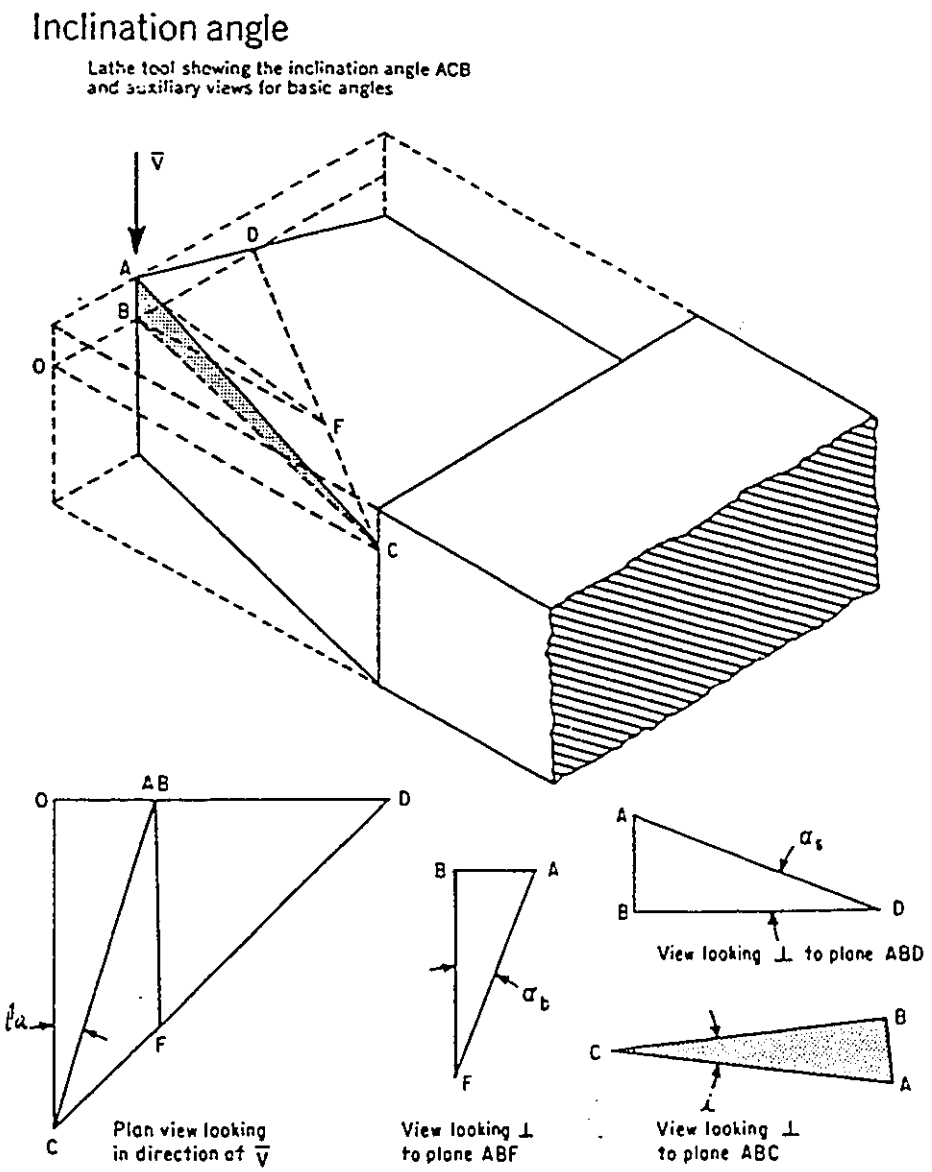

Fig. A.1 Inclination Angle. (Kuhl, 1985)

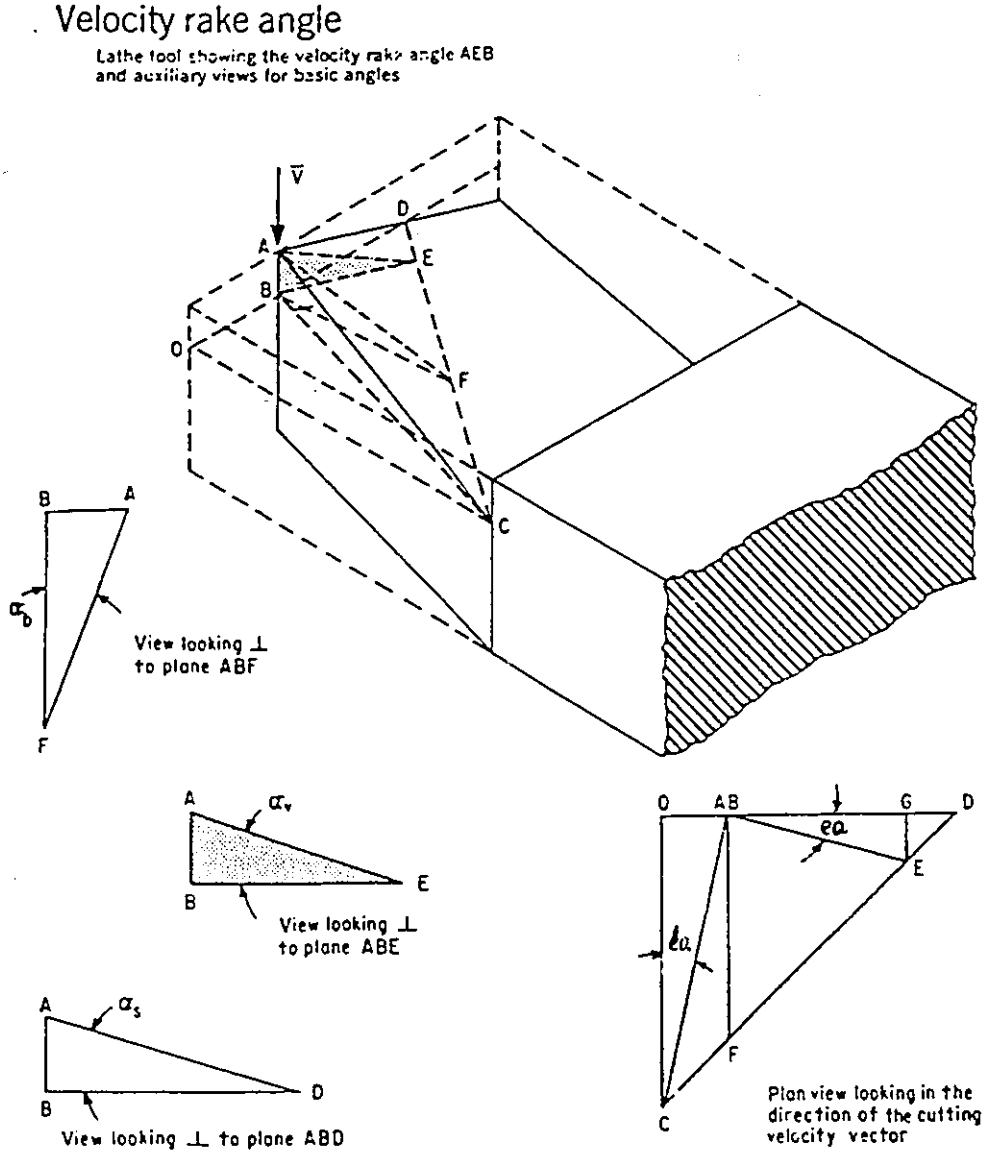

Fig. A.2 Velocity Rake Angle. (Kuhl, 1985)

Normal rake angle

Lathe tool showing the normal rake angle GEB and auxiliary views for velocity rake and equivalent inclination angles

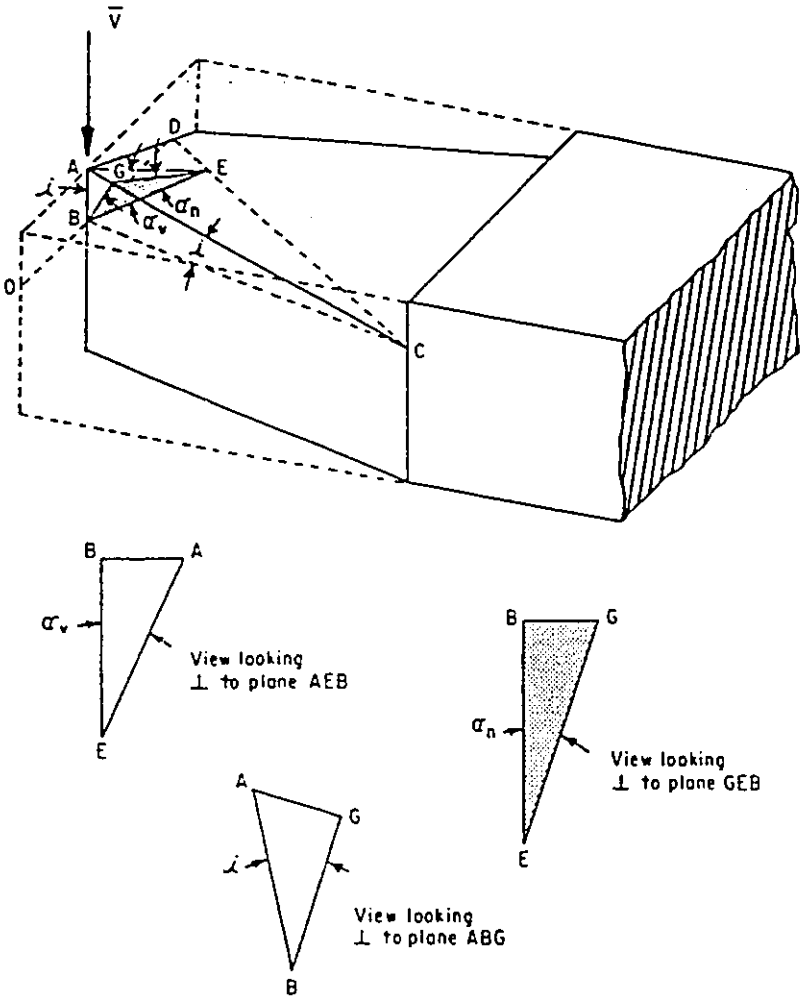

Fig. A.3 Normal Rake Angle. (Kuhl, 1985)

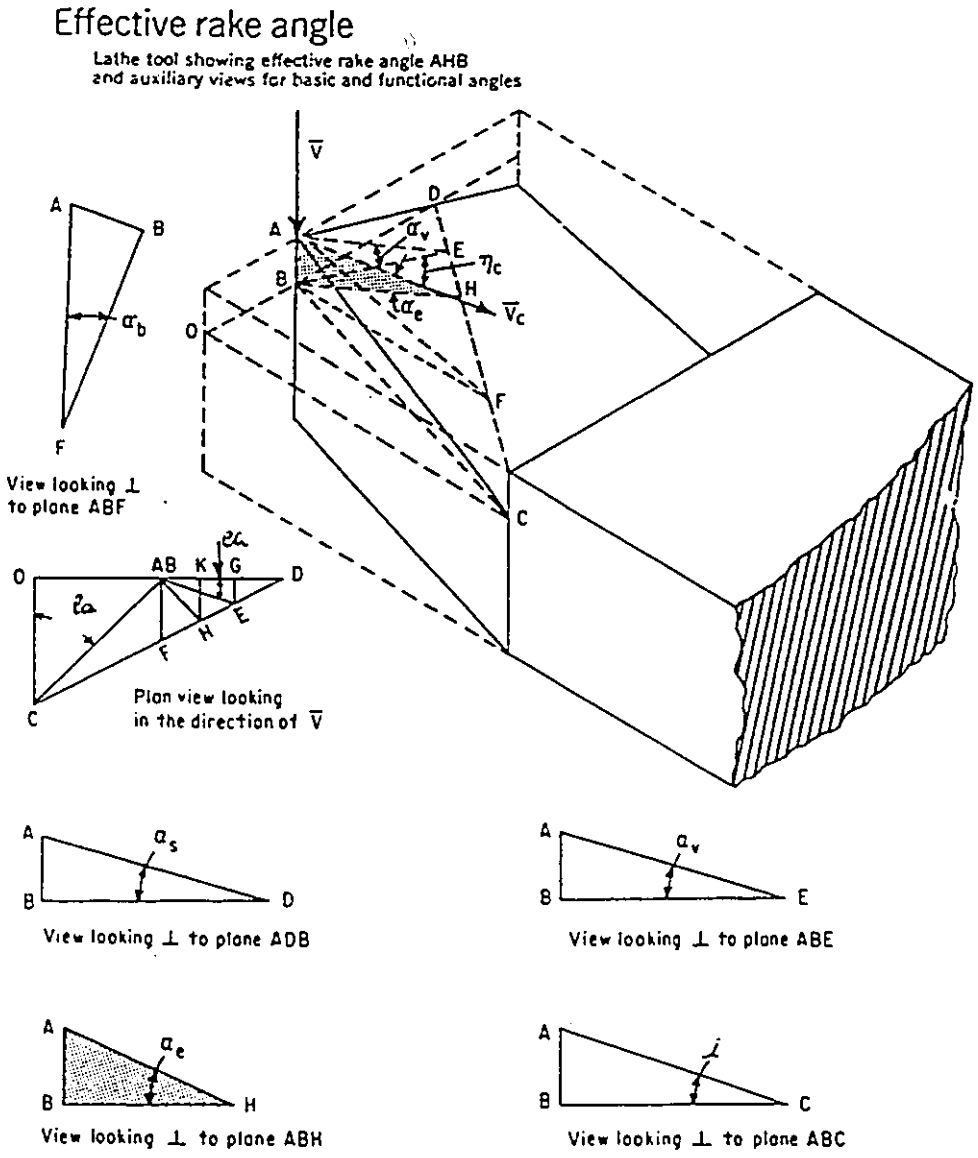

Fig. A.4 Effective Rake Angle. (Kuhl, 1985)

APPENDIX B

CALCULATIONS OF EQUIVALENT CHIP THICKNESS AND EFFECTIVE LEAD ANGLE

B.1 EQUIVALENT CHIP THICKNESS

The equivalent chip thickness is calculated as the ratio of the chip load area $A_c(t)$ to the width of cut $b(t)$. The chip load area is calculated as shown in section 3.1. Therefore, the main concern here is the calculation of the width of cut. The width of cut is taken as the average of the lengths of profiles $P(t)$ and $P(t-T)$ that are in contact with the chip, $l_c(t)$ and $l_c(t-T)$, respectively. The chip length $l_c(t)$ is the algebraic summation of the three elements $L_S(t)$, $L_C(t)$ and $L_E(t)$ as shown in Fig. B.1. The three latter elements represent the contribution of side cutting edge, tool nose radius and end cutting edge to the total to the chip length $l_c(t)$, respectively. The determination of $L_S(t)$, $L_C(t)$ and $L_E(t)$ is based on the knowledge of coordinates of the points *LIM1* and *LIM2* as defined in section 3.1. Each of $L_S(t)$ and $L_E(t)$ is calculated as the linear spatial distance between their respective start and end points, while $L_c(t)$ is calculated as follows:

$$L_C(t) = R \cdot (\phi_o - \phi_1) \qquad \textbf{(B.1)}$$

where, ϕ_o and ϕ_1 are equal to the lead angles at the start and end points of arc *'C'*, respectively, as shown in Fig. B.2. Thus, the width of cut can be calculated from

$$b(t) = \frac{L_S(t) + L_C(t) + L_E(t) + L_S(t-T) + L_C(t-T) + L_E(t-T)}{2} \quad \textbf{(B.2)}$$

Hence, knowing both the chip load and the width of cut, the equivalent chip thickness is directly calculated from,

$$t_c(t) = \frac{A_c(t)}{b_c(t)} \quad \textbf{(B.3)}$$

B.2 EFFECTIVE LEAD ANGLE

The nominal lead angle *'la'* is the angle measured between the cutting edge and the normal to the workpiece axis of rotation. In the case of a multi-edged cutting tool, the local lead angle ϕ changes along the cutting edge profile as shown in Fig. B.3. On the side cutting edge $\phi = la$; along the nose ϕ changes continuously, reaching a maximum of $\phi = \pi/2 + ea$ on the end cutting edge. The local effective lead angle ψ_a at any point *'A'* represents the direction of the normal force F_N at that point measured from a vector parallel to the workpiece axis of rotation and in a plane normal to the cutting velocity. Applying Stabler's Rule ($\eta = i$), the direction of F_N (*i.e,* ψ_A) is defined by the local inclination angle $i(\phi_A)$ and the local lead angle ϕ_A (as shown in Fig. B.4) by the following relation:

$$\psi(t_c) = \phi + \tan^{-1}\left[\frac{\tan i(\phi)}{\cos \alpha_n(\phi)}\right] \quad \textbf{(B.4)}$$

The $\cos \alpha_n$ term transforms the local chip flow direction from the rake face plane into the plane normal to the cutting velocity, where the friction force is measured (see Fig. B.5). The dependence of the inclination angle on ϕ is known by:

$$i(\phi) = \tan^{-1}(\tan\alpha_b \cdot \cos\phi - \tan\alpha_s \cdot \sin\phi) \qquad \textbf{(B.5)}$$

The effective lead angle is a weighed average of the elemental local effective lead angles $\psi(\phi)$. The distribution of the normal force is assumed to follow that of the chip thickness shown in Fig. B.5. Thus, the values of $\psi(\phi)$ are basically weighed by the corresponding values of $t_c(\phi)$. Hence, the generalized formula for determining the effective lead angle may be written as,

$$la_e = \frac{\int \psi(l_c)\, t_c(l_c)\, dl_c}{\int_{l_c} t_c(l_c)\, dl_c} \qquad \textbf{(B.6)}$$

The dependency of the la_e calculation on t_c requires the knowledge of the local chip thickness $t_c(\phi)$ at every increment $d\phi$. Referring to Fig. B.6, for every increment, the coordinates of the corresponding points *'A'* and *'B'* are determined using the set of intersection functions. Points *'A'* and *'B'* are the intersections of *AB* with *P(t)* and *P(t-T)*, respectively; except for zone *'Q'*, where, *'B'* is the intersection with the workpiece surface. Vector *AB* represents the chip flow direction in a plane perpendicular to the cutting velocity. Thus, the local value of $t_c(\phi)$ is equal to the length *AB*.

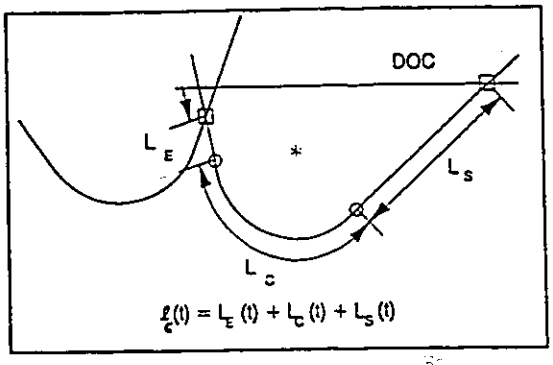

Fig. B.1 Chip Length $l_c(t)$.

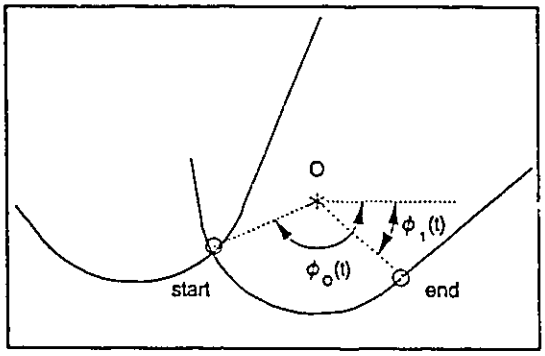

Fig. B.2 Nose Radius Contribution to $l_c(t)$.

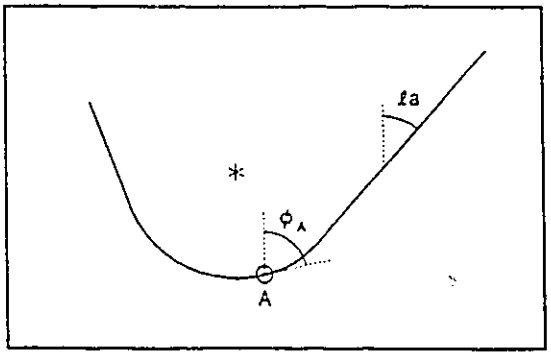

Fig. B.3 Lead Angle *la* at point *A*.

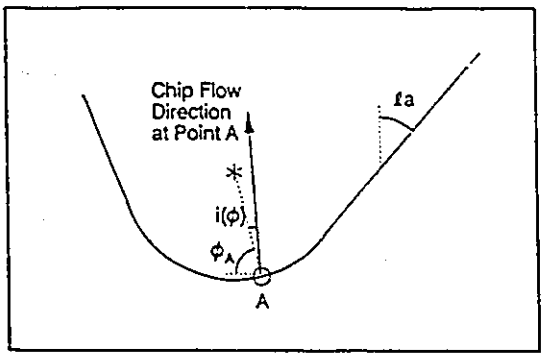

Fig. B.4 Local Friction Force Direction.

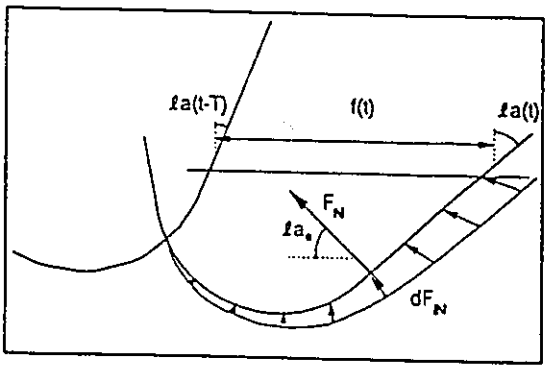

Fig. B.5 Friction Force Distribution.

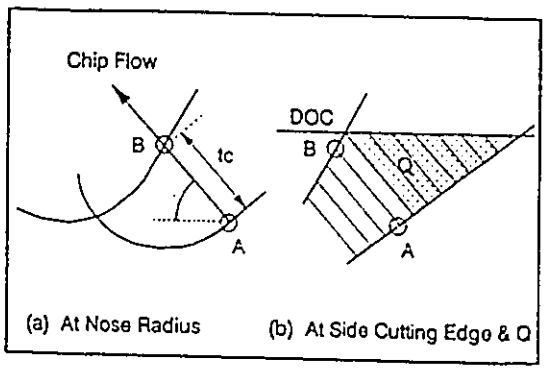

Fig. B.6 Local Chip Thickness t_c.

APPENDIX C

THE THREE-POINT METHOD

In roundness and spindle error measuring systems there are three errors in total. These errors are out of roundness of the workpiece, X and Y components (or amplitude and phase) of the radial error motion of the spindle. All these errors are functions of the angle of rotation. If three probes are used as shown in Fig. C.1 we get three sets of equations. By solving the combined equations we are able to determine all three errors. This method is called "three-point method" and it can be used for separating spindle error of the machine from the roundness error of the workpiece, even if the spindle does not repeat.

If the roundness error of the workpiece is expressed as $dr(\theta)$ and the X and Y components of the spindle error motion are $x(\theta)$ and $y(\theta)$ respectively then three sets of readings can be acquired from the probes:

$$S_1(\theta) = R_1 - dr(\theta) - y(\theta) \qquad \textbf{(C.1)}$$

$$S_2(\theta) = R_2 - dr(\theta - \phi_2) - y(\theta)\cos\phi_2 + x(\theta)\sin\phi_2 \qquad \textbf{(C.2)}$$

$$S_3(\theta) = R_3 - dr(\theta - \phi_3) - y(\theta)\cos\phi_3 + x(\theta)\sin\phi_3 \qquad \textbf{(C.3)}$$

where, R_i is the reading of the *ith* probe ($i = 1$ *to* 3) at the initial position, while roundness error $dr(\theta)$ and error motion $x(\theta)$ and $y(\theta)$ equal zero. Build a new function,

$$S_0(\theta) = S_1(\theta) + a_2 S_2(\theta) + a_3 S_3(\theta) \quad \textbf{(C.4)}$$

After expanding $dr(\theta)$ into Fourier series,

$$dr(\theta) = r_0 + \sum_{k=1}^{\infty} (A_k \cos k\theta + B_k \sin k\theta) \quad \textbf{(C.5)}$$

substituting into equation C.4 and expressing,

$$1 + a_2 \cos k\phi_2 + a_3 \cos k\phi_3 = \alpha_k \quad \textbf{(C.6)}$$

$$a_2 \sin k\phi_2 + a_3 \sin k\phi_3 = \beta_k \quad \textbf{(C.7)}$$

we get,

$$\begin{aligned} S_0(\theta) = {} & R_1 + a_2 R_2 + a_3 R_3 - r_0 (1 + a_2 + a_3) - a_1 y(\theta) + \beta_1 x(\theta) \\ & - \sum_{K=2}^{\infty} [(A_k \alpha_k - B_k \beta_k) \cos k\theta + (B_k \alpha_k + A_k \beta_k) \sin k\theta] \end{aligned} \quad \textbf{(C.8)}$$

Selecting a_i and ϕ_i ($i = 2 - 3$) to make $\alpha_i = 0$, $\beta_i = 0$ we can make $S_0(\theta)$ independent from spindle errors $x(\theta)$ and $y(\theta)$. $S_i(\theta)$ ($i = 1 - 3$) are the acquired measurements. After selecting a_i ($i = 1 - 3$), $S_0(\theta)$ can be determined. By expanding $S_0(\theta)$ into Fourier series we get,

$$S_0(\theta) = S_0 + \sum_{K=1}^{\infty} (F_k \cos k\theta + G_k \sin k\theta) \quad \textbf{(C.9)}$$

where,

$$A_k = -\frac{\alpha_k F_k + \beta_k G_k}{\alpha_k^2 + \beta_k^2} \qquad \textbf{(C.10)}$$

and,

$$B_k = \frac{\beta_k F_k - \alpha_k G_k}{\alpha_k^2 + \beta_k^2} \qquad \textbf{(C.11)}$$

Once all A_k and B_k are determined from Eqs. C.10 and C.11, the roundness error $dr(\theta)$ is determined. Error motions $x(\theta)$ and $y(\theta)$ can be also determined from Eqs. C.1-C.3.

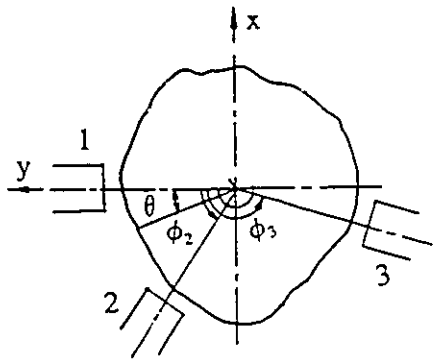

Fig. C.1 The Three Point Method.